A STUDY, USING A WILSON CLOUD CHAMBER, OF THE ELECTRONS EMITTED WHEN LIGHT MESONS ARE STOPPED BY ELEMENTS OF LOW ATOMIC NUMBER

Thesis

Submitted by

JOHN R. NORBURY, B.Sc. (Edinburgh)

for the degree of

Doctor of Philosophy

University of Edinburgh

March, 1966.

PREFACE

The research described in this thesis has been conducted in the Department of Natural Philosophy of the University of Edinburgh, under the joint direction of Professor N. Feather, F.R.S. and Dr. G.R. Evans.

C O N T E N T S

C O N T E N T S (Contd.)

C O N T E N T S (Contd.)

C O N T E N T S (Contd.)

CHAPTER 1

THE INTRODUCTION

When a slow negative meson is captured by an atom, by the replacement of an atomic electron, a mesic atom in a high state of excitation is formed. The meson reaches the ground state of the atom through de-excitation by the emission of photons and electrons. These electrons, because they are emitted in a similar manner to atomic Auger electrons, are also termed Auger electrons.

The μ-meson, due to its relatively long half life and weak interaction with the nucleus, invariably reaches the ground state of the μ-mesic atom. Either decay or nuclear absorption is possible from this level, the ratio of the rates of these two processes being a function strongly dependent on the nuclear charge. After nuclear absorption, a process similar in some respects to K-capture, the daughter nucleus may exhibit a β-activity. Under certain conditions, confusion between the β-decay and μ-meson decay electrons might occur.

In a series of previous experiments[1, 2] conducted with a Wilson High Pressure Cloud Chamber, using an argon filling, several examples of stopped μ-mesons were observed associated with electrons of energies between 2-5 Mev. Among the total number of μ - e decay events of these

experiments, no decay electrons in this energy group should have been seen. They were alternatively interpreted as arising from the β-decay of a nucleus formed by μ-meson absorption. However as the available evidence in favour of this theory was not completely convincing, a further study of these anomalous low energy electrons was conducted. More information in support of the β-decay hypothesis was gathered, together with approximate limits on its half life.

Prior to the start of this project, Auger electrons associated with μ-mesic atoms had only been studied in a quantitative manner, when observed in nuclear emulsions. A technique, which utilizes the photographs of stopped μ-mesons in a high pressure cloud chamber, for the estimation of Auger electron yields in gaseous targets is the subject of one of the following Chapters, whilst the available results of those experiments conducted with nuclear emulsion, the topic of another.

As a consequence of the method adopted to obtain some of the above experimental results, it was also possible to study in a preliminary way, the phenomena of direct pair production by μ-mesons. Although the number of events was small, at least qualitative agreement with the current theoretical predictions was achieved and this experiment could serve as a useful basis for further research in this direction.

The high pressure cloud chambers, its associated electronics and operational properties are described in the next Chapter. However, the complete account of a cloud chamber and counter system, which was used to obtain further results, is included in an appendix form, only necessary details being mentioned in the main part of the text.

CHAPTER 2

THE CLOUD CHAMBER

Section 1. The Experimental Approach

The high pressure Wilson Cloud Chamber, used to observe both low energy electrons (energy, a few Mev) associated with stopped μ-mesons and Auger electrons (energy 10-100 keV) produced by the de-excitation of μ-mesic atoms, could be operated in three different ways:- 1) in conjunction with a counter system designed to detect incident μ-meson stopping in the chamber gas, 2) by purely random photography of cosmic rays, 3) operated in conjunction with a beam of artificially produced μ-mesons.

1) Counter Control System

The satisfactory recycling time of the cloud chamber at the start of this project was 15 minutes. The low counting rate expected by such a system would have rendered the existing cloud chamber operation perfectly satisfactory, with no further improvement necessary. The quality of counter controlled tracks would be very good, the effects of thermal distortion in the chamber being reduced to a minimum by the long waiting time between successive events. If the counter system could be refined sufficiently the stopping power of the chamber gas could be reduced, allowing the detection of low energy Auger electrons. This reduction could be achieved, either by merely lowering the gas pressure, or by using a hydrogen filled chamber with a small percentage of a heavier gas. (In the latter case, the μ-meson initially atomically captured by a proton would

invariably be transferred to an atom of a larger atomic number). If the experimental counting rate was too low to be practicable using cosmic rays, the counter system and chamber might possibly be used with a particle accelerator, where a greater efficiency for the selection of events would be expected, compared with method 3).

However the design and operation of this technique would pose rather difficult problems, the low counting rate expected (about 1 genuine event per 10 hours from cosmic radiation) making calibration a difficult and lengthy procedure.

2) Random Photography

Although information concerning other events would be collected in such an experiment, where no bias existed for one particular type, a very large number of photographs would be required (10,000 photographs) if a significant number of events were to be obtained.

The existing recycling time would have to be reduced to as low as 5 minutes and the conditions for optimum chamber operation investigated. Although the cloud chamber control circuit would be simpler than in the other two methods, extreme reliability would be required and continuous operation on a 24 hour basis necessary, if the experiment was to be completed in a sensible time.

Little possibility existed of lowering the gas pressure below some 50 atmospheres as the number of events recorded would depend on the stopping power of the chamber gas.

3) The Accelerator Experiment

In this method, the experiment could be completed quickly with the double advantage of knowing the type of particle entering the chamber and a more consistent quality of tracks than method 2).

The maximum recylcing time acceptable for accelerator operation would be of the order of 2 minutes. Large improvements in the recycling time would have to be achieved before this type of experiment would be considered. Again, as in method 2), the gas pressure would have to be relatively high.

Conclusions

Thus having examined the relative merits of each method, the counter control system 1), although possibly the most difficult technically, would appear to yield the greatest advantage. Although a counter system was constructed and several hundred cloud chamber photographs obtained, no evidence that the system was selecting slow or stopping particles was apparent. A closer examination of the electronics of this first system suggested that the necessary time resolution had not been achieved, and considerable improvement would be required for a satisfactory arrangement.

During the time spent on this counter system, the operation of the chamber had been improved, resulting in a satisfactory recycling time of less than 5 minutes. Although method 3) was still not feasible, the possibilities of method 2) could then

be explored. An investigation of the cloud chamber properties which led to optimum operation, together with a redesigned automatic control circuit enabled 5,000 photographs to be obtained with both nitrogen and argon fillings.

The counter controlled system was considered at least of technical interest. After prolonged development, a system which achieved the selection of stopped particles was designed, resulting in a three fold increase in the rate with which information could be gained over the random method.

The problem of detecting Auger electrons in a manner other than that described in Chapter 6 was considered too difficult, when using cosmic ray μ-mesons. If the electron tracks were to be clearly resolved, a pressure as low as 6 atmospheres of argon would be necessary. At this stopping power only one event a month would be collected.

Section 2. The Cloud Chamber Design

The details of the construction of the high pressure cloud chamber are shown in Fig. 1. The working volume (dimensions 20 cm long by 20 cm diameter), illuminated by three flash tubes through three ports symmetrically placed around the chamber, was viewed through the front window by a stereoscopic camera. The cloud chamber clearing field was an arrangement of rods supported between two ebonite rings.

At the rear region of the chamber a velvet cloth,

FIG I

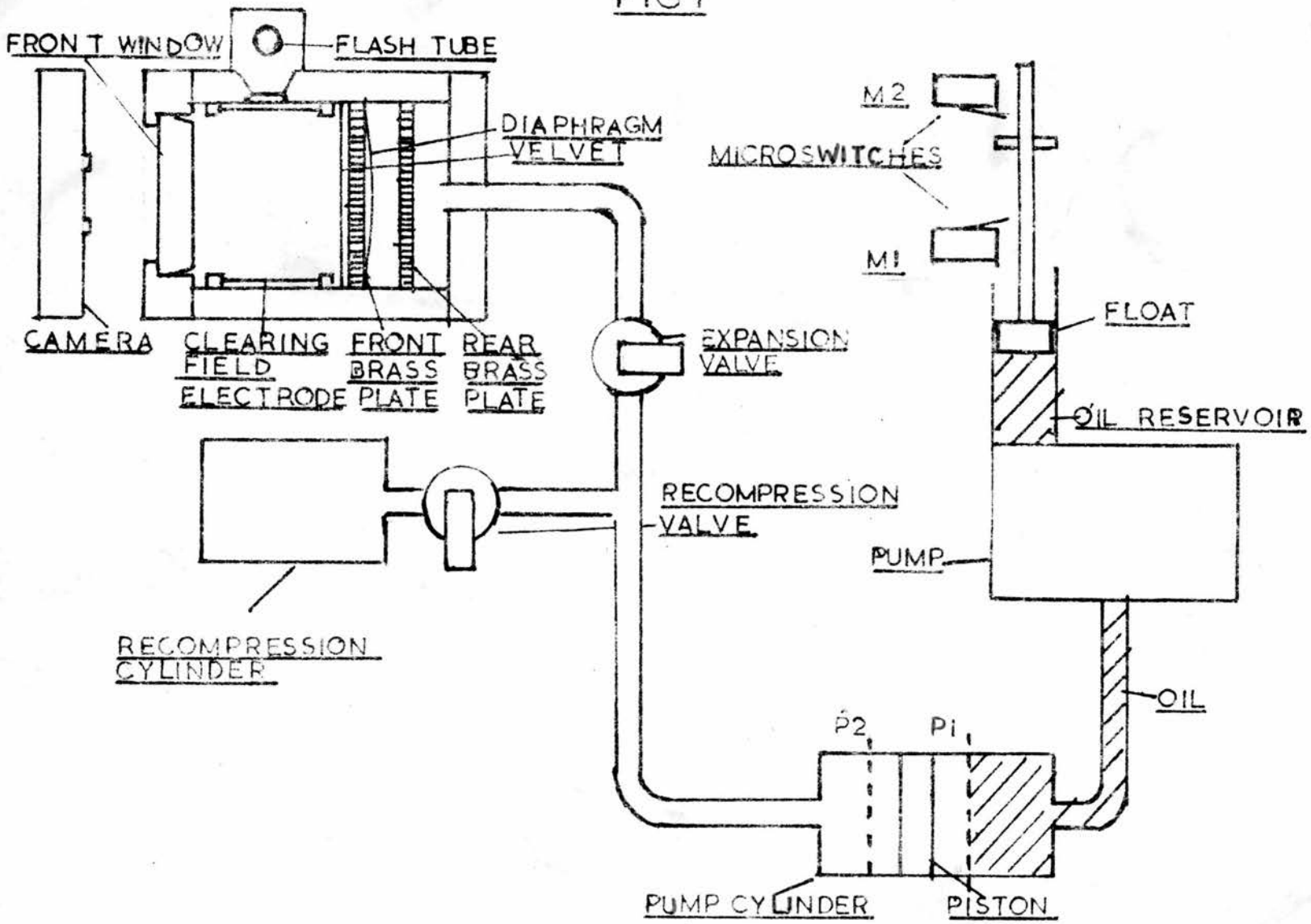
FRONT WINDOW
FLASH TUBE
DIAPHRAGM
VELVET
M2
MICROSWITCHES
M1
FLOAT
CAMERA
CLEARING FIELD ELECTRODE
FRONT BRASS PLATE
REAR BRASS PLATE
EXPANSION VALVE
OIL RESERVOIR
RECOMPRESSION VALVE
PUMP
RECOMPRESSION CYLINDER
OIL
P2
P1
PUMP CYLINDER
PISTON

stretched over a coarse wire mesh secured both a good photographic background and smooth gas flow during an expansion. The rubber diaphragm was constrained to move between two brass plates each of which had some 900 small bore holes drilled in them. The expansion ratio of the chamber, determined by the separation of the two brass plates, could be altered by changing the position of the rear one.

A 0.75 inch diameter pipe connected the rear of the chamber through the expansion valve to the pump or expansion cylinder. A float, situated in the oil reservoir of the high pressure pump, operated two microswitches, the vertical position of which, determined the two limiting positions of the piston in the pump cylinder.

A second pipe led from the pump cylinder side of the expansion valve to the recompression cylinder via a second valve (recompression valve). Water was passed through the lead pipes wrapped around both cylinders to maintain the gas at a constant temperature.

Both valves were identical and have been described in some detail by Donald[1]. The gas sealing of these valves was achieved by seating a polished steel cone-shaped valve onto a brass seat. The cone-shaped valve was part of a spindle which moved along its axis when rotated by means of a threaded section, located in a fixed nut. The opening and closing of the valves was performed electro-mechanically by two solenoids which struck a cam fixed to the valve spindle.

Pressure gauges were attached to various sections of the

chamber, two of which incorporated an electrical contact which could be set to open at a predetermined pressure.

The stereoscopic camera had two lenses which photographed each event on the same piece of film, the images being 7.5 cm apart. In order to conserve the length of film used, successive events were interleaved, which required the camera wind on motor to pull through alternate lengths of film in the ratio of 3 : 1. The details of the camera wind on mechanism are shown in Fig. 2 and described later (section 3).

The cloud chamber and auxiliary components (except the pump) were enclosed in a well insulated hut. The temperature of the system was kept constant by a heating and cooling arrangement operated by a thermostat.

The Cloud Chamber Cycle with Fast Recompression

Both parts of the cloud chamber (i.e. the volumes in front and behind the diaphragm) were filled with gas to some predetermined pressure, of the order of 50 atmospheres. Finally the rear portion of the chamber had an excess pressure over the front of 1 to 2 atmospheres, thus ensuring the diaphragm was held firmly against the front brass plate (Fig. 1). During this procedure both valves were kept in the open position and the piston in position P1. The expansion valve was then closed, the pump operated until the piston reached position P2 (Fig. 1). The pressure of both the expansion and recompression cylinder was thus increased (approximately 100 atmospheres). The recompression valve was closed and the piston returned to its original

FIG 2

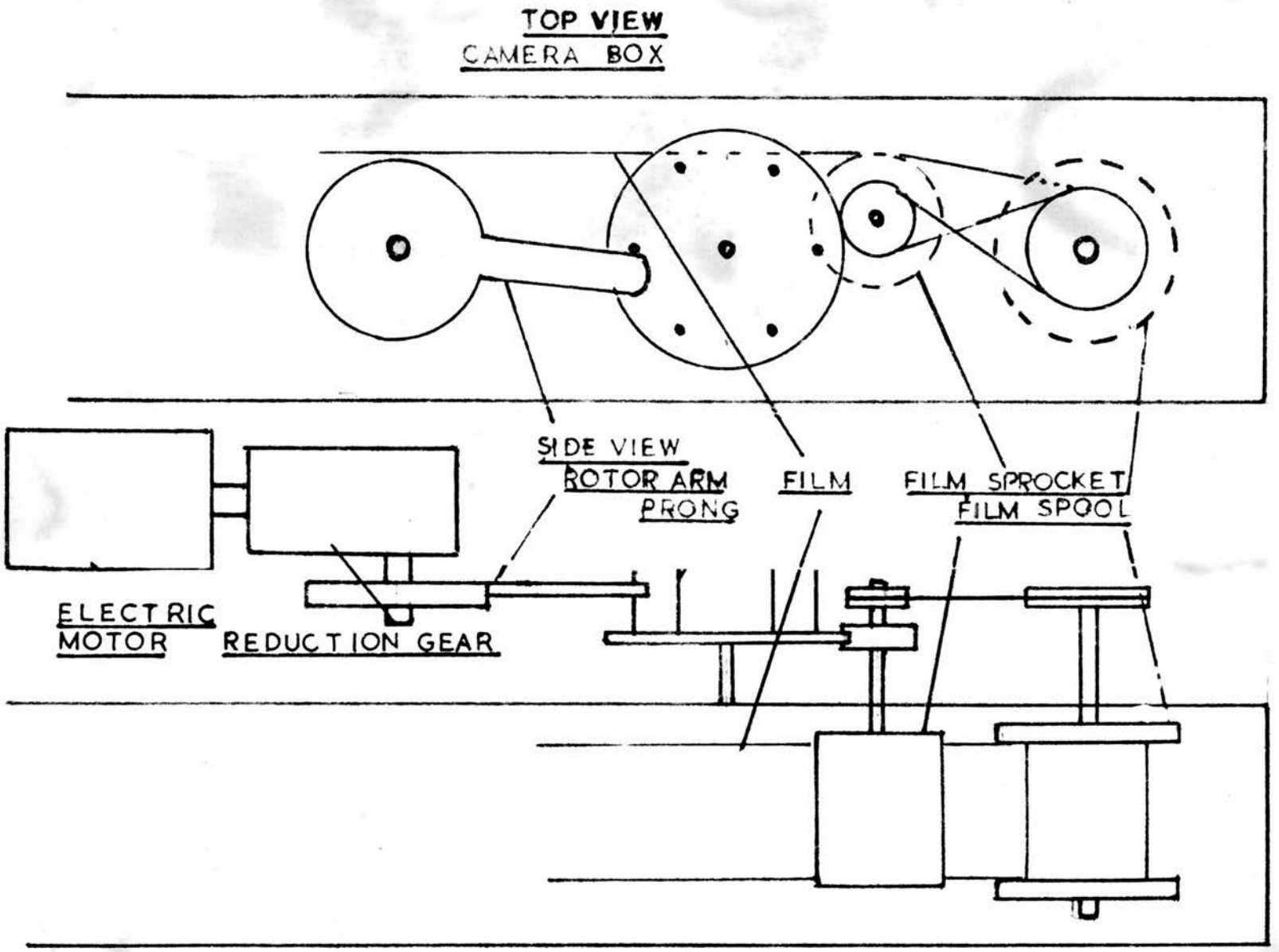
TOP VIEW
CAMERA BOX
SIDE VIEW
ROTOR ARM
PRONG
FILM
FILM SPROCKET
FILM SPOOL
ELECTRIC MOTOR
REDUCTION GEAR

position P1 by allowing the oil to flow back into the pump reservoir from the pump cylinder. The pressure in the expansion cylinder was then of the order of 20 atmospheres.

The chamber was then ready for the start of a cycle. Initially, before an expansion in which events were to be photographed, the camera was in position, the clearing field had been switched on and the flash tube condensers fully charged.

The operations in one cycle using fast recompression were:-

1) The clearing field was switched off and the expansion valve opened at the same time. The diaphragm moved from the front to the rear brass plate due to the large pressure difference between the chamber and pump cylinder.

2) The flash tubes were triggered (~ 0.5 second after the expansion), the appropriate time for drop growth to have increased to a photographable size.

3) The recompression valve was opened, the diaphragm returning to the front brass plate (~ 0.6 seconds after the expansion).

4) a. The expansion valve was closed, isolating the chamber from the pump mechanism.

b. The film wind on operation was started.

5) The pump motor was started, thus moving the piston from P1 to P2.

6) When the pump piston reached P2, the motor was turned off, and the recompression valve closed.

7) The oil was returned to the reservoir until the piston reached position P1.

8) The clearing field was switched on again.

9) A delay mechanism operated which rendered the control circuit inactive for the waiting period (2-5 minutes) in order that chamber gas could regain thermal equilibrium.

The flash tube condensers were charged continuously throughout the cycle, except during the interval between expansion and recompression, when they were connected to the flash tubes. The flash tubes required a triggering pulse at a voltage substantially higher than that of the charged condensers to initiate the discharge. This pulse was supplied (in operation 2).

The minimum possible recycling time (i.e. of the operation 1 to 8) was of the order of one minute.

The operations described were achieved automatically by a control circuit into which a safety system was incorporated. This system stopped the cycle if one of four possibilities occurred:-

10) The forward pressure across the diaphragm exceeded 10 atmospheres,

11) The pressure in the pump cylinder became greater than 130 atmospheres.

12) The expansion valve was not shut at the appropriate time.

13) The current flowing through the solenoids which operated the valves was not switched off in a time of 8 seconds. (Normally they were in operation for 1-2 seconds).

If possibilities 10) or 12) occurred, then damage to the rubber diaphragm was likely. Replacement represents a considerable amount of labour before the chamber can be rendered operational again. Invariably, some of the pump oil which could seep past

the piston found its way into the working portion of the chamber, if a punctured diaphragm occurred. The contamination caused by this oil must be removed before the chamber would function successfully and might take a matter of days.

The pressure limit of 130 atmospheres was set for the recompression cylinder as it was only tested to this value. This pressure was also the upper satisfactory working limit of the pump.

The solenoids were run at a current twice their continuous working rating. Although perfectly safe for short time operation, any failure of the control system which left the solenoids switched on, would have resulted in serious overheating and damage.

When the chamber was operated continuously, the termination of operation 9 could be arranged to start the next cycle. When operated in this way, a facility for switching off the clearing field between 0 and 2 seconds before the start of the expansion was available. Thus tracks formed by a particle passing through the chamber immediately prior to expansion remained relatively undistorted.

Slow expansions when necessary were performed by opening the expansion valve manually. As this chamber could be operated in a perfectly satisfactory manner without the need for slow clearing expansions, this facility was not built into the control circuit.

Section 3. Cloud Chamber Control Circuit

A control circuit which produced the necessary cycle of functions for automatic cloud chamber operation had been constructed by Donald (1958)[1] and modified by Tait (1960)[2]. A sequence of pulses was obtained from a uniselector driven by a thyratron valve, the timing of each stage being achieved by an R-C circuit. However as this system had been modified considerably during the series of experiments on cloud chamber operation (Section 4), it was difficult to maintain. It had also become unreliable due to ageing of some of the components.

An entirely new transistorized circuit was constructed, in which a series of almost identical circuit sections replaced the uniselector system which had been one of the sources of poor reliability. These sections consisted of an R-C timing circuit operating a transistor actuated post office relay. The necessary sequence of pulse for cyclic operation was obtained by triggering each section by the previous one. The operation of the cloud chamber mechanism (i.e. valves, pumps etc.) was achieved by a bank of large relays, which in turn were controlled by the post-office relays in the individual sections.

The layout of the circuit was arranged so that all the relays and transistors could be easily replaced in event of failure. However, after a few initial modifications the control system operated the cloud chamber for some 15,000 cycles, the only maintenance required being the replacement of two transistors.

Basic Section

The circuit of the basic section 2 is shown in Fig. 3. However, as both the preceding and following sections play some part in its operation, the relevant components of these sections (i.e. 1 and 3) are also shown. The relay contacts (i.e. RL1,1 RL2,3) are shown in the position they occupy when the relay is not energised, the first digit referring to the relay, the second to the contact number on that relay.

Initially transistor T1 is turned on, resulting in current flowing in relay RL1. Even if this transistor is now switched off, relay RL1 remains energised as current can now by-pass the transistor through contacts RL1,1 and RL2,3.

Contact RL1,2 is opened as soon as relay RL1 is switched on, allowing the condenser to charge through resistance R1. (This condenser is normally almost discharged as a result of resistance R2). When the potential of point x becomes sufficiently negative, base current flows in transistor T2, resulting in sufficient collector current to switch on relay RL2. The energising of relay RL2 disconnects the coil of relay RL1 from the earth line via contact RL2,3. Thus as contact RL1,2 is also returned to the closed position by this process, transistor T2 is switched off.

As in the operation of these relays (i.e. post office relays) the "break contacts" are opened before the "make contacts" are closed, this cycle of operations would also result in the switching off of relay RL2. However the condenser C2 placed across the coil of relay RL1 ensures a slight delay in the switching off

FIG 3

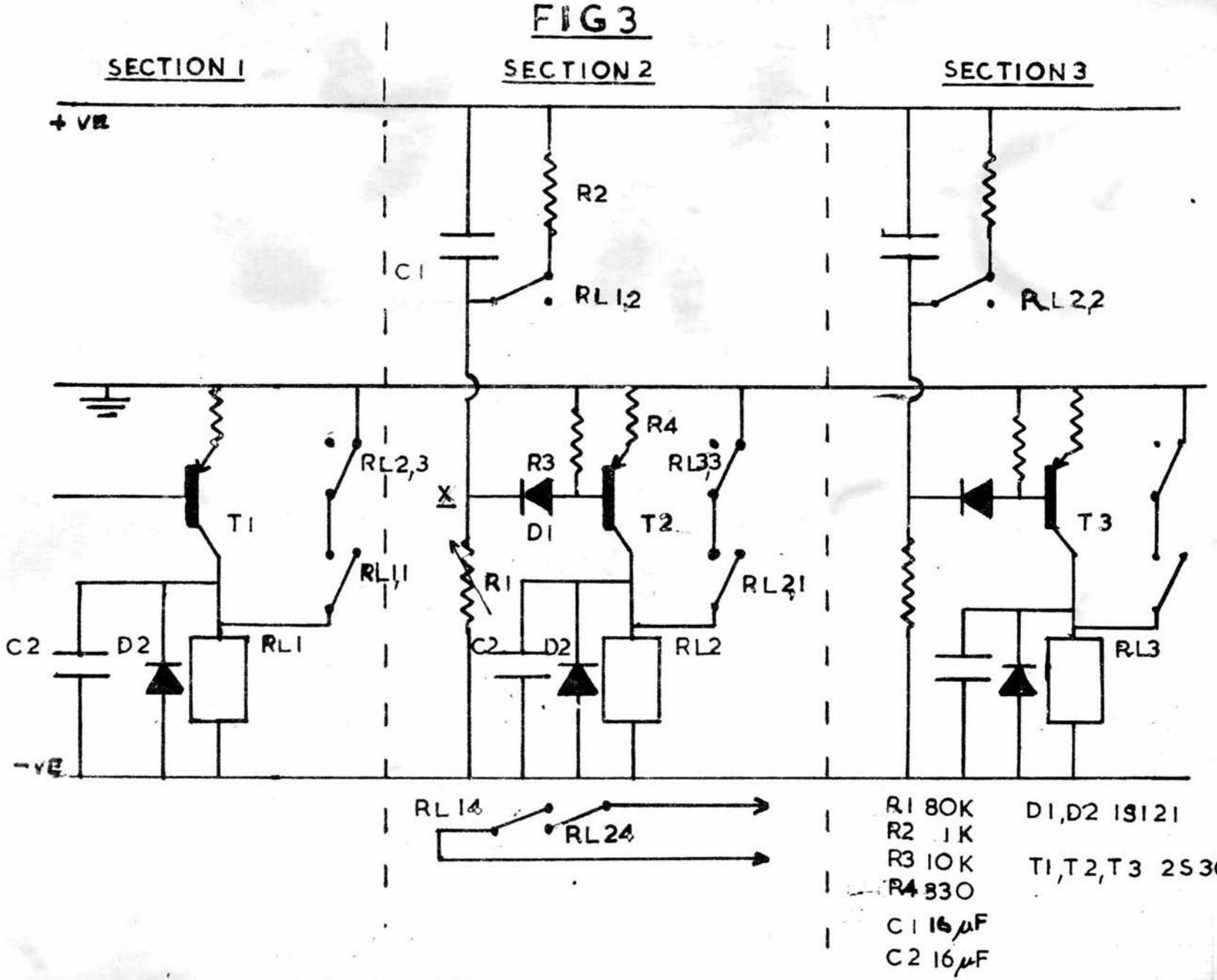
SECTION 1
SECTION 2
SECTION 3
+ VE
R2
C1
RL1,2
RL2,2
R4
RL2,3
R3
RL3,3
X
T1
D1
T2
T3
RL1,1
R1
RL2,1
C2
D2
RL1
C2
D2
RL2
RL3
-VE
RL14
RL24
R1 80K
R2 1K
R3 10K
R4 330
C1 16μF
C2 16μF
D1,D2 IS121
T1,T2,T3 2S301

process of this relay. Thus the make contact RL2,1 has sufficient time to close properly before transistor T2 is turned off. A diode D2, connected in parallel with the coil of relay RL1, limits the negative voltage pulse induced when contact RL2,3 is broken. (Limiting this pulse is necessary to avoid transistor failure).

The diode D1 in section 2, connected between point x and the base of the transistor T2, stops any communication of the large positive voltage in the off state of this section, the base being held close to earth potential by resistance R3. The self-biasing resistance R4 ensures that no large current can be drawn through the transistor until the point x is well negative.

The operation of this cycle turns on relay RL1 for a length of time depending on the values of R1 and C1. This same cycle is repeated for the relay RL2, the period for which this relay remains energised depending on the time constant of section 3. This type of circuit will operate with time constants between about 0.1 to 5 secs, the limiting factor being the value of R1. The size of this resistance cannot be increased indefinitely as the current gain in the transistor would not be sufficient to operate the relay with any degree of reliability. The maximum value of R1 with these transistors was of the order of 100 KΩ. Increases in the time constant could be achieved by a larger condenser, but the volume occupied by this component imposes its own limitations.

Timing calibration of this circuit was achieved through the two relay contacts RL1,4, RL2,4 connected in series to the

appropriate socket of an Isotope Development Scalar Type 500/A, driven by a pulse generator at a known frequency (1000 kc/s). Thus the scalar will count only when both relay contacts are in the closed position, i.e. the time between the switching on of relays RL1 and RL2.

Complete Control Circuit

When the power supplies are initially switched on to the circuit (Fig. 4) none of the relays are energised. Before the cycle can be started, relay RLI must be switched on, either by the completion of the previous cycle or, as in the case of the first cycle, by the momentary closure of the spring loaded toggle switch SW2. A neon indicator lamp (L1) is illuminated when this relay is energised (contact I6).

The cycle is started by the push button P1 which switches on relay RLQ (section Q). As the switch SW3b is closed for push button operation, the -60 volt line is connected to the 8K resistor of section A, when contact Q3 is closed. (The other functions of section Q will be referred to later). Transistor TA is thus turned on causing relay RLA to operate. Thus relay RLI is switched off (contact A5) and the charging of the timing condensers in sections B and C started (contacts A2 and A3). Both the time constants of the sections are variable but they are connected in such a way that relay RLB cannot operate after relay RLC has been energised. When relay RLC is switched on relay RLA is switched off (contact C1). The relays of sections D and E are switched on and off in sequence, in a similar manner.

FIG 4

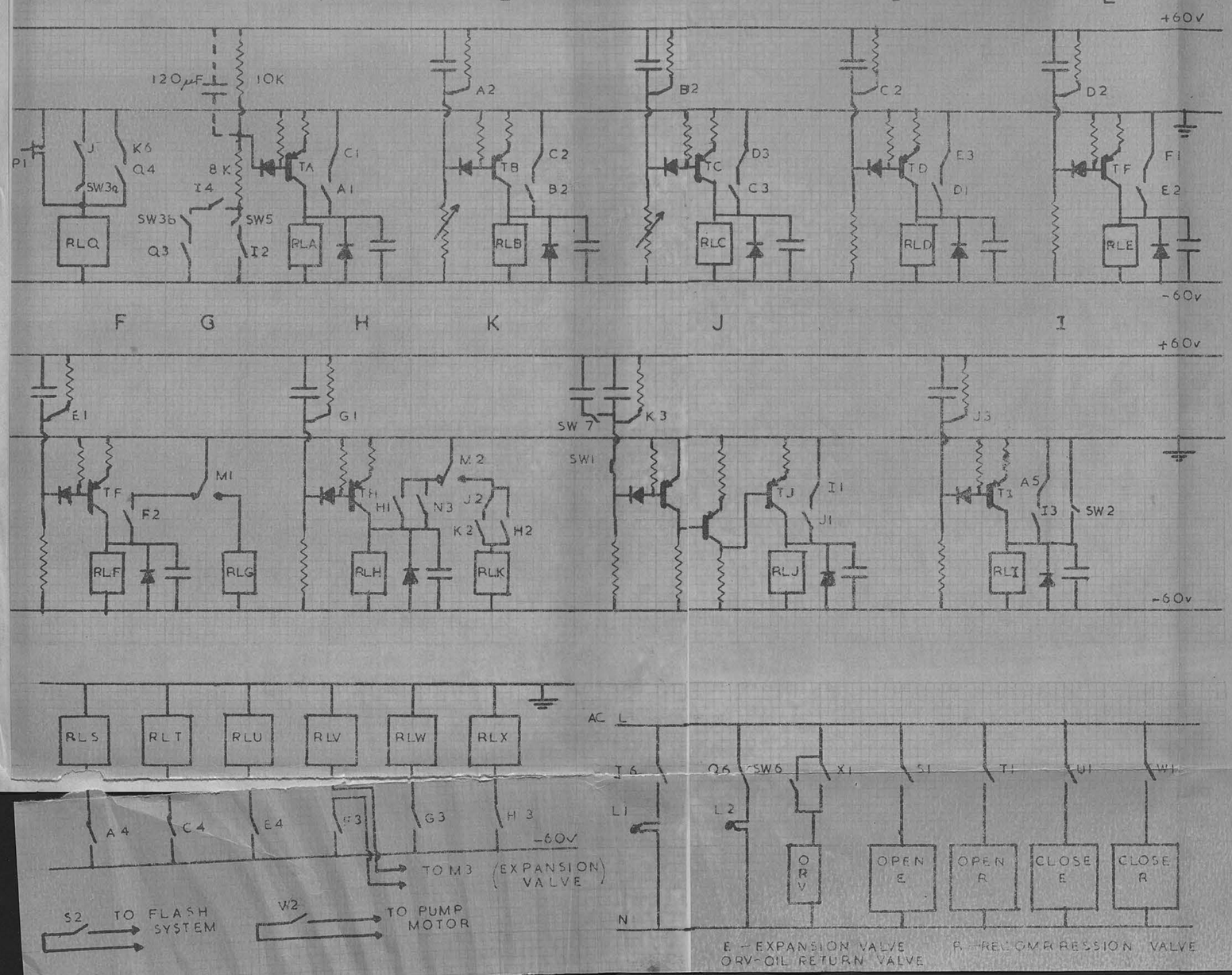
Q
A
B
C
D
E
+60v
120μF
10K
A2
B2
C2
D2
P1
J
K6
Q4
8K
I4
SW3b
SW3a
SW5
I2
Q3
TA
TB
TC
TD
TF
C1
A1
C2
B2
D3
C3
E3
D1
F1
E2
RLQ
RLA
RLB
RLC
RLD
RLE
-60v
F
G
H
K
J
I
+60v
E1
G1
SW 7
K3
J3
SW1
TF
TH
TJ
TI
F2
M1
H1
M2
N3
J2
K2
H2
I1
J1
A5
I3
SW2
RLF
RLG
RLH
RLK
RLJ
RLI
-60v
RLS
RLT
RLU
RLV
RLW
RLX
AC L
T6
L1
N
Q6
SW6
X1
S1
T1
U1
W1
L2
A4
C4
E4
F3
G3
H3
-60V
TO M3 (EXPANSION VALVE)
S2 TO FLASH SYSTEM
W2 TO PUMP MOTOR
ORV
OPEN E
OPEN R
CLOSE E
CLOSE R
E - EXPANSION VALVE
R - RECOMPRESSION VALVE
ORV - OIL RETURN VALVE

Relay RLF, energised a short time after the operation of relay RLE, is only switched off when the contacts of the microswitch M1 are transferred from their normal position.

When the contacts M1 are held over, relay RLG is energised but is again switched off by the action of the relay in section H. Relay RLH remains switched on until the contacts of a second microswitch M2 are opened, thus energising relay RLK. The time constant of section J, which determines the period for which relay RLK remains switched on, is of the order of minutes. Finally relay RLI is switched on by the operation of the relay RLJ, the circuit being returned to its original starting state.

Operation and Functions of the Bank of Large Relays

1) Relay RLS, switched on by the action of relay RLA operates the opening of the expansion valve by applying 250 volts A.C. to the solenoid of the opening mechanism (contact S1). This relay also controls the connection of three banks of charged condensers to the flash tubes on the cloud chamber.

2) Relay RLT, which operates the opening of the recompression valve, is switched on by relay RLC at a time after the opening of the expansion valve determined by the time constant of section C.

3) Relay RLU actuates the closing of the expansion valve in a similar manner.

4) Relay RLV controls the start of the pump motor by the action of relay RLF. When the float in the oil reservoir of the pump reaches the lower level, the contact of the microswitch M1 is

broken, thus turning off these two relays and stopping the pump motor. The coil of relay RLV is attached through another microswitch M3 to the negative line. This microswitch is only closed when the expansion valve is closed. Thus the pump motor can only be operated by the control circuit under this condition.

5) Relay RLW is energised when the relay RLG is switched on and thus facilitates the closing of the recompression valve.

6) Relay RLX is switched on by relay RLH and operates the return of the oil from the pump cylinder to the reservoir by opening the pump return valve. When the float reaches the upper level the contacts of microswitch M2 are opened, thus switching off relays RLH and RLV which in turn closes the oil return valve. A switch SW6, wired in parallel with contact V1, allows manual return of the oil to the reservoir.

Clearing Field Circuit

The high voltage for the clearing field of the cloud chamber is supplied by the circuit shown (Fig. 5). The secondary windings of the transformer supply 2,500 volts A.C. which is rectified by an arrangement of diodes, capacitances and resistors. The resistances R2 lead the positive and negative lines to earth. The variable contact on this resistance allows a continuous range of voltages to be obtained, the value of which can be read on a voltmeter. This voltage, communicated to the cloud chamber via the resistance R3 and relay contact Q1 and Q2, is switched off when relay RLQ is energised. A neon indicator lamp L2 is illuminated when this relay is not energised.

At the start of the cycle the clearing field is removed

FIG 5

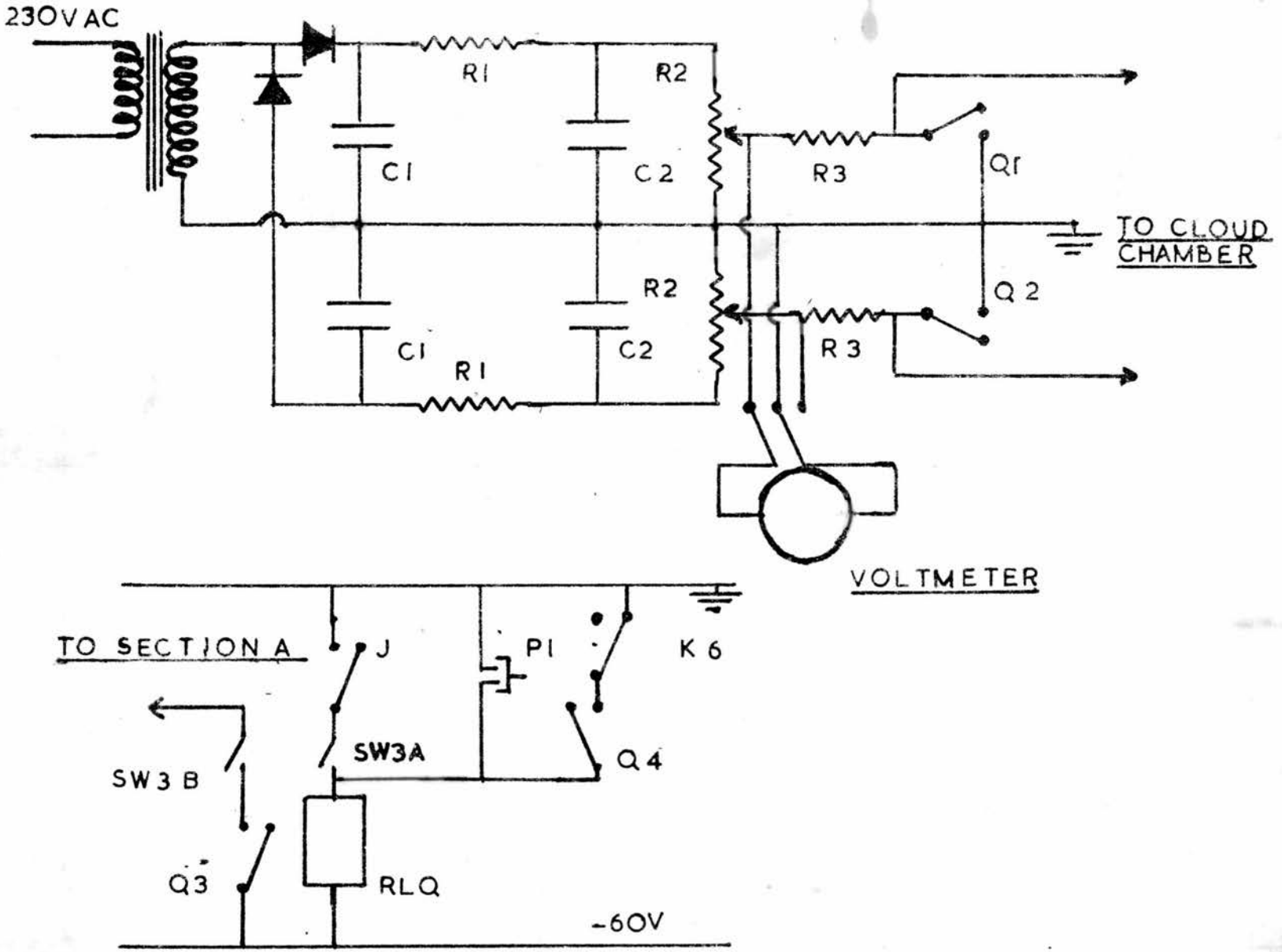
230V AC
R1
R2
C1
C2
R3
Q1
TO CLOUD CHAMBER
R2
C1
C2
R1
R3
Q2
VOLTMETER
TO SECTION A
J
P1
K6
SW3A
Q4
SW3B
Q3
RLQ
-60V

from the cloud chamber when relay RLQ is switched on. When relay RLK is energised, contact K6, between the coil of relay RLQ and earth, is broken, thus restoring the clearing field to the cloud chamber (Fig. 4).

When in continuous operation switches SW3a and SW5 are closed, SW3b is open. Thus the clearing field is switched off by the operation of relay RLJ, the period between the start of the expansion (i.e. when relay RLI is energised) and the switching off of the clearing field being determined by the time constant of section I. This time is variable between 0.1 and 3 seconds .

Operation of Section J

As the time constant required for the waiting period (Section J) was of the order of minutes, the simple circuit (Fig. 3) was not satisfactory. However, as it was intended to use the same principle of a condenser charging through a resistance for a timing device, a stage of current amplification was preferable if a very large capacitance was to be avoided.

When the contact K3 is opened (Fig. 6) the condenser C1 charges through resistance R1, conduction in the transistor T1 taking place, when the potential of the point X is sufficiently negative. The current flowing in the resistor R2 causes the potential of point Y to fall. As transistor T2 is normally conducting, this fall in potential at Y causes this transistor to be almost switched off. The resulting rise in the potential of Z then allows transistor T3 to conduct, the current gain in the proceding stages being sufficient to energise relay RLJ.

FIG 6

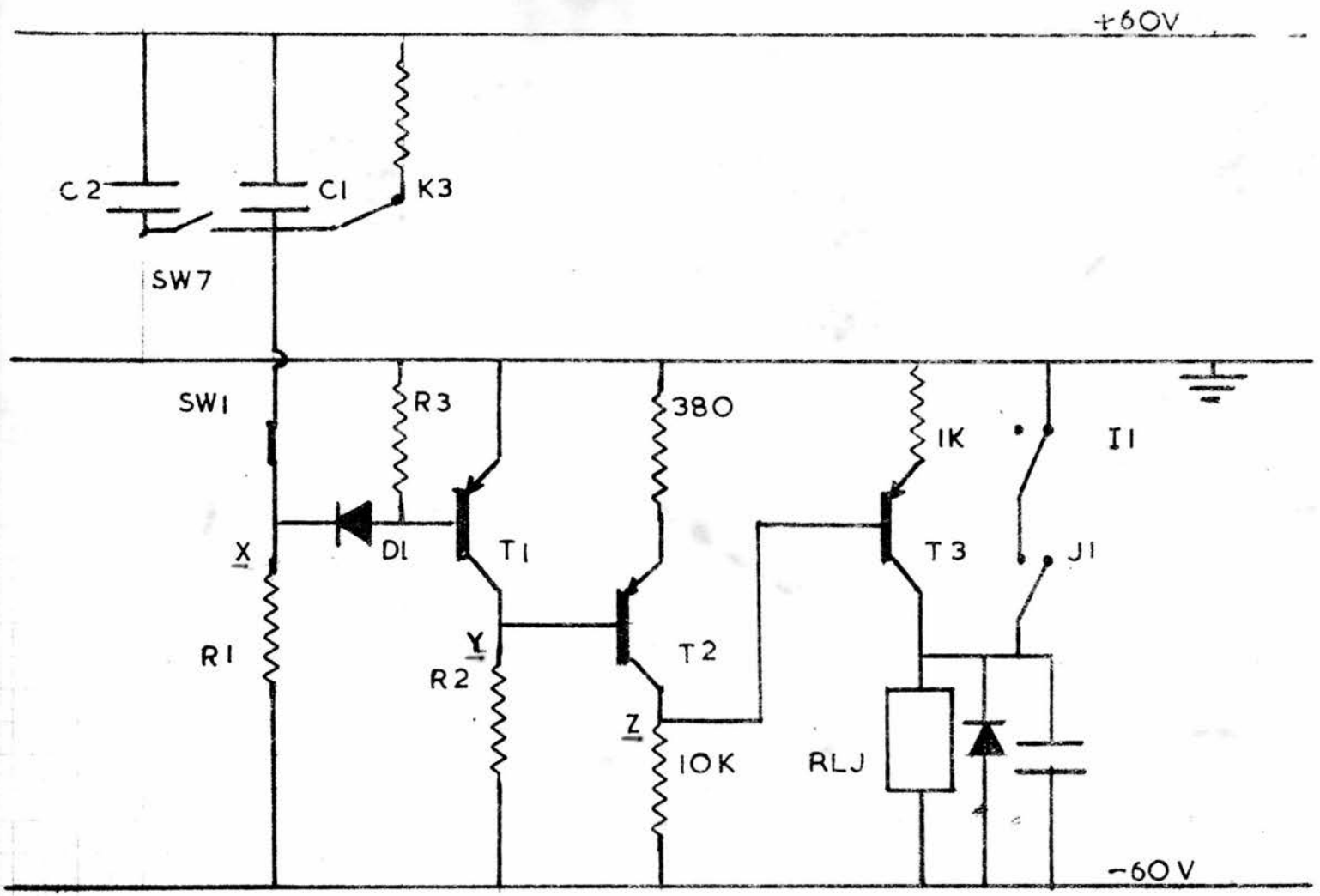

R1 4M
R2 100K
R3 1 7 M

C1 16 μF
C2 32 μF
D1 IS121

T1 2S301, GAIN 40
T2 T3 2S301

The length of the waiting period can be changed by closing switch SW7 which brings capacitance C2 in parallel with C1, resulting in a time constant three times as long.

The waiting period can be eliminated, as is required in certain test conditions, by opening the contacts of switch SW1.

Operation of the Flash Tubes

The flash tubes which illuminate the chamber are connected by the closing of the points of relay RLS, to a bank of condensers (99μF each), charged to 2000 volts by a system constructed by Donald[1]. In order to initiate the discharge in the flash tubes a high voltage pulse is supplied from the secondary winding of a car ignition coil.

The 4μF condenser (Fig. 7) is charged through the normally closed contacts of relay RLB, and a resistance and diode from the A.C. line. When relay RLB is energised, the charged condenser is transferred to the primary windings of the ignition coil, the resulting discharge producing a high voltage pulse in the secondary circuit, which is sufficient to trigger the flash tubes.

As relay RLB operates the timing of the flash, no photograph can be taken after the start of the recompression, as this relay will only operate before relay RLC is energised.

Operation of the Camera wind on

As previously mentioned, the length of film wound on after successive photographs was in the first instance 3 frame lengths, the next, one frame length, then alternately 3 and 1 frame lengths.

FIG 7

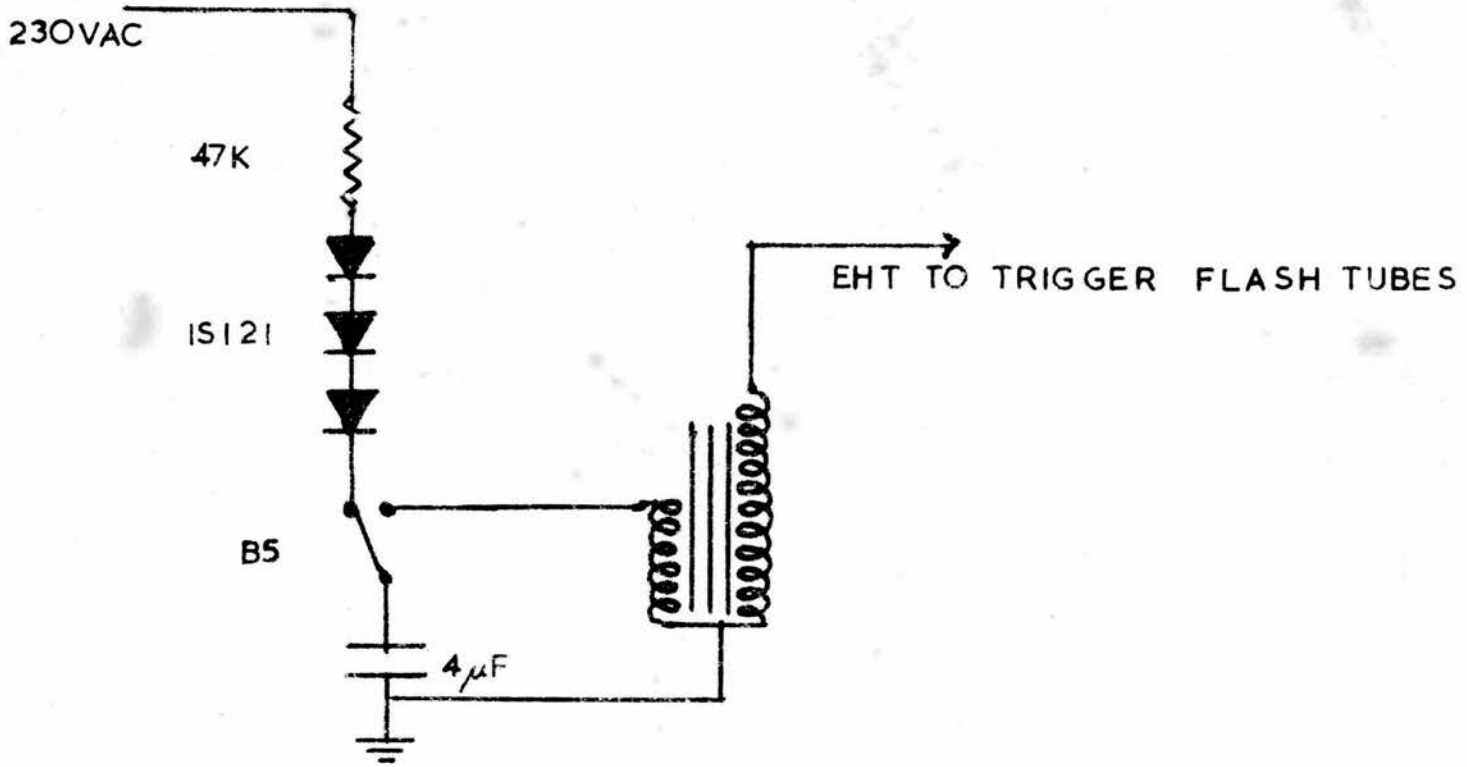

A rotor arm, driven through a reduction gear by an electric motor, winds the film on at the rate of one frame per revolution. This rotor arm strikes one of six vertical prongs attached symmetrically to a horizontal gear wheel which in turn drives the sprocket wheel, over which the film in the camera is fed. (Fig. 2). The rotor is in contact with the prong for only 30° per revolution. The film is thus wound on in short bursts, rather than a continuous process. A twin rise cam, running at one quarter of the rotor speed, operates an electrical contact x in such a manner that opening occurs alternately after three and one rotor revolutions.

The contacts of relay RLP connect the camera motor to a variable A.C. supply. When relay RLE is energised (Fig. 4) in the control cycle, relay RLP is thus switched on (Fig. 8). This relay is kept energised provided the contact x remains closed. When the rotating cam breaks this contact, the relay RLP is switched off and the motor stopped. However the inertia of the system is sufficient to allow the cam to rotate past the open position of x, so that when the next signal arrives from relay RLE, relay RLP can be held on.

The supply voltage to the motor is adjusted so that about half a revolution of free wheel occurs after the power is switched off. This is sufficient to allow rotation of the cam past the open position of x, but not enough to wind the film on one frame too many.

FIG 8

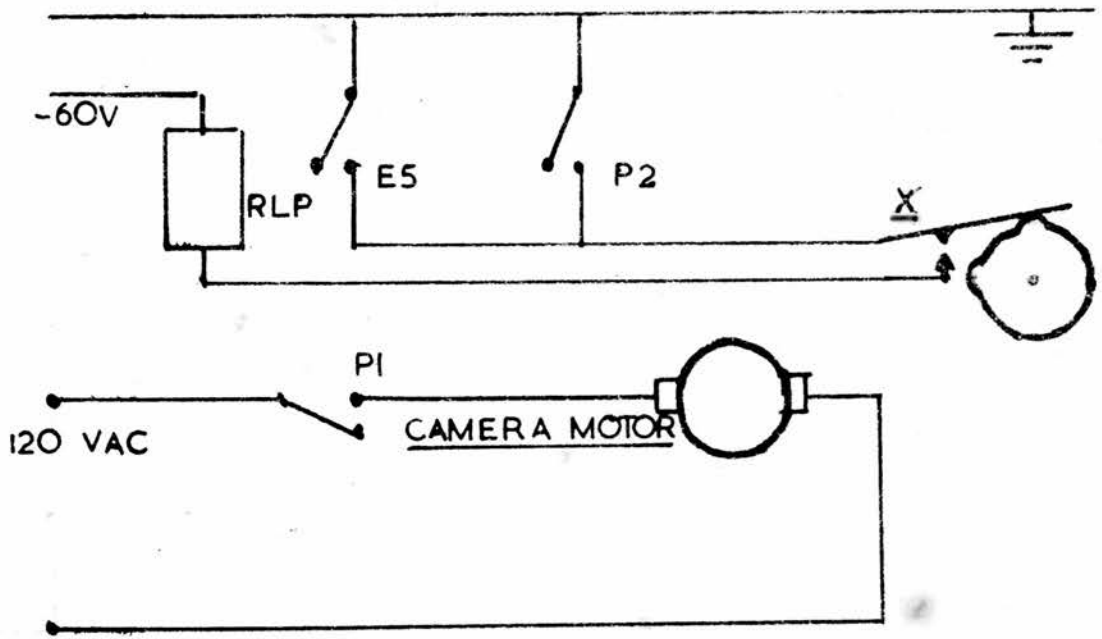

CAM ROTATES
1/4 ROTOR SPEED

Safety System

If the relays which switch current to the solenoids which operate the valves are left energised for more than 8 seconds, the safety system operates.

One set of normally closed contacts from each of these relays (i.e. RLS, RLT, RLU, RLW) are connected in series (Fig. 9). The operation of this circuit is similar to that of Fig. 3, with one stage of current amplification included, due to the relatively long time constant. Thus if any one of these relays remains energised for more than 8 seconds, due to some fault in the system, relay RLN is switched on and remains held on by contacts N1. Relay RLN actuates the larger relay RLZ which, when energised, removes all the power supply lines from the control system except those to relays RLH and RLX.

In Fig. 4 the contact N3 operates the relay RLH, thus activating relay RLX. Thus if the pumping cycle had been in operation when the safety system was triggered, then the oil would be returned to the reservoir by the operation of relay RLX. When the float makes contact with the upper microswitch M2, relays RLH and RLX are switched off.

Relay RLN can also be switched on by the dial gauge contacts DG1 and DG2 if excess pressures are recorded. This could result from either a leaking valve or a failure of the system.

Power Supply

An Admiralty rectifier unit (W3995) supplies 120 volts D.C. at a maximum current of 2.5 amps. Both the lines are led into a

FIG9

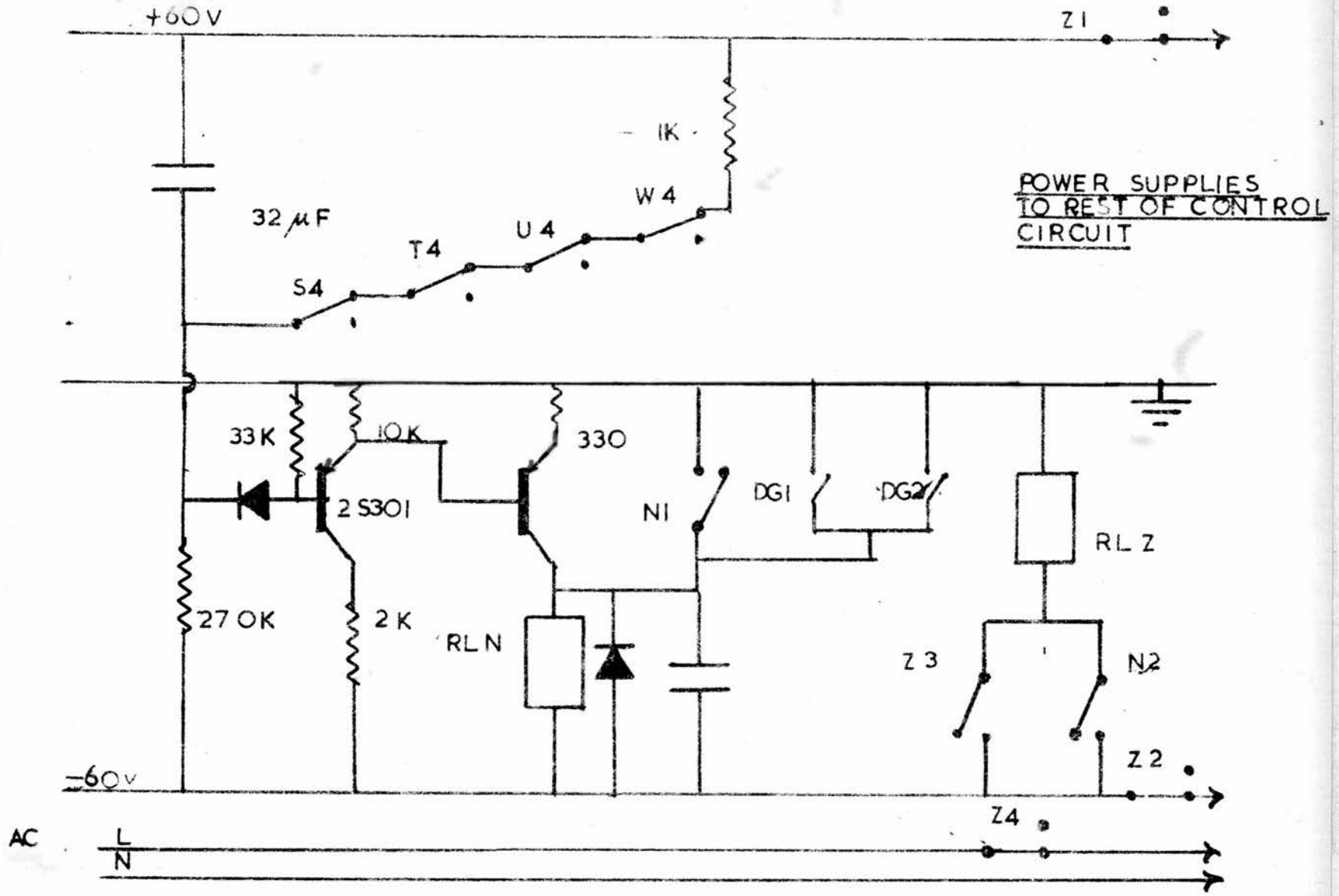
+60V
Z1
1K
W4
32 μF
U4
T4
S4
POWER SUPPLIES
TO REST OF CONTROL
CIRCUIT
33K
10K
330
2S301
N1
DG1
DG2
RL Z
27 OK
2K
RL N
Z3
N2
Z2
-60V
Z4
AC
L
N

FIG 10

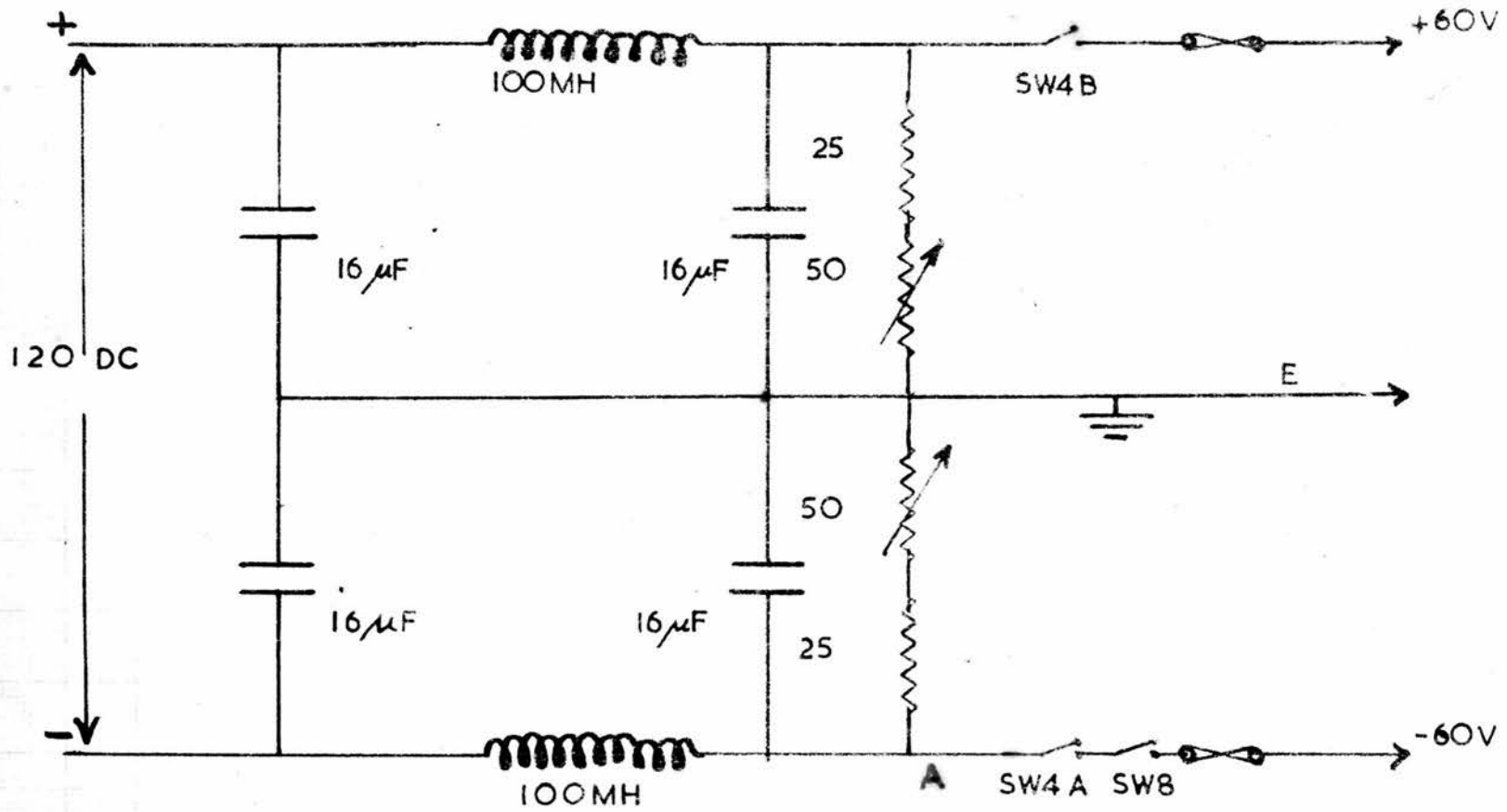
+
100MH
+60V
SW4B
25
16 μF
16 μF
50
120 DC
E
50
16 μF
16 μF
25
-
100MH
A
SW4A SW8
-60V

smoothing circuit (Fig. 10) and then to earth through a 75Ω variable resistor. The approximate current through this resistor is 1 amp. Current variations from 30 ma to 150 ma are recorded on the negative line, whereas the positive bias line remains at about 30 ma during the control cycle. Thus the voltage of the point A varies by about 10 per cent depending on the different loads.

As it is important that the positive line is switched on first, a double switch SW4 ensures that the negative line cannot be connected without the positive line. If the negative line only was switched on, all the relays would switch on simultaneously.

Section 4. Cloud Chamber Operation

Introduction

An attempt to reduce the recycling time of a high pressure cloud chamber using fast recompression techniques was made by varying both the expansion and recompression processes. A minimum recycling time of two minutes was obtained when using gases (argon and nitrogen) at approximately 50 atmospheres pressure. A qualitative understanding of the processes which initiate background cloud in the chamber was also achieved through this investigation.

Expansion and Recompression processes

When the gas in a cloud chamber is cooled by a fixed amount (depending on the physical properties of the gas and condensant), condensation takes place on ions. (The condensant used in all experiments was ethyl alcohol). This cooling is obtained

by a pressure reduction of the chamber gas (section 2), the ratio of the initial to final pressures being termed the expansion ratio. The time is short compared with the time necessary for heat to be conducted into the chamber from the walls[3] for a high pressure chamber, provided the initial expansion of the gas is sufficiently fast. However shortly after drops grow to a visible size, the thermal effects of both condensation and their motion due to gravity produce local heating in the chamber. The resulting gas motion from convection and conduction takes an appreciable time to settle down after an expansion ($\sim$15 minutes). However when fast recompression of the chamber gas is used, the drops are re-evaporated in the position in which they were formed, thus minimising both sources of thermal disturbance and reducing the recycling time considerably.

In Fig. 11 the pressure P_1 is that of the chamber gas before an expansion. In order to produce condensation on ions, a sufficient temperature reduction is produced by lowering the pressure adiabatically to P_2. If the expansion is initially started at zero time, t_1 is the time when the pressure reduces to P_2. At a time t_2 drops are visible and recompression can be started. The gas reaches its initial pressure P_1 at time t_3 on completion of recompression. If the time taken by the expansion and recompression processes could be reduced, thermal disturbance of the chamber gas would also be expected to be diminished, resulting in a shorter recycling time.

FIG II

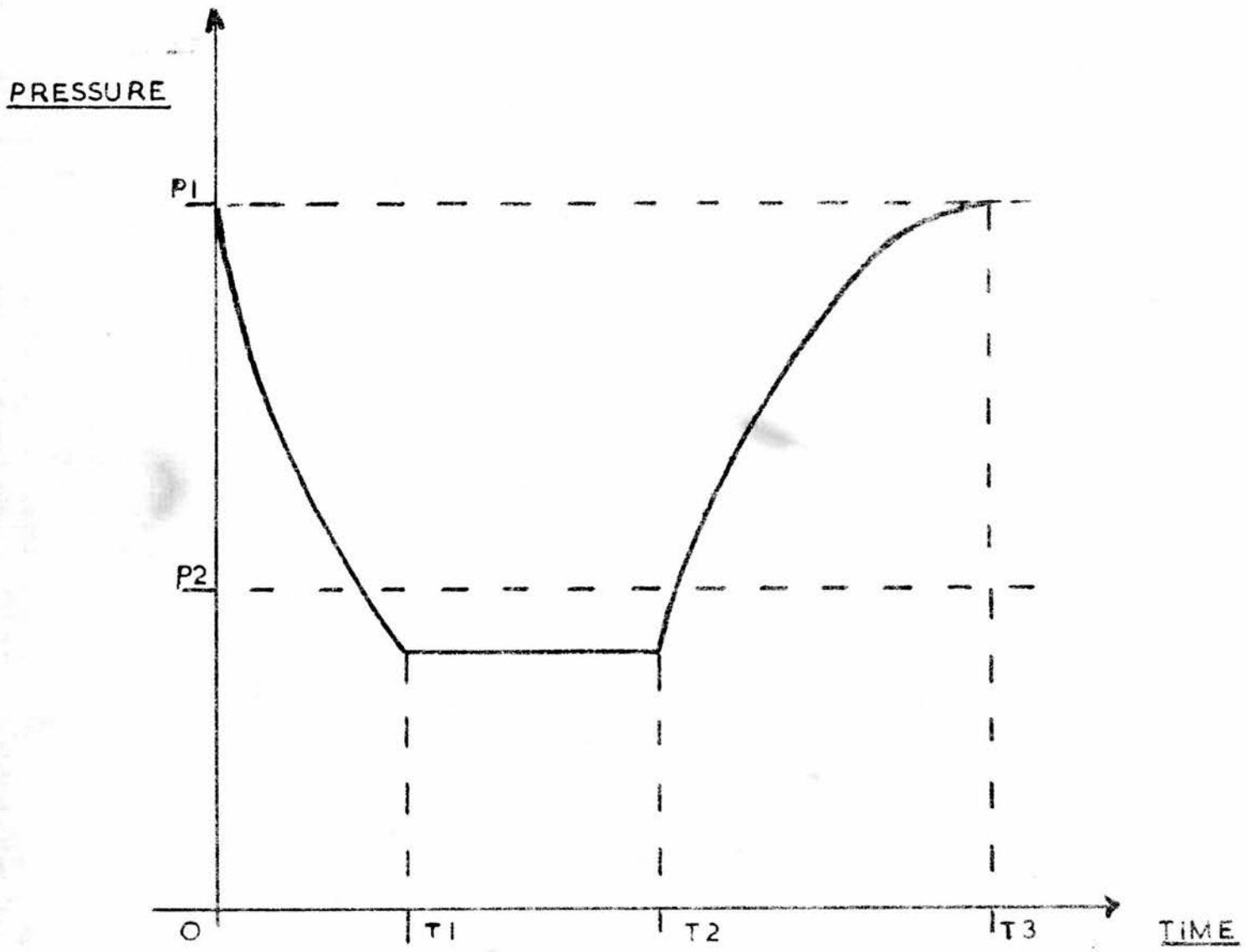

The Valves Controlling the Expansion and Recompression Speeds

Originally the high pressure cloud chamber[1] was fitted with valves which had opening apertures of 0.5 inches. Operation when using fast recompression was satisfactory with a recycling time of 2 minutes. As a delay of 0.4 seconds between the start of the expansion and recompression was sufficient to eliminate visible condensation with the original valves, the introduction of larger valves was expected to improve operation with respect to recycling time.

Larger valves were constructed[2] having apertures of 1 inch and twice the opening speed, producing an effective increasing in the valve aperture of a factor of eight.

However when the chamber was operated with these larger valves, a marked deterioration in its performance was noted. With a two minute recycling period, a steady increase in background cloud (which had been absent with the smaller valves) on successive expansions was sufficient to almost obscure particle tracks on the tenth of a series of expansions. Before the chamber could be operated again, cleaning expansions followed by a wait of 15 minutes was necessary. Only when operated with a 15 minute recycling period were tracks observed successfully on subsequent expansions without the need of cleaning expansions.

Experiments with a Floating Diaphragm

All the previously mentioned expansions had been performed with a "fixed diaghragm technique" in which it was initially held against the front brass plate. Another method of operating a cloud chamber of this type was a "float diaphragm technique".

In this method, the diaphragm was held just off the front brass plate (Fig. 1), it being maintained in a position of zero pressure difference across the front and rear of the chamber.

Although more difficult to operate with fast recompression, a successful method was developed. Instead of allowing the piston (Fig. 1) in the expansion cylinder to return to an arbitrary position P1, the end of the expansion cylinder was used as a stop. Thus, provided the temperature of the gases in the various parts of the chamber remained constant, the diaphragm would always be reset in its original position at the appropriate part of the cycle. When using this technique, it was important to run at a fixed recycling speed, as any small temperature variations resulting from an irregular cycle would alter the diaphragm position.

When the chamber was operated with the larger valves with a floating diaphragm, a large number of successful expansions were performed in which background cloud did not occur. A minimum recycling time of $\sim$ 3.5 minutes was obtained with a nitrogen filling, in which track distortion rather than background cloud proved the limiting factor.

Thus the source of background cloud was eliminated by using a floating diaphragm technique, an observation noted by others[4].

Variation of the Speed of Expansion

A series of experiments were performed to investigate the possibility of eliminating this build up of background cloud by altering the expansion speed, when a fixed diaphragm technique was used.

When the aperture of the outlet pipe between the expansion valve and pump cylinder was reduced, in order to slow down the rate of the expansion, a slight improvement in the rate at which background cloud increased on successive expansions was observed.

As operation with a floating diaphragm had indicated that the source of background cloud appeared to arise from the initial part of the expansion (i.e. when the diaphragm separated from the brass plate) a compound valve was constructed (Fig. 12) which consisted of the larger and smaller valves connected in parallel, to facilitate expansions in which the initial separation of the diaphragm from the brass plate was slow, the remainder being as fast as in the floating diaphragm case. A modification of the control circuit constructed by Donald[1] was made to achieve this compound expansion. The speed of the recompression remained unchanged, as the gas returned mostly through the larger valve.

Again a general improvement of the performance was noted, but the recycling time could never be reduced to the two minutes originally achieved with the small valves.

As all these experiments had indicated that an over-expansion (discussed later) took place during the initial part of the expansion, any reduction in the restriction imposed on the gas flow by the first brass plate (Fig. 1) would improve the performance. The holes in this plate were enlarged to 0.125 inches from their original diameter of 0.063 inches.

FIG 12

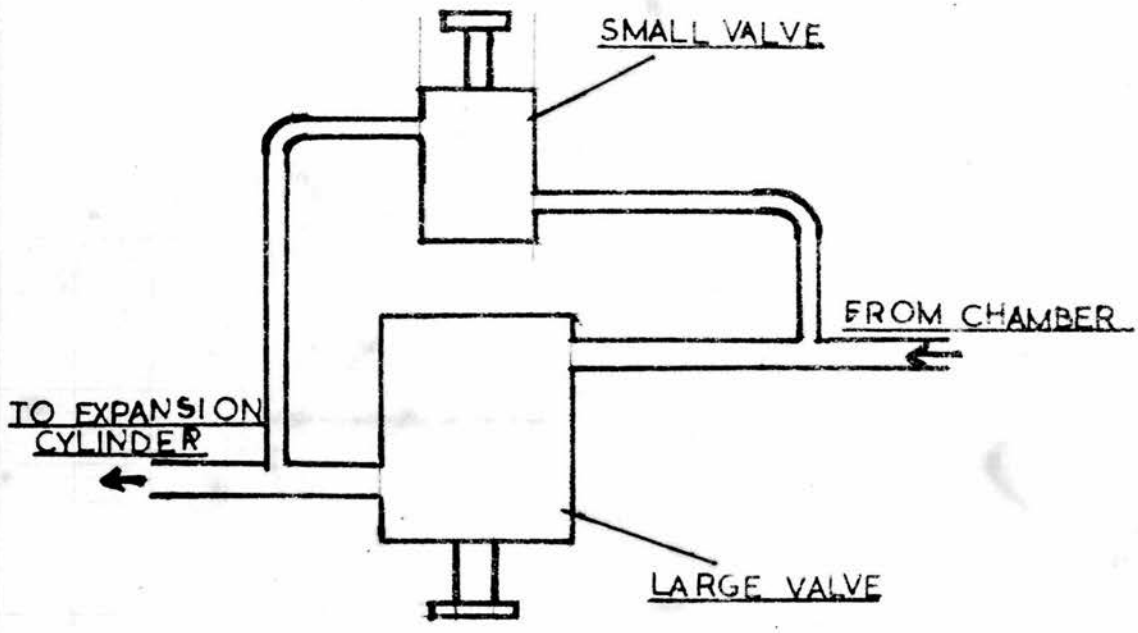
SMALL VALVE
FROM CHAMBER
TO EXPANSION CYLINDER
LARGE VALVE

The chamber now operated in a perfectly satisfactory manner with a two minute cycle. With fillings of argon and hydrogen little growth in background cloud was experienced in runs of over one hundred cycles. However with nitrogen a tendency to produce background cloud still persisted, although by no means obscuring the tracks. For comparison Figs. 13 and 14 are photographs of the first and one hundredth expansions respectively, of a run with a filling of argon. Figs. 15 and 16, and Figs. 17 and 18 are similar to the above, but with fillings of nitrogen and hydrogen respectively. In all these photographs the source of particles was cosmic rays.

Degree of Supersaturation of the Condensant

When the vapour pressure of the condensant was the maximum at a given temperature, the cloud chamber was saturated or "wet". This could easily be observed by a pool of alcohol lying at the foot of the chamber and the generally wet appearance of the various components.

On the other hand chamber operation was still possible, although at an increased expansion ratio, when the vapour pressure was not 100 % at the initial temperature. This condition of operation is termed "dry".

It was found that when using the chamber with a fixed diaphragm (after the holes in the front brass plate had been enlarged) that a "wet" chamber gave the most satisfactory results. No change in the expansion ratio occurred from day to day and little trouble resulted in prolonged runs.

However when operated with a floating diaphragm technique,

FIG 13

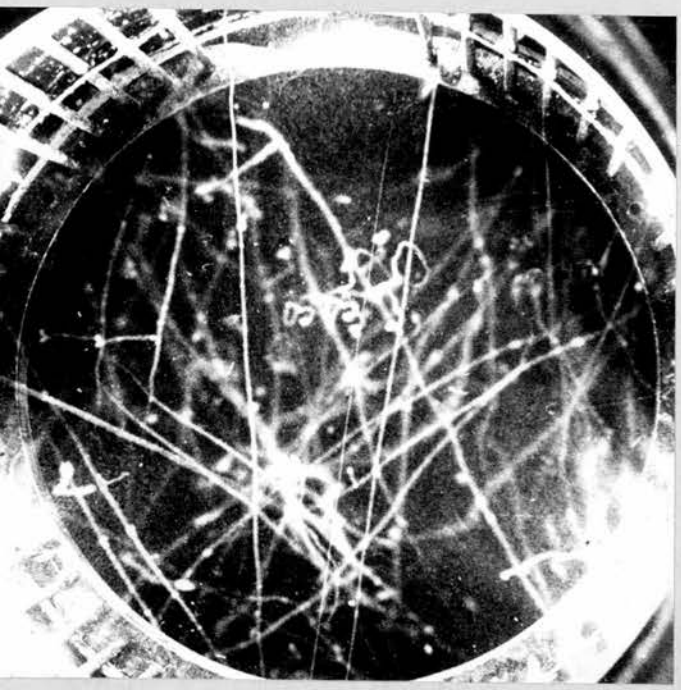

FIG 14

FIG 15

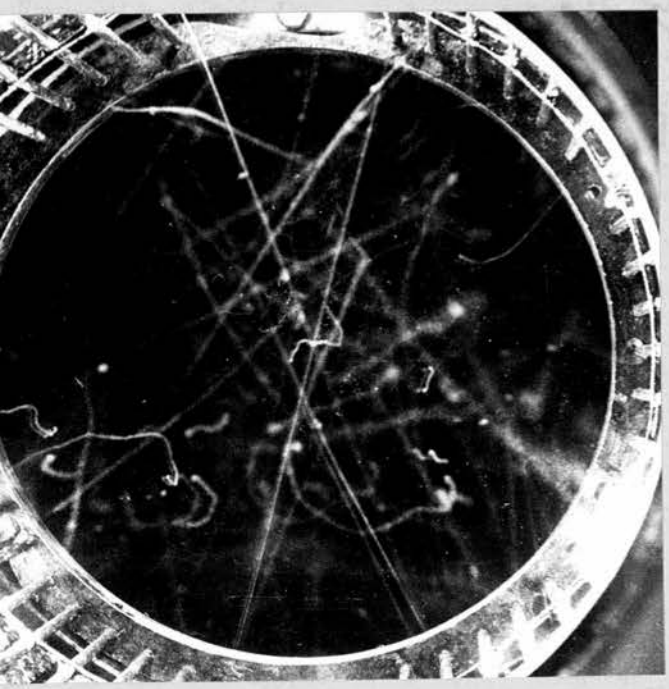

FIG 16

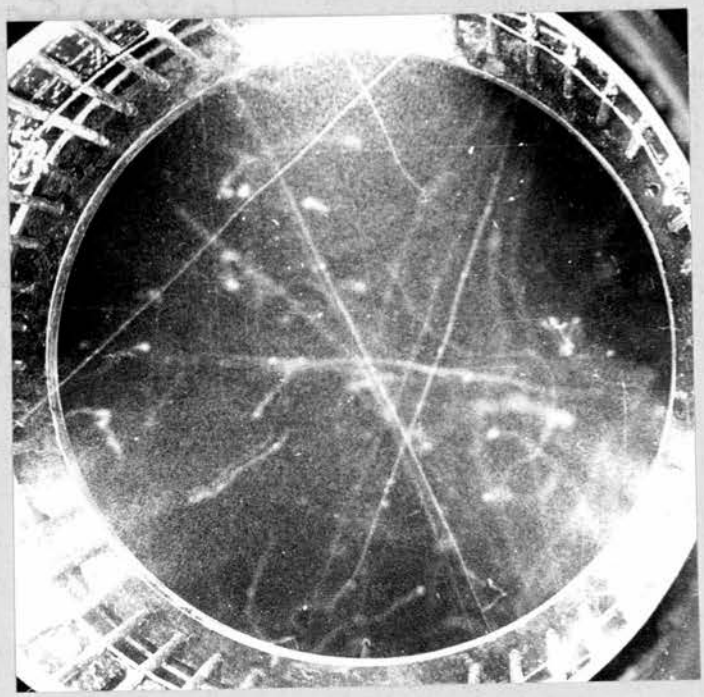

FIG 17

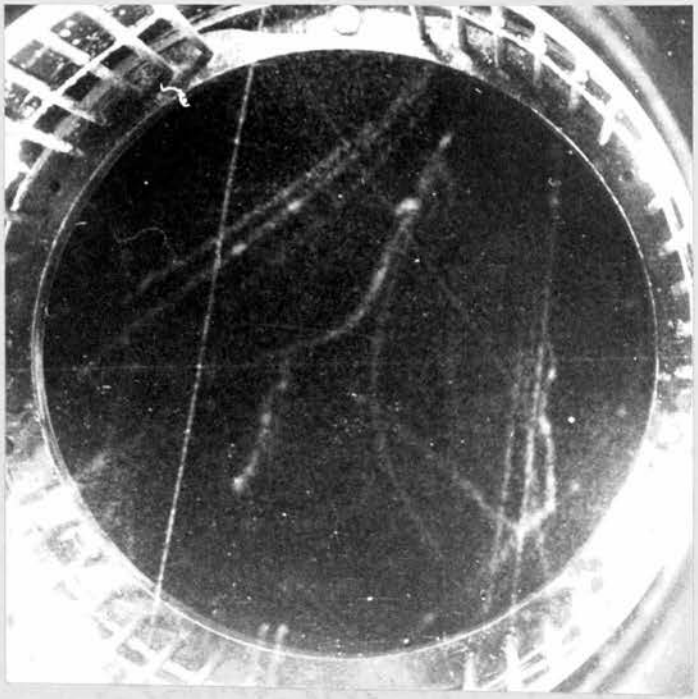

FIG 18

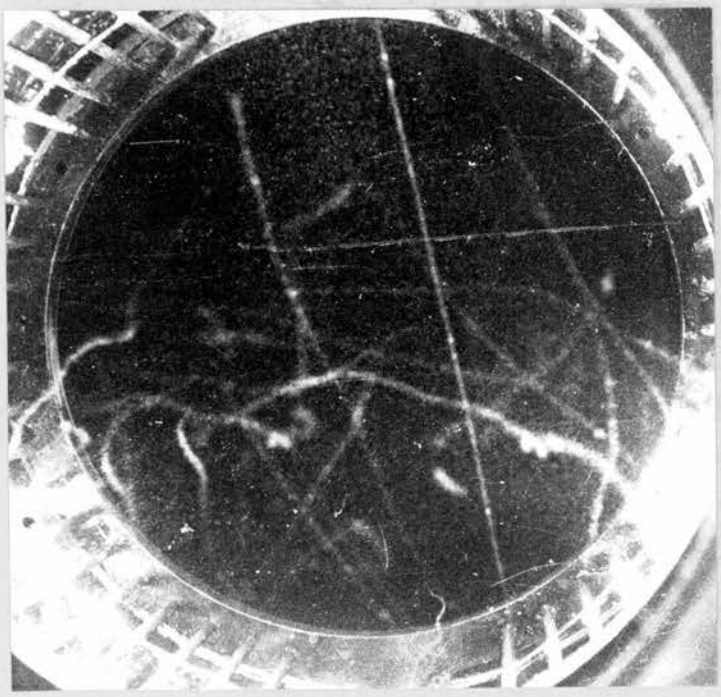

a "dry" chamber gave better performance. In this case the expansion ratio is not quite so critical and small variation in the diaphragm setting position did not produce over expansions so easily as in the case of a "wet" chamber.

However as the condensant gradually permeated the seals and diaphragm after prolonged use, the degree of supersaturation changed and thus altered the working expansion ratio. This process could be slowed down by injecting alcohol into the rear of the chamber, but nevertheless, a constant watch on the chamber was necessary during long runs, to ensure satisfactory condensation on ions.

Discussion of the Observations

Origin of Background Cloud:

At a certain expansion ratio condensation on ions occurs. A slightly larger expansion ratio produces homogeneous condensation in the form of a dense cloud which disappears on recompression. When an over-expansion has taken place in which homogeneous condensation has occurred, subsequent expansions even at ratios less than that necessary for ionic condensation produce the same dense cloud. Only after several small clearing expansions, in which the condensation centres which produce this homogeneous condensation are removed, and a long period of time (at least 30 minutes), can expansions be made in which this kind of condensation does not occur, provided of course the expansion ratio is sufficiently small not to produce it once again.

These experiments and others[5, 6] have shown that condensation on ions in itself did not produce nuclei which form condensation centres in following expansions. Otherwise operation of a cloud chamber without slow clean expansions would be impossible. The background cloud observed in these experiments resembled that produced by homogeneous condensation. Thus one may assume that when background cloud of this type occurred an over-expansion must have taken place, in some region of the chamber in the previous expansion to account for the existence of the necessary condensation nuclei.

Possible Explanation of the Source of Background Cloud

A section of the chamber (Fig. 19) shows the front brass plate and diaphragm during the course of an expansion. Gas will pass through the holes in the plate by virtue of the pressure difference $P_1 - P_3$ acting across it. The pressure of the gas P_2 inside each hole will be less than P_1 and P_3, the reduction being a function of the velocity of the gas traversing the hole. At the start of an expansion the greatest acceleration of the diaphragm will occur, as the pressure difference $P_3 - P_4$ will be largest and the resistance to motion offered by the stretching of the diaphragm least. Thus the velocity of gas through the holes will reach a maximum very shortly after the start of the expansion.

If at any instant the ratio P_1/P_2 is greater than that necessary for homogeneous condensation, an over-expansion occurs producing nuclei which will act as condensation centres. As

FIG 19

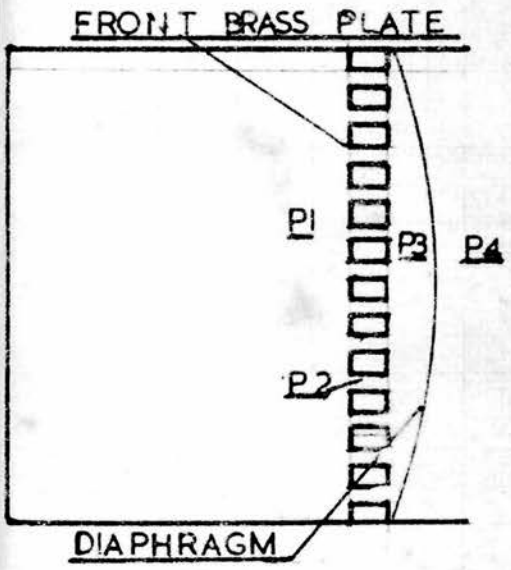

the nuclei will be transferred to the portion of the chamber behind the first plate in this expansion, no sign of an over-expansion will be seen. (This portion was not visible). After recompression, these nuclei will be returned to the working volume and act as condensation centres on following expansions.

In a chamber specially constructed by Watson[6] so that this region between the diaphragm and front plate could be viewed, an over-expansion has been observed in this portion at a nominal expansion ratio theoretically less than that necessary for ionic condensation, after a certain rate of expansion speed had been exceeded. No condensation was observed in the region in front of the brass plate.

Discussion of the different chamber operation techniques

The different modes of operation were:-

(a)	fixed diaphragm	small valves	0.063 inch diameter holes in front brass plate.
(b)	fixed diaphragm	large valves	
(c)	floating diaphragm	large valves	
(d)	fixed diaphragm	compound expansion valve	
(e)	fixed diaphragm	large valves	0.125 inch diameter holes in front brass plate.
(f)	floating diaphragm	large valves	

When used with a fixed diaphragm technique, satisfactory operation was obtained in cases (a) and (e). The ratio A_1/A_2 was the ratio of the area of the restrictions to gas flow imposed by the rear brass plate, expansion valve and piping, added in series, to the area of the holes in the front brass plate.

For (a) $A_1/A_2 = {}^1/12$

(e) $A_1/A_2 = {}^1/20$.

In case (a) the velocity of the gas flowing through the expansion valve would be less than in (e) as the port area is smaller. Thus, if the velocity of the gas through the holes in the front brass plate is controlled by the ratio A_1/A_2 and the velocity of the gas through the expansion valve, then (a) and (e) would be expected to give much the same condition as the smaller ratio of (a) would be compensated by a lower gas velocity through the valve.

The ratio $A_1/A_2 = {}^1/5$ for case (b) and would by the above argument be expected to yield much larger gas velocities through the holes in the plate. In (c) this ratio is the same as that of (b) but as has been noted satisfactory operation was possible for case (c). Initially (c), the diaphragm was slightly pre-stretched in the floating position, thus offering some resistance to motion when subjected to a pressure difference, whereas in (b) this condition does not occur initially, the motion of the diaphragm being controlled completely by the pressure difference. It could be argued that only during the initial part of the expansion (i.e. when the diaphragm was in a position between the front plate and the starting position of (c) that gas velocities were large enough to cause an over-expansion. After this initial stage much smaller ratio A_1/A_2 could be tolerated.

This supposition was not completely borne out by case (d). The diaphragm was moved very slowly initially. The large valve

was opened only after separation of the diaphragm had occurred. Although a general improvement in operation was observed, the performance was never as satisfactory as case (e). The best results were obtained when a delay of 0.3 seconds between the opening of the large and small valves was used. The relatively long time necessary for the expansion and recompression process could have accounted for the poorer performance caused by lack of thermal equilibrium. In (d) the ratio A_1/A_2 was $^1/50$ initially, but increased to $^1/5$ when the large valve was opened. (The low value of A_1/A_2 was obtained by connecting a small bore pipe between the chamber and valve).

In (f) satisfactory operation was achieved as would be expected. ($A_1/A = {}^1/20$) the performance being slightly better than (e).

The most likely cause of an over-expansion during the course of the expansion would be the initial separation of the diaphragm from the brass plate. If an over-expansion followed by condensation did occur, then the gas flow would be further impeded by the condensation and a larger over-expansion would result. Thus once the condition which causes the initial over-expansion is fulfilled, the effect is liable to be accumulative.

Conclusions

With fixed diaphragm operation

1) For satisfactory operation $A_1/A_2 = {}^1/12$ to $^1/20$ for this chamber.
2. If the ratio $A_1/A_2 = \frac{1}{5}$, background cloud was formed on successive expansions.

3) The most likely source of the over-expansion, which produced the condensation nuclei for background cloud, was the initial separation of the diaphragm from the brass plate.

4) The ratio A_1/A_2 could not be reduced indefinitely before the chamber operation suffered.

Recycling Time

The minimum working recycling time after the larger valves had been fitted and suitable modifications made, was still two minutes, the figure originally achieved by the smaller valves. Although the time in which tracks could be first observed was reduced from 0.4 to less than 0.2 seconds after the start of the expansion no comparable reduction in the recycling time had been gained.

Thus as the time the chamber was actually expanded had been reduced by more than a factor of two, it was concluded that the heating effect of condensation was dominant, thus producing an absolute limit in the recycling time of the chamber. Only by using a gas of larger thermal conductivity could the recycling time be reduced any further.

When the cloud chamber was used with a effective time of 3 seconds (described in Chapter 4) by switching off the clearing field some seconds before the expansion, the increase in ionization resulting from a greater number of tracks, and the effect of very slow gas motion which still persisted after two minutes, tended to increase the working recycling time to ~ 4 minutes. At a recycling time of less than this figure, the

distortion in the chamber, which affects pre-expansion tracks much more than post-expansion tracks, rendered momentum determination of particles by multiple scattering measurements subject to unacceptably large systematic errors.

CHAPTER 3

THE ABSORPTION OF THE μ-MESON BY A NUCLEUS

Section 1. Total Capture Rate

The capture (or absorption) rate of a μ-meson by a complex nucleus was shown by Wheeler[7] to depend on the fourth power of the effective nuclear charge. The law could be expressed simply

$$\lambda = \frac{1}{\tau_o} \frac{Z_{eff}^4}{Z_o^4} \qquad (1)$$

where 1) τ_o was the mean life time of the μ-meson

2) Z_{eff} was the effective nuclear charge

3) Z_o was a constant to be determined experimentally

4) λ was the capture rate.

The effective nuclear charge Z_{eff} occurs in the expression rather than the actual nuclear charge Z because of the finite extent of the nucleus. The relationship between the two quantities was derived by Wheeler[7] where

$$Z_{eff} = Z\left[1 + \left(\frac{Z}{37.2}\right)^{1.54}\right] - \frac{1}{1.54} \qquad (2)$$

The basic reaction concerning the capture of a μ-meson by a nucleus was considered to be of the form[8]

$$\mu^- + P \longrightarrow \mu_o + N \qquad (3)$$

where μ, P, N and μ_o are μ-meson, proton, neutron and a neutral meson more recently thought to be the μ neutrino.

In order to derive certain properties about the charge

exchange process (equation 3) an interaction Hamiltonian was established:

$$H = g\ O_{HL}\ (T_H\ T_L + T_H\ T_L)\ \delta(X_H - X_L) \qquad (4)$$

where 1) The suffixes H and L refer to nucleons (proton or neutron) and leptons (meson or neutrino) respectively.

2) T_H is an operator which converts a proton into a neutron, and T_H the reverse process.

3) T_L is similar to T_H, but refers to the meson conversion into a neutrino.

4) O_{HL} is an operator which is a relativistic invariant combination of the Dirac spin operators for nucleon and meson fields.

5) X_H and X_L refer to the coordinates of nucleons and leptons respectively.

6) g is the coupling constant for the interaction and has dimensions of erg-cm^3.

Using the above interaction Hamiltonian (equation 4) the capture rates, coupling constant and degree of excitation of the final nucleus were evaluated using three different nuclear models.

Although it was accepted that at least in two of the nuclear models, drastic idealizations had been made, the value of the coupling constant g, in all three of the separate calculations, was approximately the same as that for β-decay and μ-meson decay.

The average degree of excitation transferred to the final nucleus differed in the three cases, but was of the order of 10 - 15 Mev, i.e. considerably less than the rest mass of the

μ-meson. This excited nucleus was expected to lose its energy, by either neutron or γ-ray emission rather than by the ejection of a proton, in agreement with experimental evidence.

Later experimental evidence indicated agreement with Wheeler's law (equation 1) for light nuclei, but significant differences in the observed and predicted capture rates occurred for heavier nuclei[9].

Kennedy[11] suggested that the earlier theory[8] was too approximate in certain respects and evaluated the capture rates for two nuclei (Ca^{40} and Pb^{208}, both having closed neutron and proton shells) using a shell model of the nucleus. He suggested that a dependence, not only on the nuclear charge, but also on the number of neutrons, should exist.

In previous calculations, the specific character of the interaction had been neglected and the term O_{HL} was made equal to unity.

The most general interaction Hamiltonian could be expressed:

$$H = g\left(C_S H_S + C_V H_V + C_T H_T + C_A H_A + C_A H_P\right) \qquad (5)$$

where the suffixes S, V, T, A and P refer to scalar, vector, tensor, axial and pseudo-scalar, interactions respectively.

Tolhoek and Luyten[12] evaluated the capture rates for several nuclei, using essentially the same shell model calculation used by Kennedy[11], by means of a simplification of the above Hamiltonian (equation 5). They assumed the kinetic energy of the nucleons to be small compared with their rest masses, an approximation which rendered V interactions indistinguishable from S type and T from A. The P type interactions vanished.

The calculations for nuclei, having between 20 and 28 protons and 20 and 32 neutrons for two different radii of potential well, indicated capture rates which would depend on the form of the interaction. The predicted Z dependence[8] was not generally true, as the capture rate also varied considerably with neutron number, as suggested previously[11]. Although it was not expected that the rather approximate theory could predict the character of the interaction completely, an indication existed, that T or A type predominated when compared with the experimental capture rates[15]. However the possibility of an equal mixing of S or V with T or A could not be eliminated.

A general theory for μ-meson absorption by a complex nucleus was evolved by Primakoff[13], which took into account the limited number of final neutron states available, due to the Pauli exclusion principle.

This theory was further refined by Primakoff[14], by using an effective Hamiltonian developed by Fujii and Primakoff[16]. This Hamiltonian corresponded to the most general Lorentz covariant transition matrix element for the interaction, in which the lepton bare nucleon coupling was V and A. Both the numerical relationship between the induced pseudo-scalar and axial coupling constant (i.e. $g_\mu = 8g_A$)[17] and the hypothesis of conserved vector currents[18] were incorporated in this interaction Hamiltonian.

The calculation of the total μ-meson capture rate involved the use of the closure approximation, in which the individual

transition rateswere summed up over all states of the final nucleus, rather than just those which were energetically allowed. When using this approximation, it was necessary to estimate the average neutrino energy. Primakoff[14] indicated that, as the transition rates to the lowest states predominated, the use of the closure approximation would not produce any large inaccuracies.

The capture rate Λ for a nucleus (A,Z) was expressed:-

$$= Z^4_{eff} (\langle\eta\rangle_a)^2 (272 \text{ sec}^{-1}) R \left(1 - \frac{A - Z}{2A} \partial\right)$$

where

$\langle\eta\rangle_a$ was the estimated average neutrino energy divided by the μ-meson rest mass.

R was a factor which depended on the coupling constants involved in both μ-meson capture and β-decay.

∂ was a nuclear correlation parameter and estimated with a 10 per cent accuracy. $\partial = 3.0$.

Experimental confirmation of Primakoff's theory was demonstrated by Sens[15] who measured the μ-meson capture rates in 29 elements. A plot of the reduced capture rates ($\frac{\Lambda}{Z^4_{eff}}$) versus the corresponding value of $(A - Z)/2A$ gave a straight line, the values of $\partial = 3.15$ and $\langle\eta_a\rangle^2 R(272 \text{ sec}^{-1}) = 1.88$ sec.$^{-1}$ being achieved by a least squares fit.

A further experiment in which the μ-meson capture rates of elements in the region Z = 40 to 70 by Filippas et al.[19] has again confirmed the general predictions of the theory, yielding a value of $\partial = 3.19$.

Although Primakoff[14] and more recently Telegdi[22] have indicated that the value of the quantity $(\langle\eta\rangle_a)^2$ 272 R obtained experimentally was in good agreement with the assumption of a

Universal Fermi interaction (UFI) on which this theory was based, theoretical criticism by Klein and Wolfenstein[20] and Luyten et al.[21], concerning some of the approximations made in the original calculation, suggested that it was difficult to test the validity of the UFI by using the experimental results of μ-meson capture.

Klein and Wolfenstein[20] have established an alternative theory for μ-meson capture which removed some of the approximations made by Primakoff[14]. However the experimental results of Filippas et al.[19] showed better agreement with the earlier theory[14], than that of Klein and Wolfenstein. The value of the coupling constant derived from this later theory[20] was twice that required for the UFI.

Further calculations on the μ-meson capture rate by O^{16} and Ca^{40} have been made by Luyten et al.[21] Several different approaches were tried, but although in fair agreement, yielded a coupling constant which was 0.6 times that required by the UFI.

Neither of these two[20,21] suggested that their calculations were a rejection of the principle of a UFI present in μ-meson absorption, but rather that the value of the coupling constant could not be obtained to any greater accuracy than a factor of two from the total capture rates of μ-mesons by complex nuclei, due to the present theoretical difficulties.

However in the case of μ-meson capture by He^3 and He^4, considerably less approximations were necessary and recent experimental evidence of Zaimidoraga et al.[23] on μ-meson

capture by these nuclei indicated more positive evidence in favour of the UFI.

The capture of μ-mesons by protons is rendered difficult by two effects, 1), Only about one μ-meson out of a thousand, bound to a proton, will be captured. 2) Meso-molecular effects which cause the μ-meson to be captured not by a single proton, but by a meso-molecule $(p\mu p)^+$. The capture of μ-mesons by protons has however been measured by several investigators[24,25] in order to obtain information about the basic reaction, uncomplicated by nuclear effects.

The resulting capture rates by protons indicated that the assumed numerical relationships between the various coupling constants (i.e. $g_A/g_V = -1.21$, $g_\mu/g_A = 8$) were inconsistent with the experimental results.

Rothberg et al.[24] have suggested that if it was assumed that $g_A/g_V = -1.21$, then $g_p/g_A = 15.5 \pm 3.5$ when derived from the capture rate. Only if the ratio $g_A/g_V = -1.05 \pm 0.08$ would $g_p/g_A = 8$.

Partial Capture Rates

Whilst the total capture rate to all states of the final nucleus is relatively easy to measure experimentally, the character of the absorption interaction is difficult to predict theoretically because of the large number of allowed final nuclear states. When only the partial capture rate to one specific level of the final nucleus is required, then this difficulty is removed.

Godfrey[27] first measured the partial rate of μ-meson capture by carbon 12 leading to the ground state of Boron 12, by observing the subsequent β-decay of the Boron nucleus. The contribution to the capture rate, of μ-meson initially captured in excited bound states of Boron, then decaying to the ground state by γ-emission, was estimated to be small. Thus the partial capture rate from ground to ground state was measured.

In order to establish a theoretical value for this partial capture rate, a relationship between the matrix elements for μ-capture to the ground state of Boron 12 and the reverse process of β-decay was determined. By this calculation the coupling constants effective in μ-capture and β-decay were shown to be approximately equal.

Further calculation concerning partial capture rates in light nuclei have been made by Fujii and Primakoff[16] in which use was made of the effective Hamiltonian discussed in the previous section. Wolfenstein[28] has made analogous calculations for the partial capture rate of C^{12} leading to the ground state of B^{12}, whereas Flamand and Ford[29] have extended their accuracy. A more general theory, concerning the transition probability to a particular state of known spin and parity of the final nucleus, has been derived by Morita and Fujii[30].

It has been demonstrated by Primakoff[14] that the partial μ-meson capture rate to the ground state of B^{12} would depend on the ratio g_p/g_A and also on the weak magnetism term arising from the hypothesis of conserved vector currents.

Several experimental values [31-34], which are not in complete agreement, have been obtained for the partial μ-meson capture rate by C^{12} to the ground state of B^{12}, using different techniques. Maier et al.[34], who claim the most accurate experimental value, suggested however that owing to the difficulties involved in the theoretical calculations which lead only to an accuracy of some ten per cent, the measured capture rate did not confirm definitely the presence of the weak magnetism term. One further experimental difficulty was the estimated contribution to the transition rate resulting from capture to bound excited states. Only in one experiment[32] was this measured and found to account for about ten per cent of the observed β-decays of the B^{12} nucleus.

Partial capture rates have been measured in the case of μ-meson capture by oxygen[35]. In the reaction

$$\mu^- + O^{16} \longrightarrow N^{16} + \nu$$

the transition rates to three of the bound states of the resulting nitrogen nucleus were measured. The ratio of the two transition rates to the 0^- and 1^- excited states of N^{16} is very sensitive to the ratio g_p/g_A. Based on the calculations of Duck[36] for the transition rates, a value of $g_p/g_A = 15$ was shown to be consistent with the experimental values.

Conclusions

Although the experimental evidence available suggests that the basic interaction involved in muon capture is the U.F.I., several details concerning the theoretical predictions are not in complete agreement with the measured values.

Notably the ratio g_p/g_A suggested by Goldberger and Treiman[17] appears at present not to agree with the experimental values observed in either μ-capture[24,25] or in the asymmetries of neutrons emitted after μ-meson capture[40]. The capture rate for radiative μ-meson capture, i.e. in the reaction

$$\mu^- + p \rightarrow n + \gamma + \nu$$

is strongly dependent on this ratio and results, based on a theory by Rood and Tolhoek[39], from an experiment performed by Conversi et al.[38] have indicated the value of $g_p/g_A = (13.3 \pm 2.7)$.

Yovnovich and Erseer[40] have discussed the situation with regard to the interaction constants in μ-meson capture. They concluded that in order to accommodate all the existing experimental evidence, two more interaction constants (including the existing four g_A g_V g_p g_m) must be incorporated in the theory.

CHAPTER 4

μ-MESON ABSORPTION BY AN ARGON NUCLEUS

Introduction

In a series of previous experiments[2, 41], μ-meson absorption by an argon nucleus had been studied, using a high pressure cloud chamber. In addition the reaction $A^{40}(n,p)Cl^{40}$ had also been investigated[2] in an attempt to clarify the results of the absorption experiments.

In photographs of cosmic rays obtained with an argon filled high pressure cloud chamber[41], three examples of stopped μ-mesons were observed which emitted β-particles in the energy range of 2-3 Mev. In one case, the event was observed whilst the cloud chamber operated with a magnetic field, the curvature of the track indicating that the β-particle was an electron. Although the number of stopped μ-mesons was not counted, an estimated number of 35 μ-mesons was calculated from knowledge concerning the ratio of positive to negative μ-mesons and the capture rate of μ-meson by an argon nucleus. Thus 3 stopped negative μ-mesons out of an estimated total of 35 were associated with electrons of this energy (2-3 Mev).

In a further experiment, negative μ-mesons from the Liverpool cyclotron were stopped in the high pressure cloud chamber with a filling of argon[2]. A total of 66 stopped μ-mesons with no secondaries were counted, (the contamination of π^- mesons in the beam was ~ 5 per cent) with 25 apparent μ - e decays. However in 9 decays, the energy of the electrons

was less than 10 Mev. In both the cloud chamber experiments the momenta of the decay electrons, rather than their energy, was determined by multiple scattering measurements.

The energy distribution[42] of the decay electrons resulting from μ-mesons, indicated that only in 1 decay in 1000 should an electron have an energy in the range of 0-5 Mev, or 1 in 40 in the range 0 - 10 Mev. Clearly if these events were to be accepted as genuine decaying μ-mesons with a very low energy electron, then they were in violent disagreement with a well established theory. Out of several possibilities, it was considered most plausible to interpret these events as the β-decay of a radioactive nucleus formed by μ-meson capture.

The basic interaction manifest in μ-meson absorption is:-

$$\mu^- + p \rightarrow n + \nu$$

Thus when a μ-meson is captured by an argon nucleus one of the protons is converted into a neutron with some excitation energy, the remainder of the energy resulting from the rest mass of μ-meson being carried off by the neutrino. As the neutron would receive enough energy to be emitted from the daughter nucleus, this μ-meson capture reaction could result in the formation of Chlorine isotopes Cl^{40} Cl^{39} Cl^{38}. An argument[2] based on the energy available for β-decay demonstrated that Cl^{40} was the most likely chlorine isotope which could exhibit such a β-decay. Although Cl^{40} does exhibit a β-decay mode with an end point energy of ~ 7 Mev, the measured half life[43] is 1.42 minutes, a period far too long to account for the observation of so many events in a cloud chamber which has a sensitive time of only 0.5 seconds. In order to account for

the observed events, it was suggested that the activity could arise from the β-decay of an isomeric state of Cl^{40} which could have a half life of the order of tenths of seconds. In none of the recorded events did the age of the electron appear any different from that of the incident μ-mesons, indicating, although not conclusively, a half life for the decay mode of less than 0.1 seconds.

As no experimental evidence concerning the excited states of Cl^{40} existed, a further experiment[2] was performed in which an attempt was made to produce this isomeric state by the reaction

$$n + A^{40} \rightarrow p + Cl^{40} .$$

Neutrons, of 14 Mev energy, were injected into the argon filled high pressure cloud chamber, the resulting (n, p) reactions being identified by the tracks of the recoil protons. The neutron flux was calibrated by a small percentage of hydrogen in the chamber. The experimental values of the energies of recoil protons gave evidence that the reaction had been successful in exciting the ground state and some excited states about 2 - 4 Mev above the ground state. If the postulated isomeric state were excited, then the subsequent β-particle (energy 0 - 7 Mev) would have been observed associated with a recoil proton track.

In 92 events which were attributed to the formation of Cl^{40} in either its ground or excited states, only one event exhibited a proton track associated with an electron of relevant energy. This event could be assigned to the β-decay of either the ground state or the isomeric state. This experiment yielded a cross-section for the formation of Cl^{40} in the

proposed isomeric state by (n, p) reaction of less than 0.6 m.b.

No conclusive confirmation of the existence of this isomeric state had been achieved by the $A^{40}(n, p)C\ell^{40}$ experiment. Several possibilities existed for the explanation of these experimental results.

1) The predicted isomeric state did not exist, the low energy electrons being in fact genuine electrons resulting from decaying μ-mesons.

2) The measured values assigned to the electrons were incorrect, their low values resulting from some experimental error.

3) The isomeric state, from which this β-decay was observed, was too high in energy to be excited by the (n,p) reaction, or the cross-section for production to this particular state was too low to be observed in the previously conducted experiment.

Experiment a)

In order to investigate the first two possibilities an experiment was planned in which the energies of electrons from μ - e decays could be measured when 'atomically bound' to a nucleus other than argon. If no low energy electrons were observed, both these suggestions 1) and 2) could be eliminated, the explanation falling back on the isomeric state hypothesis.

As the experiment was to be conducted using a high pressure cloud chamber, the element used would be gaseous. Nitrogen was the most convenient gas, its physical properties being reasonably suitable for a cloud chamber and its stopping power per atmosphere, not much different from argon. Due to its low atomic number (Z = 7), the number of captured negative μ-mesons

would be less than in an equivalent run in argon, resulting in more μ - e decays.

Experiments b1) and b2)

As the results of experiment a) proved negative, no low energy electrons being recorded, a further experiment was conducted, both to repeat the previous experiments of μ-meson capture by an argon nucleus and to make some estimation of the limits of the half-life of this isomeric state of Cl^{40}. In experiment b1) the cloud chamber was used with a effective time extended to 2-3 seconds, this increase being sufficient to demonstrate that the half-life of this isomeric state was less than 0.5 seconds. Further examples of stopping μ-mesons were obtained when the argon filled cloud chamber was operated in conjunction with a counter system (experiment b2)).

The details of experiment a)

The necessary μ - e decays were obtained by the previously mentioned random photography method of cosmic rays with the cloud chamber filled with 55 atmospheres of nitrogen and operated by the redesigned control system. Preliminary experiments, where the clearing field of the cloud chamber had been switched off at varying times before the start of an expansion, had demonstrated that the tracks of electrons which entered the chamber as much as 2-3 seconds before the expansion were sufficiently undistorted that energy determinations of less than 5 Mev could be made with reasonable confidence. Above this figure, the

reliability with which the limit could be fixed was a function of the age of the track.

Thus by switching off the clearing field 2.5 seconds before the start of the expansion and photographing 0.5 seconds after the expansion, a total sensitive time of 3 seconds was achieved. Photographing at any later time produced severe distortion of all pre-expansion tracks, which resulted from the local heating effects of condensation.

The chamber was operated with a floating diaphragm technique for this experiment. (Only at a date after the completion of this experiment was it found possible to operate with a fixed diaphragm technique when nitrogen was used). However as the quality of photographs was remarkably good in general (i.e. very low background), the possibility of increased track distortion resulting from this technique and the more stringent operating conditions were somewhat offset.

In all, 5,000 photographs were obtained, an extra 1,000 being discarded due to faulty operation after perforation of the rubber diaphragm. The recycling time of the chamber was maintained at 5 minute intervals, which resulted in about 300 photographs in a 24 hour period. Most of the photographs were obtained in the space of two months.

Photographic development of the 5G91 Ilford recording film was achieved by Ilford ID2 developer, in 25 ft, lengths. Care was taken to see that both the developing and fixing processes remained as constant as possible during the course of the experiment.

The processed film was scanned for interesting events with the use of a micro method Film Reader (Fig. 1), the projected film image being slightly larger than life size (i.e. chamber size). Both the stereoscopic images were viewed, producing a scanning rate which could match the production rate of photographs. The relevant results of scanning are shown in Table 1, together with photographs of typical events (Figs. 2, 3, 4).

The details of experiment b1)

A similar experiment to a) was performed, in which the chamber was filled with 47 atmospheres of argon. The clearing field was switched off 1.5 seconds before the start of the expansion, giving an overall sensitive time of 2 seconds. An increase in the sensitive time above this figure resulted in so many old tracks that scanning became difficult. Some 5,000 photographs of cosmic rays were obtained with the cloud chamber operated with a fixed diaphragm technique, very few photographs being discarded because of poor quality.

Satisfactory operation of the chamber was obtained with a 3 minute 40 second recycling time. With this recycling period, a 24 hour run consumed 100 ft. of film, thus eliminating the wasted time where film had run out during the night in experiment a). The film processing and scanning in this experiment were conducted in a similar manner to that of a), with the exception that film was developed in 100 ft. rather than 25 ft. lengths.

FIG 1

MICRO METHODS FILM READER

FIG 2

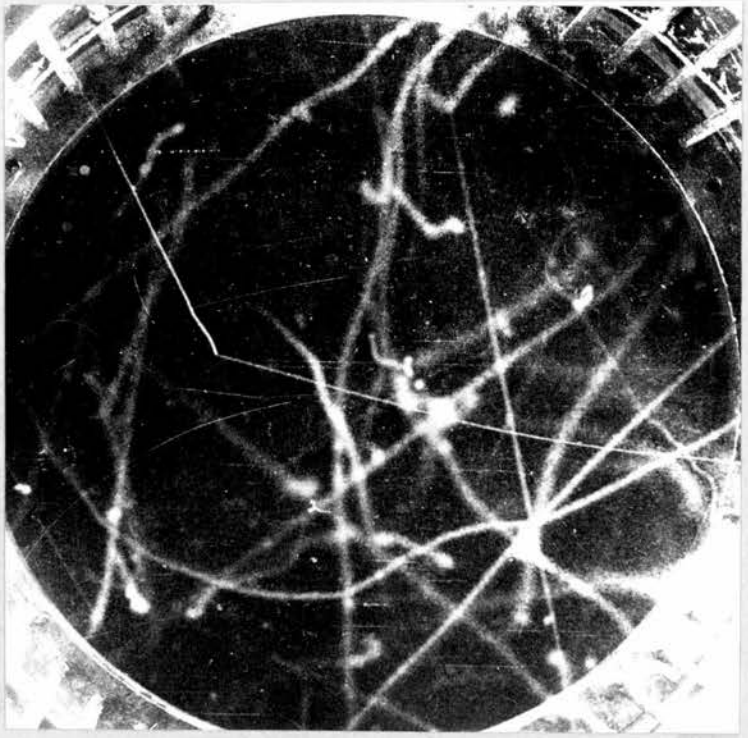

DECAYING MUON

FIG 3

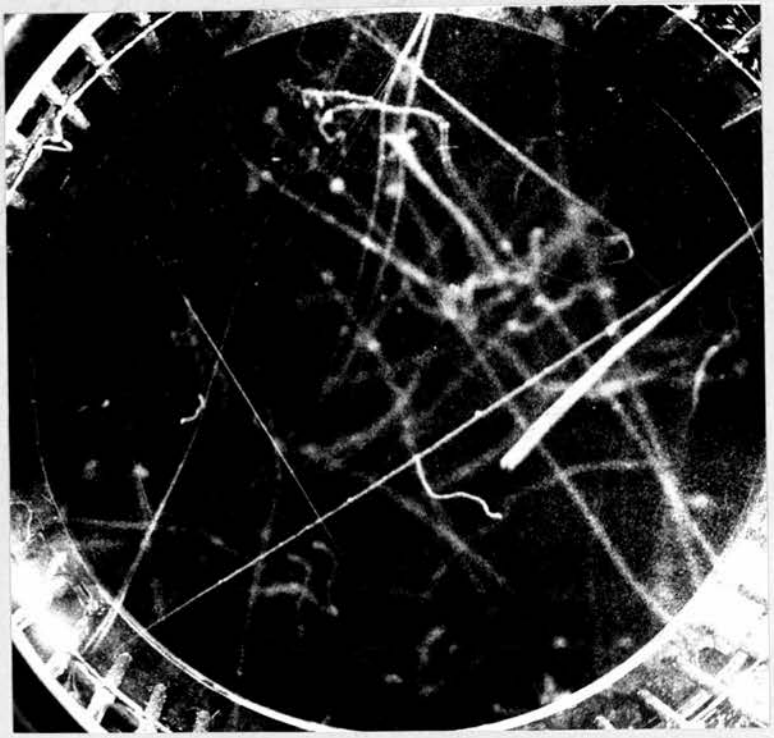

STOPPED PROTON

FIG 4

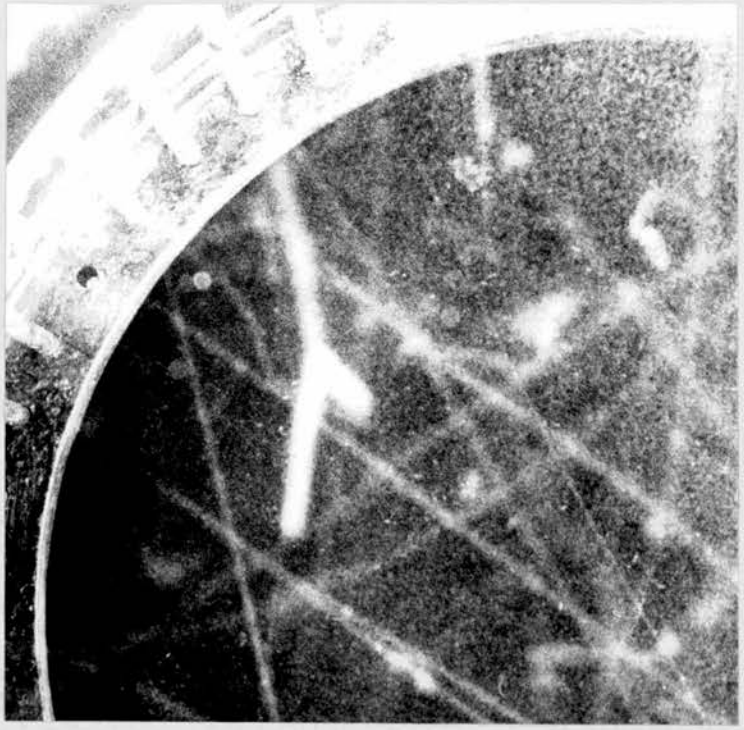

STAR

FIG 5

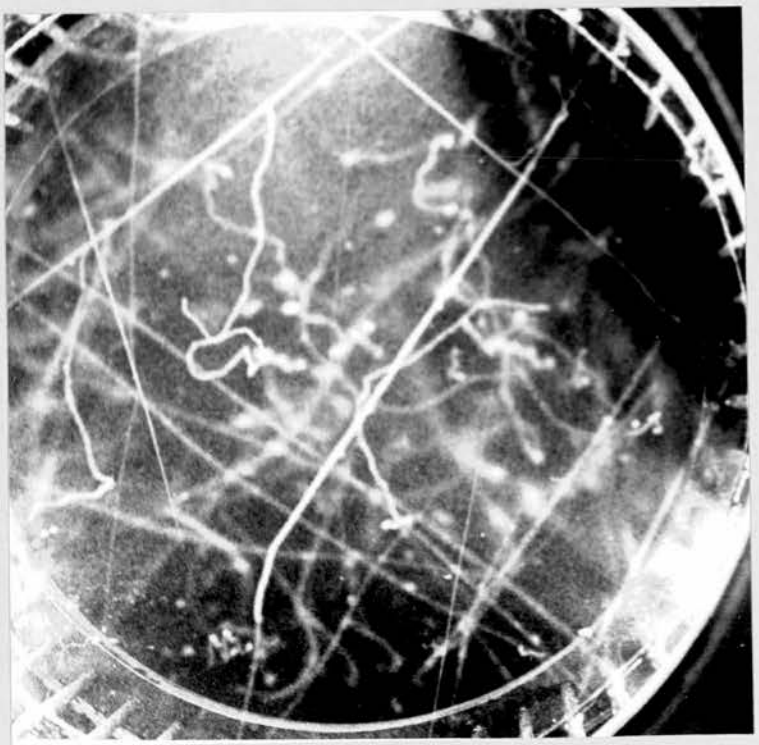

DECAYING MUON

FIG 6

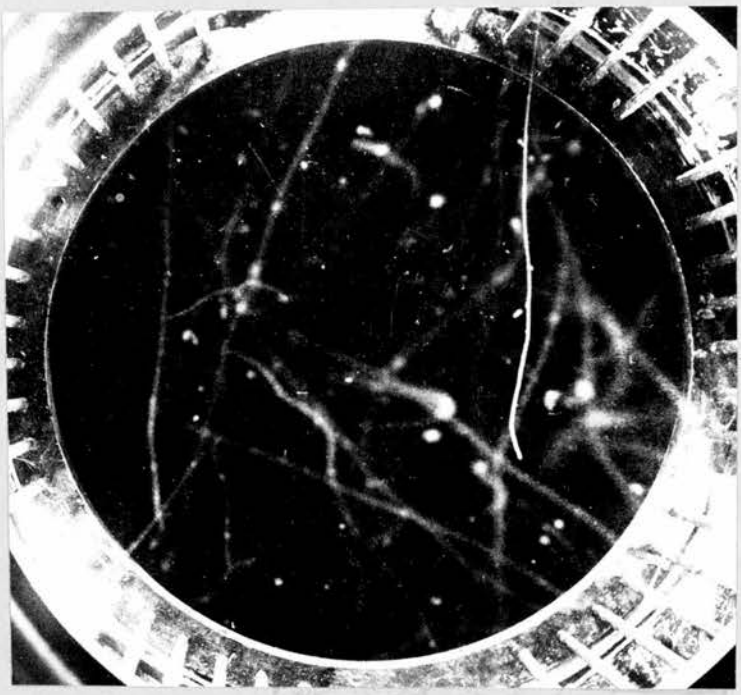

CAPTURED MUON

FIG 7

STOPPED PROTON

FIG 8

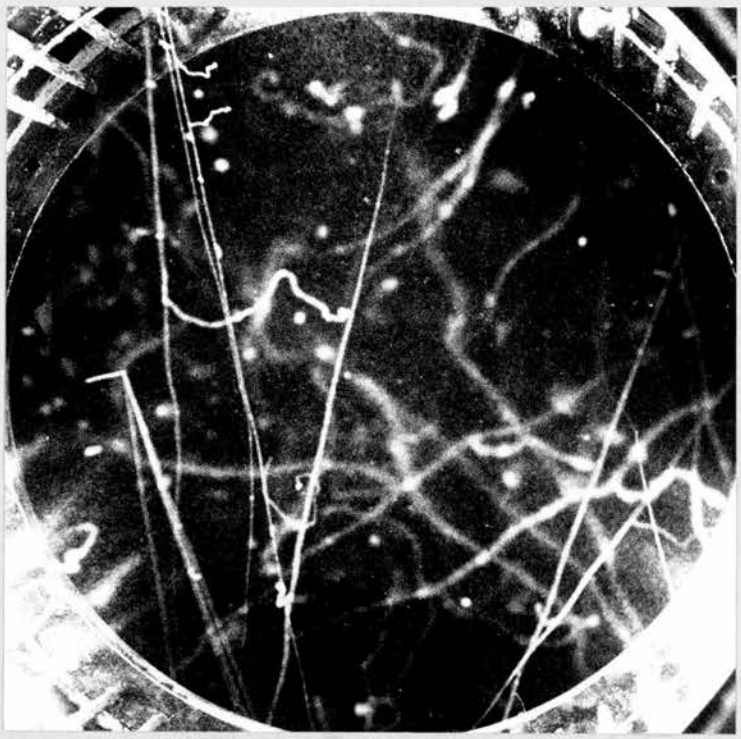

STAR

FIG 9

DECAYING MUON

FIG 10

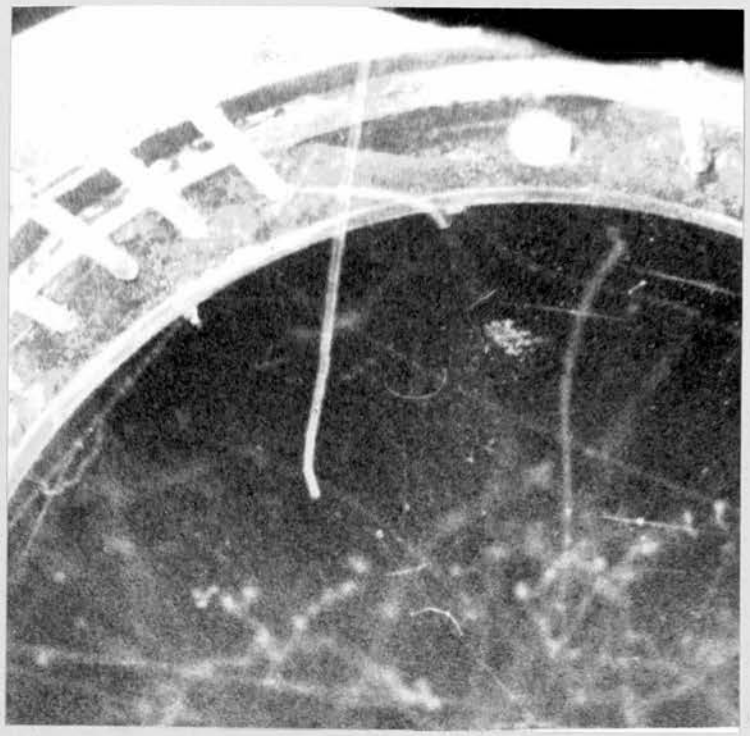

CAPTURED MUON

FIG 11

EVENT 3 (a)

The relevant results of the scanning in this argon experiment are shown in Table 2 (a) with some photographs of typical events (Figs. 5, 6, 7, 8). (Other results of the scanning pertaining to an experiment concerning direct pair production by μ-mesons are contained in Chapter 7). In general the degree of background cloud was slightly larger than in experiment a) but never sufficient to impair relatively easy scanning.

The details of experiment b2)

When the chamber was filled to a pressure of 60 atmospheres of argon, further examples of captured and decaying μ-mesons were obtained with the cloud chamber operated with a counter system which is described in detail in Appendix 1. In this system, the clearing field of the cloud chamber was switched off some 50 m secs after the arrival of the trigger pulse from an incoming particle. Thus counter controlled tracks were in general easily recognized by the very slight field separation of the +ve and -ve ions. Any β-decay event arising from a μ-meson capture by an argon nucleus would give the appearance of a "double" μ-meson track with only a "single" electron track, provided the half-life of the β-decay was greater than 50 m secs.

The results of scanning 3,800 photographs obtained with this system are shown (Table 2(b)). The events have been separated into two categories, namely counter controlled and purely random events. Typical photographs of counter controlled decaying

TABLE 1

Type of event	Number
μ-e decay	20
Stopped μ-meson	-
Stopped proton	7
Stars	2

TABLE 2a

Type of event	Number
μ-e decay	15
Stopped μ-meson	14
Stopped proton	11
Stars	7

TABLE 2b

Type of event	Counter controlled	Random
μ - e decay	15	16
Stopped μ-meson	7	8
Stopped protons	0	9
Stars	1	4

and captured μ-mesons are shown (Figs. 9 and 10).

The average recycling time of the cloud chamber system with the counters was of the order of 15 minutes. Thus effects caused by distortion would be expected to be less than in experiments a) and b1), where much shorter recycling times were used.

Further notes on scanning.

The criterion adopted for the selection of μ - e decays was that an observable difference in the ionization of the incident μ-meson and its decay electron could be clearly noted. In all the events recorded, the difference between the intensities of ionization was so large that no single particle scatter could have been selected.

Selection of stopped heavy particles was again possible by the large ionization of these tracks. The end points of the tracks were shown to be inside the chamber by measuring the distance between the track endings on the two stereoscopic views. Assignment of the stopped heavy particles to μ-meson or proton groups was achieved by the method suggested by Burhop[44], of noting the distance of the last observable δ-ray from the endpoint and by an inspection of the relative increase in ionization along the track length.

Comparison of the scanning results from a), b1) and b2)

In both experiments a) and b1) the numbers of stopped and decaying particles (i.e. μ-mesons, protons etc.) were expected

to be comparable, the slightly higher pressure and longer sensitive time of the nitrogen experiment being compensated by its lower stopping power.

In experiment a) 20 μ - e decays and 7 stopped particles all protons or heavier were observed, whereas in b1) 15 μ - e decays, 14 stopped μ-mesons and 11 stopped protons or heavier particles were recorded.

In nitrogen only 8 per cent of the negative μ-mesons would be captured by the nitrogen nucleus, resulting in an expected number of less than one stopped μ-meson with no secondaries in experiment a). In argon, and using Tait's figure (2) for the ratio of apparent decays to stopped μ-mesons with no secondaries, the total number of stopped negative mesons, which are captured, should be of the order of 9 when 15 μ - e decays of positive and negative mesons were observed. (Note the observed number of 14). However the statistical variation on such small numbers would be rather large.

When the results of experiments b1) and b2) are added together, the total of 29 absorbed μ-mesons is in good agreement with the expected number of 27

<u>Determination of the momenta of the decay electrons in experiments a), b1) and b2).</u>

The momenta or rather the pB values of the decay electrons associated with stopped μ-mesons were determined by suitable calculations from multiple scattering measurements. The method

adopted was similar to that described by Tait[2], in some detail, but a short account of the relevant facts have been included in Appendix 2. The multiple scattering measurements were performed using a reprojection machine[51].

Experiment a).

The momenta of all 20 decay electrons could not be determined for one of several reasons.

1) The illumination of the track or its intensity of ionisation was not sufficient to be observed clearly when viewed in the reprojection apparatus. Thus no reliable measurements could be made.

2) The length of track was too short (i.e. less than 2 cm.).

The momenta in units of Mev/c of the 13 decay electrons which could be obtained, together with the track thickness of the stopping μ-meson near the endpoint, are listed in Table 3.

In no fewer than 5 events was the estimated momentum less than 10 Mev/c (i.e. events 3, 7, 8, 9, 11). However all the tracks in these events were pre-expansion, in which the possible existence of track distortion could not be discounted. For instance, event 3 (Fig. 11) must have occurred some 5 seconds before the start of the expansion as judged by the amount of field separation of the two sets of ions. Signs of track distortion due either to slow movement of the chamber gas or by the effect of field separation are clearly present.

A correlation of the age of the event, when not field separated, with the thickness of the μ-meson track would not

TABLE 3

Event Number	Momentum p (Mev/c)	Cell Length	Track thickness (cm)
1	12^{+4}_{-2}	1.0	0.047
2	14^{+6}_{-3}	1.0	0.130
3	7^{+1}_{-1}	1.0	0.152
4	11^{+10}_{-3}	1.0	0.101
5	25^{+12}_{-7}	1.0	0.057
6	10^{+2}_{-2}	1.0	0.118
7	6^{+7}_{-2}	0.5	0.185
8	8^{+5}_{-2}	0.5	0.188
9	5^{+2}_{-1}	1.0	0.220
10	11^{+5}_{-2}	1.0	0.169
11	8^{+7}_{-3}	1.0	0.166
12	10^{+5}_{-3}	0.5	0.209
13	25^{+17}_{-8}	1.0	0.164

be expected to yield more than qualitative success. The μ-meson track thickness, apart from being a function of the age of the event, would depend on several factors:- 1) The expansion ratio, 2) The degree of background cloud, 3) The variation of illumination and magnification of the event from one position to another, 4) The different development conditions of the individual film. All these four factors would inevitably vary in an experiment of this duration. However an indication does exist that the thicker the μ-meson track (i.e. the older the event) the lower was the measured momentum value.

Returning to the five events in question, two of these (i.e. events 8, 11) could be included in the higher energy category if the upper limit of their error is taken. As no event was observed in which the momentum was less than 5 Mev/c and those in the region of 5-10 Mev/c are suspected to be too low due to distortion, it can be asserted with reasonable confidence, that in none of the 13 events was an electron associated with a stopped μ-meson which had an energy as low as those recorded in the previously mentioned experiments in argon (i.e. energy in the region of 2-5 Mev).

A qualitative inspection of the tracks of the other 7 decay electrons, whose momenta could not be determined empirically indicated a small degree of multiple scattering. If measurements had been possible, they would most probably have been included in the momentum group above 10 Mev/c.

Experiment b1)

Out of 15 μ - e decays observed in argon, reliable multiple scattering measurements could only be performed in 11 cases (Table 4(a)). In all but two of these events (i.e. events 7 and 8) the measured momenta were greater than 10 Mev/c. Leaving event 8 aside (discussed in some detail later), the electron in event 7 suffered a large angle scatter which was included in the multiple scattering measurements due to the very short length of track available for the determination ($\sim$ 3 cm). Thus the value of 4 Mev/c obtained on such a short track could be very far from the correct value and the electron momentum of event 7 should be treated with some caution.

In this experiment b1) even those electron tracks which resulted from events which had occurred some time before the expansion, yielded momentum values greater than 10 Mev/c. Events 1 and 4, which were field separated, fall into this category. Thus provided no difficulty is encountered in the measuring procedure, it would appear that the amount of distortion in this chamber was too small to impair momentum measurements below 10 Mev/c when the gas was argon.

In event 8 (Fig. 12) the apparent decay electron can be seen at only one of the μ-meson endings. As both the heavy particle tracks are in the same plane as the direction of the clearing field and have endpoints at the same height, the chance that the two tracks were caused by different particles, rather than field separation of a single event seems, very remote. The distance between the two sets of ions indicated that the

TABLE 4a

Event Number	Momentum p(Mev/c)	Cell Length	Track Thickness (cm)
1	13^{+3}_{-4}	1.0	0.259
2	10^{+25}_{-4}	1.0	0.146
3	31^{+28}_{-10}	1.0	0.092
4	13^{+46}_{-5}	1.0	0.112
5	13^{+22}_{-3}	1.0	0.118
6	18^{+28}_{-9}	1.0	0.069
7	4^{+5}_{-1} *	1.0	0.067
8	4^{+3}_{-1}	1.0	0.257
9	18^{+24}_{-7}	0.5	0.067
10	8^{+14}_{-2}	1.0	0.321
11	14^{+61}_{-8}	1.0	0.183

* unreliable result - see text

FIG 12

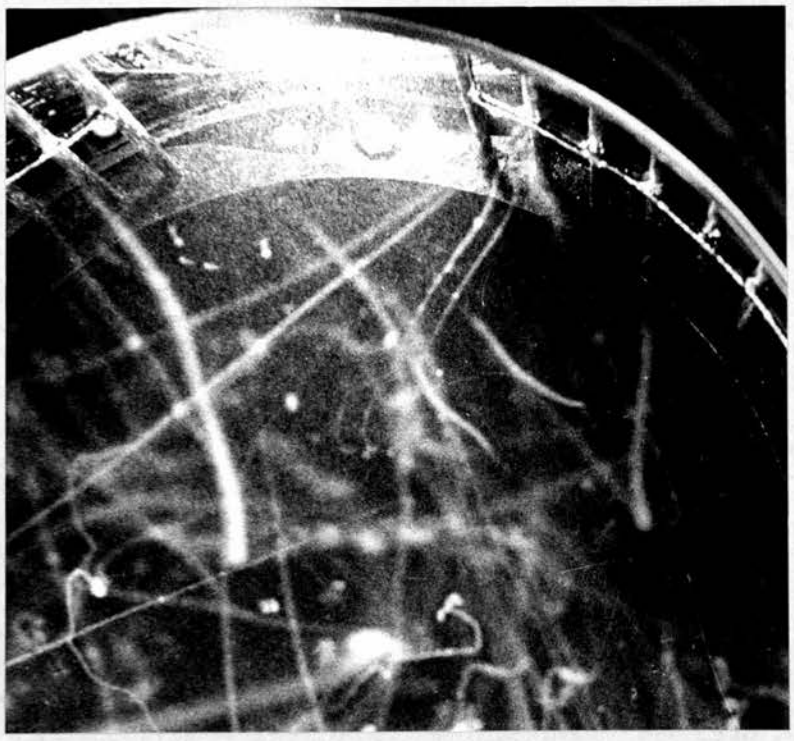

EVENT 8 (b1)

FIG 13

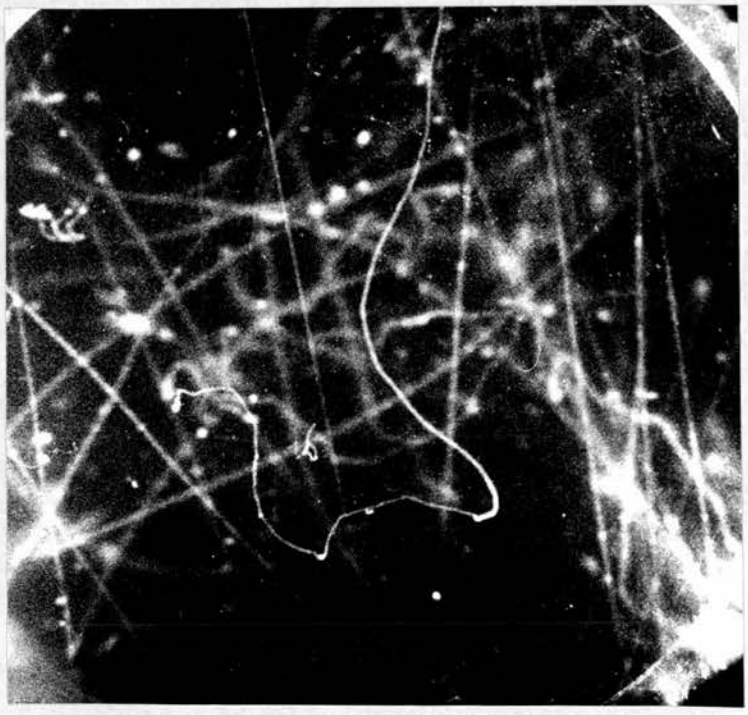

EVENT C8 (b2)

μ-meson entered the chamber 2 seconds before the clearing field was switched off. The electron track, which was emitted from only one μ-meson endpoint, shows no sign of a field separated partner and must have occurred after the field was removed, in an interval 2-4 seconds after the initial capture of the μ-meson by an argon nucleus.

This event cannot be an example of a μ - e decay and in fact must be the β-decay of some radioactive nucleus formed by μ-meson capture by an argon nucleus, the momentum value of 4 Mev/c being consistent with the β-decay of Cl^{40}.

Thus in experiment b1) only one doubtful event, which could be assumed to be a μ - e decay, exhibited an electron of momentum less than 10 Mev/c.

Experiment b2)

Out of the 15 examples of counter controlled μ - e decays, 14 events were suitable for momentum determination of the emitted electron. In the case of event C8 , the electron stopped in the chamber (Fig. 13), its momentum being computed from a range measurement. Only in 9 out of the 15 random events were measurements possible. The results are shown in Table 4b where the suffixes C and R refer to counter controlled and random event respectively.

Only one event (C8) among the counter controlled events had a momentum value significantly less than 10 Mev/c. Those estimated values of momentum of events C11, 12, and 13, although of the order of 10 mev/c, were expected to be rather low as the electron track was either very faint (C11, 12) or rather short (C13).

TABLE 4b

Event Number	Momentum p (Mev/c)	Cell Length
C1	23^{+4}_{-3}	1.0
C2	17^{+10}_{-5}	1.0
C3	24^{+3}_{-3}	1.0
C4	38^{+11}_{-7}	1.0
C6	21^{+6}_{-4}	1.0
C7	21^{+25}_{-6}	0.5
C8	$2.2^{+0.2}_{-0.2}$	(range measurement)
C9	11^{+4}_{-2}	0.5
C10	17^{+4}_{-2}	1.0
C11	8^{+2}_{-1}	1.0
C12	9^{+2}_{-2}	1.0
C13	10^{+9}_{-5}	0.5
C14	26^{+8}_{-5}	1.0
C15	19^{+23}_{-7}	0.5
R1	52^{+62}_{-18}	1.0
R2	$3.1^{+1.2}_{-0.7}$ *	0.5
R3	78^{+150}_{-42}	0.5
R4	21^{+4}_{-3}	1.0
R5	7^{+2}_{-1}	1.0
R7	19^{+8}_{-4}	0.5
R8	57^{+17}_{-12}	1.0
R9	$2.6^{+0.7}_{-0.4}$	0.5
R12	32^{+8}_{-5}	1.0

* unreliable result - see text

Although the scattering of the μ-meson of event C8 was more than would normally be observed, a measurement of the track thickness of the μ-meson near its endpoint and electron at the same magnification, indicated the μ-meson track to be at least twice as broad as that of the electron. This ratio of track thickness was that expected between a slow μ-meson and electron track for this age of event. As this event appeared to be counter controlled, the expected slight field separation of the μ-meson track should have been apparent. However if the cloud chamber was operated in a slightly under-expanded condition, condensation on the negative set of ions was difficult to observe when tracks of this sort of field separation occurred (i.e. of the order of 1 mm.). Further, confirmation of the slight underexpanded nature of the chamber was obtained by viewing adjacent photographs to this event. The event could possibly be of the random type, but this seems unlikely, as both the age and the direction of the incoming μ-meson were consistent with a counter controlled event.

Three of the random events indicated electron momenta considerably less than 10 Mev/c. However, the μ-meson of event R2 stopped near the top of the chamber, where the clearing field was least uniform. As this event was field separated, the possibility of serious field distortion could not be ruled out, and the momentum value is thus rather suspect. Event R5, also field separated, might again be expected to yield lower momentum value than the true one. As event R9 was a new event, the quoted momentum value was expected to be accurate.

Thus, in two events, low energy electrons (momenta 2.2 and 2.6 Mev/c) were found associated with the endpoints of μ-meson tracks.

Discussion of the results of a), b1) and b2).

Although only a limited number of examples of μ - e decays were obtained when nitrogen was used in the chamber, no evidence of an anomalous decay mode of the μ-meson was found. More detailed studies have indicated this negative result. In an experiment conducted by Vaisenberg et al.(83) the energies of some 200 electrons, resulting from the decay of negative μ-mesons bound atomically to the heavy atoms (Ag, Br) of a nuclear emulsion, were compared with those of positrons from the decay of positive μ-meson. No difference in the two energy spectra was found, and none of the 200 negative electron energies fell into the region 0 - 5 Mev. Even with a scanning efficiency as low as 20 per cent, some of the low energy electrons observed in the cloud chamber experiment would have been detected, if they resulted from the decay rather than the capture of negative μ-mesons.

The possibility of sufficient track distortion accounting for the low energy values observed previously appears unlikely in a gas such as argon at a pressure of 50 atmospheres. In experiment b1), even an electron track resulting from the decay of a μ-meson which occurred 3 seconds before the start of the expansion yielded momentum greater than 10 Mev/c. It would be

difficult to account for a total of 10 low energy electrons observed in an argon filled cloud chamber as arising from track distortion, especially as the value of one of these events (C8) was not subject to this criticism. (The figure of 10 low energy electrons was the total number of events where the electron energy was less than 5 Mev both in this experiment and those previously mentioned[2, 41].

Neither of the first two possibilities suggested in the introduction appear valid in the light of these experiments. It must be concluded that these low energy electrons arise from the β-decay of a mucleus formed by μ-meson capture.

Further suggestions, i.e. that these electrons arise from 1) internal conversion, 2) internal pair production, 3) radiative collision accounting for the low energy values, 4) Auger electrons, have been discussed previously[1, 2] and found to be inapplicable.

The relevant results of all these experiments conducted with an argon filled cloud chamber are listed in Table 5.

Comments on the isotope Cl^{40}

Life-time of the isomeric state

In the previous experiments[1, 2], where these low energy electrons had been observed, no difference between the ages of the μ-meson and electron tracks had been detected. The half life of the β-decay from these considerations should be of the order of $\lesssim$0.1 seconds. However as one experiment was counter

TABLE 5

Experiment	μ-meson source	No. of stopped μ-mesons	No. of μ-e decays with energy > 5 Mev	No. of μ-e decays with energy < 5 Mev.	Average time between events and photography (seconds)
Ref. (41)	cosmic rays	27*	-	3	0.5
Ref. (2)	μ^- from particle accelerator	66	19	5	(0.5)
Present experiment	cosmic rays	22	16	1	2 secs.
		7	13	1	0.5 secs.

* estimated number from the actual number of μ - e decays observed.

controlled, the other performed with an accelerator, not much difference in the ages of tracks would be expected.

The results of these experiments could be alternatively interpreted. If all the μ-mesons captured by the argon nucleus formed the isomeric state of Cl^{40}, then the fact, that only one in fifteen of the Cl^{40} nuclei formed by μ-capture exhibited a β-decay observable in ~ 0.5 seconds, could indicate that the isomer had a half life of the order of 5 seconds.

In experiments b1) and b2) the sensitive time for random events was of the order of 2-3 seconds, (taking into account field separated events), each event having an average time of 1-2 seconds in the chamber before photography. If the half life of the isomeric level was of the order of 5 seconds, then proportionally more events would be expected. However with this longer half life, approximately 4 events with low energy electrons should have been observed among the random events, compared with only one actually found. Although the statistics are very poor, it seems unlikely that the half life of this isomeric state could be long compared with 0.5 seconds. Again it would be difficult to accept theoretically a process of μ-meson capture which went almost exclusively to one level. From this basis alone the half life could not be greater than 0.5 seconds.

As for event 8 of experiment b1), it has been established that 2-4 seconds elapsed between the μ-meson absorption and the emission of an electron. It can be assumed that almost all the μ-mesons captured by A^{40} yield Cl^{40} rather than Cl^{39} or Cl^{38} etc. (discussed later) and from the above argument, that the

half life of the isomeric level is less than 0.5 seconds.

The ground state half life for β-decay has been measured experimentally at 1.42 minutes[43]. Thus out of every 15 μ-meson captures, Cl^{40} in the ground state would be formed, either by direct capture in this level or by capture in an excited state and subsequent γ-decay, in 14 cases, the other one case going directly to the isomeric state. Thus the number of events expected from the ground state and the isomeric state β-decays (half life $<$ 0.5 seconds) would be 0.4 and 0.05 respectively in an interval 2-4 seconds after some 23 μ-meson captures.

Although only one event of this type was found, the rate being indeterminate, it would appear more plausible to assign this event to the β-decay of the ground state.

A decay scheme for this isotope Cl^{40} has been previously suggested[2] (Fig. 14) in which the most likely isomeric state was the 0^+ spin state a few keV above the ground state of spin 2^- (established from β-decay theory[46]). The β-decay from the 0^+ isomeric state of Cl^{40} would fall into the category of allowed transitions and have an endpoint energy of 7.5 Mev which is consistent with experimental evidence. The M2 γ-transition from the 0^+ state to the 2^- ground state could compete with the β-decay mode, the branching ratio being a function of the energy separation of the levels.

Inspection of the Fermi functions $f(z\ w_o)$[47] as plotted against endpoint energy, and typical ft values for allowed transitions (t is the half life), indicateda half life in the

FIG 14

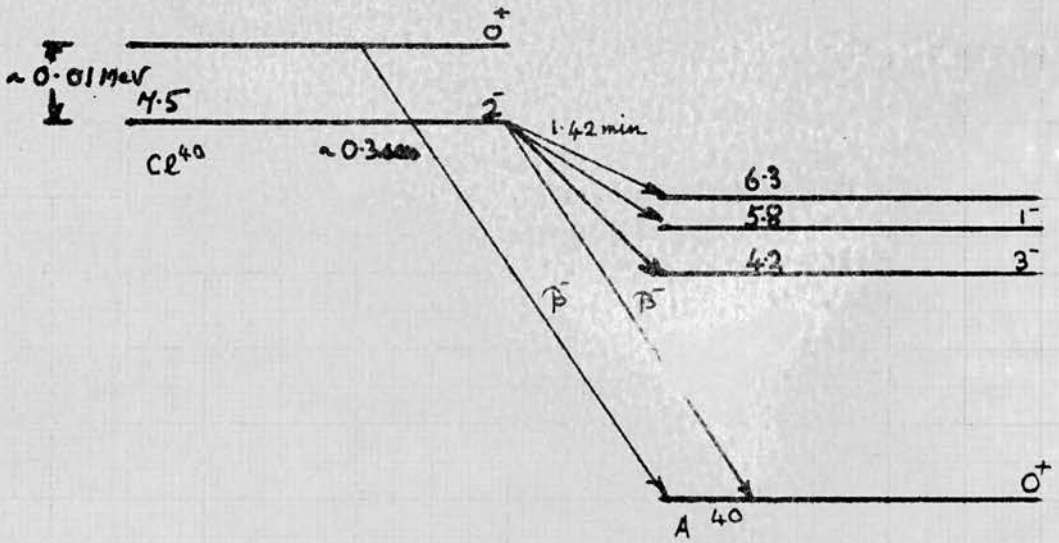

FIG 15

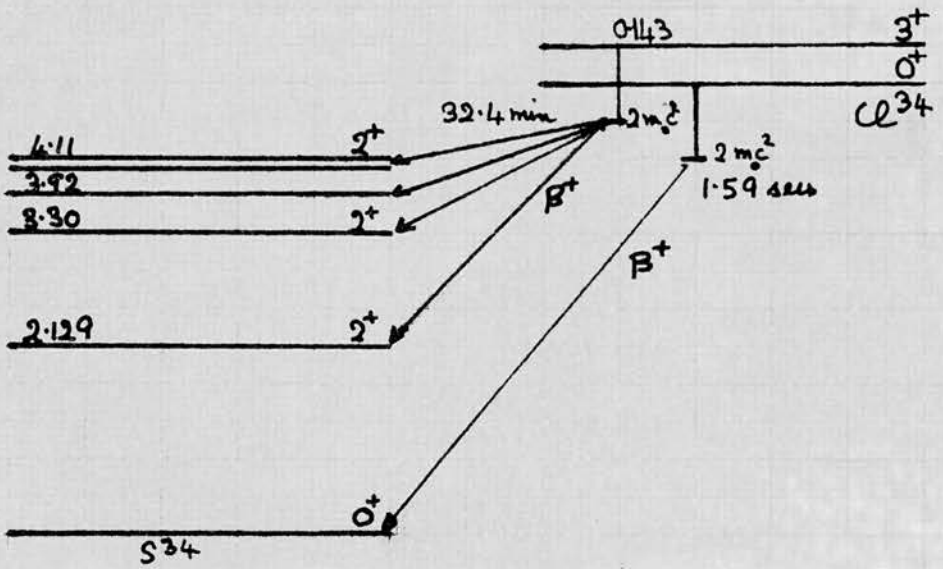

ENERGIES OF LEVELS
IN UNITS OF MEV

range of 0.3 - 3 seconds for the isomeric decay mode. Even if the β-decay came into the category of super -allowed transitions, a half life of greater than 0.03 seconds would be expected. However, as all the super-allowed β-transitions occur at very low atomic numbers, this would be unlikely, the value of 0.3 seconds being quite consistent with the experimental evidence.

Energy levels of Cl^{40}.

In the (n, p) reaction experiment[2] conducted with a gaseous argon target, no evidence for the existence of a β-decaying isomeric level was gained. An inspection of the energy distribution of the 92 protons resulting from the reaction $A^{40}(n,p)Cl^{40}$ indicated that only a cross-section of about one order of magnitude lower than the cross-section of the (n, p) reaction to the ground state of Cl^{40} would be required, if the isomeric state were never to be excited in this number of events. This would only be the case if all the excited levels produced above the isomeric state decayed by γ-emission predominantly to the ground state, thus by-passing the isomeric level.

As in Morinaga's experiment[43] an (n,p) reaction on A^{40} was used to produce Cl^{40}, the resulting half life of the activity measured at 1.42 minutes, the above suggested character of the level scheme was again confirmed.

A calculation of the first four excited levels of Cl^{40} by Talmi[49], based on the j-j coupling shell model, gave the following results.

	Spin	Energy (Mev)
Ground state	2	0.0 "
1st excited state	1	0.43 "
2nd excited state	3	0.58 "
3rd excited state	4	0.68 "

The spin of 2 calculated for the ground state is in agreement with that predicted by β-decay theory. Experimental evidence about the excited states of Cl^{40} was not available and thus the validity of Talmi's calculations has not been tested. (The resolution of the proton energies of the (n,p) reaction experiment[2] was too poor to confirm the existence of these closely grouped levels.

The calculation gave no indication of the postulated isomeric state 0^+. If it is assumed that the parities of the ground state and 1st excited state (0.43 Mev) are the same, i.e. 2^- and 1^- (the 2^- was predicted by β-decay), then γ-emission from the 1^- state would go predominantly to the 2^- ground state rather than the 0^+ isomeric state as the branching ratio for E1 to M1 transitions is of the order of 100 : 1, where the energy separations are much the same. This kind of level arrangement would be consistent with the (n,p) reaction experiment[2].

Examples of β-decay from an isomeric level

Both Cl^{34} and K^{38} exhibit β-decay from both the ground state and an isomeric, both of these isotopes being positron emitters[46]. The properties of Cl^{34} and Cl^{40} might be expected

to be somewhat similar, as the former has three neutrons inside a closed shell, the latter three neutrons outside a closed shell. The decay scheme of Cl^{34} is shown in Fig. 15 for comparison with Fig. 14. The ratio of the two β-decay half lives of Cl^{34} is two orders of magnitude, similar to that expected for those of Cl^{40}.

Comments on μ-meson capture by A^{40}

The arguments of the previous section suggest that if the μ-meson capture reaction produced a state in Cl^{40} other than the isomeric level, then the likelihood of γ-de-excitation to this state was small. The few events observed would infer that isomeric β-decay should result from direct capture of a μ-meson to the 0^+ level of Cl^{40}.

Calculation of the ratio of rates ω_o/ω_n of the two reactions (50)

$$\mu^- + (A, z) \rightarrow (A, z-1) + \nu \quad - \quad \omega_o$$

$$\mu^- + (A, z) \rightarrow (A-1, z-1) + \nu + n \quad - \quad \omega_n$$

have yielded the empirical formula

$$\frac{\omega_n}{\omega_o} = \frac{1.56}{A} .$$

Thus for μ-meson capture by A^{40}, 96 per cent of the events should produce Cl^{40}. More rigorous calculations by Luyten et al.[21] have obtained similar results for μ-meson capture by Ca^{40}.

Thus out of a total of 71 μ-meson captures[2] by A^{40}, 69 should produce Cl^{40}, 5 of these directly to the isomeric state. The half life of this isomeric state is small enough to be reasonably certain that most of the β-decays had been observed. Thus the partial capture rate to this 0^+ level of Cl^{40} would be $\sim 1 \times 10^5$/sec compared with the experimental total capture rate to all levels of Cl^{40} of $(1.6 \pm 0.9)10^6$/sec. (Both these rates were derived from the decay rate of the μ-meson).

As μ-meson capture rate selection rules are similar to those of β-decay, a capture rate of this magnitude would be acceptable for the transition from the 0^+ ground state of A^{40} to the 0^+ isomeric level of Cl^{40}. The capture rate to the 2^- ground state of Cl^{40} would be expected to be between one and two orders of magnitude less than this transition rate, as it would fall into the category of 1st forbidden transitions. If the decay mode of the isomeric state was compound, i.e. the M2 γ-transition competing significantly with the β-decay mode, then the transition rate for μ-capture would be proportionally larger.

A calculation of this partial transition rate, i.e. (0^+ A^{40} to 0^+ Cl^{40}) could be made, using the general theory of Murota & Fujii[30]. However, as many approximations would have to be made concerning the wave function which described this isomeric level and the value of the half life of its β-decay mode, only qualitative agreement could be expected, with the present results.

Although this type of reaction, in which a μ-meson capture

is accompanied by a β-decay, is similar to that studied in those experiments, where the partial transition rate of μ-meson capture by C^{12} was investigated[31-34], it would appear unlikely that any further information concerning the numerical relationships between the interaction constants (g_p, g_A, g_ν etc.) could be obtained. However, when the μ-meson capture reaction theory is better established, information concerning nuclear levels of this type could be obtained in this manner.

Further experiments on μ-meson absorption by A^{40}

If a further investigation of this isomeric level were conducted it would be desirable to obtain the following information

1) The half life of the isomeric state.
2) The shape of the spectrum of the decay electrons from the isomeric level.
3) The branching ratio of the γ and β transitions from the isomeric level.
4) The energy of the γ-transition (0^+ to 2^- level).

These properties could be achieved by a counter experiment where a liquid or solid argon target would be bombarded with slow μ-mesons. A further cloud chamber experiment could only attempt to measure the decay spectrum of the isomer and give only a qualitative result for the half life of the β-decay.

CHAPTER 5

THE μ-MESIC AUGER EFFECT

Introduction

The capture of slow negative μ-mesons by an atom, by the replacement of an atomic electron constitutes the formation of a μ-mesic atom. The μ-meson, after capture in a state of high excitation, cascades through the levels of the μ-mesic atom emitting photons and electrons until the ground state is reached[57]. The time taken for a 2 keV μ-meson to reach the ground state is approximately 10^{-13} seconds in solid materials, whereas about 10^{-9} seconds in a gas such as air[58]. Thus, as the μ-meson interacts only weakly with nucleons[7] and has a half life of 2×10^{-6} seconds, it is expected to reach the ground state of the μ-mesic atom.

The terminology of the properties of the μ-mesic atom is similar to that of the hydrogen atom. Thus, the principal quantum number $n = 1$ refers to the K level (ground state) and all photons which are emitted due to the arrival of a μ-meson in the K level give rise to the K-series radiation. The allowed values of the azimuthal quantum number ℓ ($\ell \leqslant n - 1$) produce the fine structure of each level. Further splitting of each ℓ state occurs from the intrinsic spin of one half of the μ-meson.

The formation of a μ-mesic atom was probably first observed by Conversi (1947)[59]. Quantitative measurements of many of the properties of the μ-mesic atom have been achieved since, which agree well with theoretical prediction. However, certain phenomena associated with both the X-ray and Auger electron yields from μ-mesic atoms are not easily explained by acceptable

theory. These, together with some of the relevant established properties will be the subject of the following sections.

Energy Levels

If the μ-meson is assumed to be a heavy electron moving in a Coulomb field, originating from a point nucleus of charge Ze, then the 'Bohr radius' of the μ-meson is the same as that of the K shell atomic electrons for a principal quantum number (μ-mesic) $n = 14$[7]. For lower levels ($n < 14$) the values of the particular energy levels can be estimated using the Bohr theory[60]. Thus the binding energy E_n of the n-th level is

$$E_n = -\frac{\underline{\mu}c^2}{2n^2}(Z\alpha)^2$$

where

$\underline{\mu} = \mu/(1 + \frac{\mu}{A})$ the reduced mass of the μ-meson,

$\alpha = 1/137.04$ the fine structure constant.

An exact value for the energy levels can be obtained using the solutions from the Dirac equation as the μ-meson is a spin one half particle[60]. The change in the value of the binding energies for particular j states ($j = \ell \pm \frac{1}{2}$) is only a few per cent different from that estimated by the Bohr theory, but becomes increasingly more important for large Z and small n.

The simple Coulomb potential is modified considerably near the nucleus when its finite size becomes important. The binding energy of the lowest level is much reduced, the effect becoming larger as Z increases. The values of the 2p - 1s transition

have been predicted[61] using a nuclear radius $R = 1.3 \times 10^{-13} A^{\frac{1}{3}}$ and also measured experimentally. More recent values of the lowest energy levels and some higher ones have been tabulated, using values of nuclear radius obtained from electron scattering experiments[62].

Much smaller effects which account for less than a one per cent change in the binding energies (i.e. vacuum polarization; screening of the nuclear charge by atomic electrons; and polarization of the nuclear charge by the proximity of the μ-meson) have been discussed in a review article[60].

However in light mesic atoms ($Z < 6$) the effect of vacuum polarization together with the small extent of nuclear size produces an inversion in the 2S and 2p levels, rendering the 2S a metastable state. The different Z dependence of the vacuum polarization and nuclear size effects produce a cross over of the energy levels for $Z > 5$ and thus no metastable state exists for the heavier atoms ($Z > 5$)[63].

Capture of the μ-meson into bound states.

Calculations concerning the capture of μ-mesons from the continuum to bound states of the μ-mesic atom have received little attention. Such calculations that have been accomplished[64,65] are not expected to be very reliable[66] as the Born approximation was used where it was not strictly valid.

However the capture of π and K mesons has been treated with more rigor[67,68]. In these calculations, the cross section

for capture into bound states was greatest, where n = 15 to 17 and $\ell \simeq \frac{n}{3}$ for π-mesons. A similar calculation for μ-meson would be expected to give much the same form of final result, with the maximum cross-section for capture at about n = 14 and $\ell \simeq \frac{n}{3}$.

The resulting distribution of initial states would however differ from the assumed population of the n = 14 level used by Eisenberg and Kessler (1961)[69]. The cascade calculations which are derived from this initial population[69] do however agree with some experimental results[77].

Cascade calculation and transition rates.

After capture in a high state of excitation, the μ-meson cascades through the levels of the atom by the emission of photons and Auger electrons. The reaction rates for the two processes differ in character. Whereas the radiative transition rate is strongly dependent on both nuclear charge Z (αZ^4) and the energy of the transition[7], the Auger rate is to a first approximation independent of Z and becomes less as the energy of the transition increases. These sharply contrasting characteristics tend to make the de-excitation of the μ-mesic atom initially a purely Auger process, changing rapidly over a small range of $\underline{n}$ to a purely radiative process. Both processes follow the same selection rules[70] $\Delta \ell = \pm 1$ for P type transitions. However the selection rule $\Delta \ell = 0$, whilst strictly forbidden for the radiative processes, is allowed for the Auger process, giving rise to an S type transition. This transition rate is about two orders of magnitude less than the

normal P type transition.

If the μ-meson is first captured in a state (i.e. n = 14, ℓ = 13), then the dominant transitions are of the form (n, n - 1) → (n - 1, n - 2). The rates of both radiative (Rn) and Auger (An) transition, of the above form, have been calculated[70] (Fig. 1) for different values of Z.

Further refinements to the above transition rate calculations were added by de Borde (1954)[64] namely -

1) Capture in states other than ℓ = n - 1.
2) Removal of atomic electrons by previous Auger transitions.
3) Ejection of Auger electrons from both the K and L electron shells of the atom.

If capture in several ℓ states is to be considered, some assumption concerning the distribution of the ℓ levels of the initial state of capture must be made. A statistical weight of $(2\ell + 1)$ was assigned to each ℓ state of the n = 14 level, thus giving a preference for capture in the larger ℓ values. The cascade calculation which results from the above population of the n = 14 level, together with the conditions (ii) and (iii), yield overall Auger rates which are slightly reduced compared with the simpler theory[70].

Further cascade calculations[69] have been made using four initial distributions for the n = 14 level. (The effect of ionization of atomic electrons had been shown not to contribute significantly[71] and was neglected). The expected number of transitions to each (n, ℓ) state was evaluated, allowing a determination of the relative X-ray yields (i.e. the ratio of Kα

FIG 1

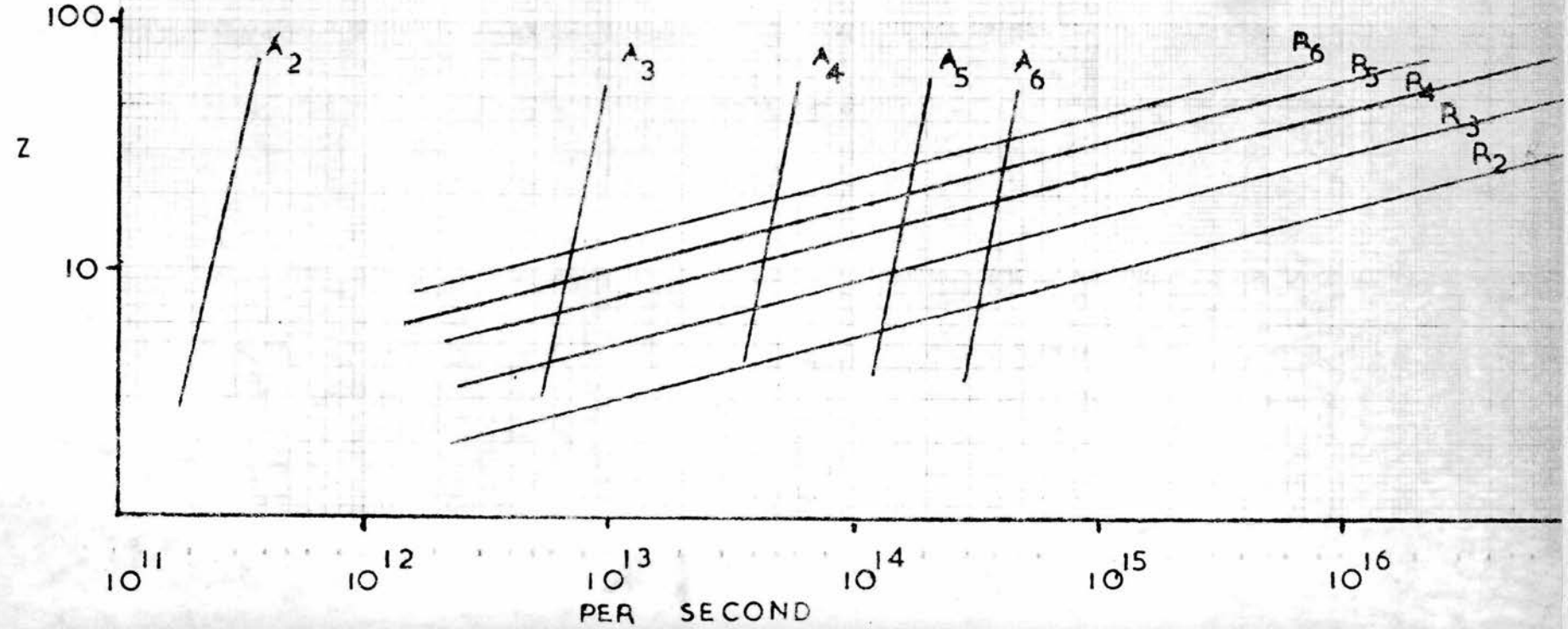
TRANSITION (N, N-1→N-1, N-2)
A_N AUGER RATE/SECOND
R_N RADIATIVE RATE/SECOND
100
10
Z
A_2
A_3
A_4
A_5
A_6
R_6
R_5
R_4
R_3
R_2
10^{11}
10^{12}
10^{13}
10^{14}
10^{15}
10^{16}
PER SECOND

to all K X-rays and similarly for L X-rays). These relative yields were shown to depend strongly on the initial distribution.

The de-excitation of the metastable 2S state in light mesic atoms ($Z < 6$) could in principle occur either by an S type Auger process or by a mixed radiative and Auger process in which the photon carried off most of the energy[71]. The latter process would be indistinguishable from a $K\alpha$ X-ray.

From the calculations of these transition rates, the yields of the various X-rays and Auger electrons per stopped μ-meson have been determined[69, 70].

Experimental X-ray yields.

When the X-ray yields for μ-mesic atoms were measured[72], a significant difference between the theoretical and experimental X-ray yields was found. The yields for the K X-rays ($Z < 6$) and the L X-rays ($Z < 18$) were much lower than the expected values. A number of theoretical explanations were offered, but no mechanism which could de-excitate the two lowest excited levels in a non-radiative form was established. When the experiment of Stearn and Stearns[72] was repeated[76] for the elements in question, a significant increase in the X-ray yields was obtained. However the K X-ray yields in Lithium and the L X-ray yields in carbon, nitrogen and oxygen were again much lower than the theoretical values calculated using the most acceptable distribution of the initial state[69] (Table 1).

However, although the absolute yields of X-rays were much reduced for small Z, the experimental relative yields [72] [76] [77]

TABLE 1

The Yield of L X-rays Per Stopped μ-Meson.

Element	C	N	O
Experimental L-Xray yield(76)	0.16 ± 0.05	0.34 ± 0.03	0.32 ± 0.03
Theoretical values of the L-X ray yield (69)	0.51	~ 0.56	0.61

appear to be in agreement with the theoretical yields calculated for one particular initial distribution (i.e. the distribution of $(2\ell + 1)e^{a\ell}$, $a = 0.2$ for each ℓ state of the $n = 14$ level(69).

The low L X-ray yields in atoms where the K X-ray yields were nearly 100 per cent made the process by which the 2p state was populated difficult to understand. It would appear that the μ-meson must arrive in the 2p state by some non-radiative process of the Auger type. However the number of observed Auger electrons of the correct energy is far too small to accommodate such a process. Thus the population of the 2p state in light mesic atoms ($Z < 8$) remains unexplained, as no initial population distribution of the $n = 14$ level could produce such low L X-ray yields(78).

Experimental Auger electron yields.

Low energy electrons associated with μ-mesic atoms have been observed by several experimenters in both nuclear emulsion (79-83) and in a diffusion cloud chamber[84]. The electrons have been interpreted as Auger electrons. In all these experiments the short range of the electrons makes an accurate determination of their energy difficult. In the emulsion technique the range straggling amounts to some 25 per cent.

The results of the more quantitative experiments using nuclear emulsions are tabulated (Table 2). The values were those obtained from observing stopped μ-mesons (i.e. not decaying), whereas the results of experiments where Auger electrons were observed associated with μ - e decays are shown in Table 3. The energy distributions of the Auger electrons are available in certain cases[80, 81, 83]. Thus the yields of Auger electrons having energies > 30 keV have been determined (last row of Table 2, last two rows of Table 3), in order to compare different experiments. Any difference in the initial criterion used to determine whether an Auger electron had occurred, would have little effect at this energy (30 keV).

A nuclear emulsion consists of two groups of elements, a light element group (H, C, N, O) and a heavier element group (Ag, Br). Fry[81] suggested that those μ-mesons which were absorbed (i.e. did not decay) were captured by silver or bromine mesic atoms, whereas those which did decay, had previously formed mesic atoms in the lighter element group. His estimate

TABLE 2

Auger electrons associated with stopped μ-mesons

	No. of stopped μ	No. of Auger electrons	Energy Range E keV.	No. of Auger electrons per stopped μ.
Fry, 1951	200*	72	$15 < E < 70$	0.36 ± 0.04
Fry, 1953	610	348	$10 < E < 100$	0.57 ± 0.03
Fry, 1951	200*	28	$30 < E < 70$	0.14 ± 0.03

TABLE 3

Auger electrons associated with decaying μ-mesons.

	No. of decaying μ-mesons	No. of Auger electrons	Energy Range E keV.	No. of Auger electrons per captured μ-meson.
Fry, 1953	358	17	$10 < E < 100$	0.047 ± 0.010
Persner et al., 1961	1000	5	$30 < E < 200$	0.005 ± 0.002
Vaisenberg et al., 1962	10,000*	166	$5 < E < 200$	0.017 ± 0.001
Fry, 1953	358	0	$30 < E < 200$	< 0.003
Vaisenberg et al., 1962	10,000*	133	$30 < E < 200$	0.013 ± 0.001

* estimated number of events.

TABLE 4

Yields of Auger electrons per captured μ-meson in both Ag and Br atoms and CNO group, using each particular experimenter's interpretation.

	Ag & Br mesic atoms	Energy range (kev)	CNO Mesic atoms	Energy range (kev)
Fry, 1953	0.57 ± 0.03	10 < E < 100	0.047	10 < E < 100
Pevsner, et al. 1961	0.04 ± 0.02	30 < E < 200	0.002	30 < E < 200
Vaisenberg et al., 1962	0.22 ± 0.02	5 < E < 200	0.004	5 < E 200
Fry, 1951	0.14 ± 0.03	30 < E < 200		
Vaisenberg et al., 1962	0.19 ± 0.02*	30 < E < 200		

* estimated by the author rather than the original experimenter.

TABLE 5

Theoretical yields of Auger electrons per captured μ-meson in Ag and Br mesic atoms.

	Ag and Br mesic atcms	Energy range E keV	Type of Calculation
de Borde, 1954	0.20	30 ≤ E < 200	$(2\ell+1)$ status
Eisenberg & Kessler, 1961	0.22	30 < E < 200	$(2\ell+1)$ status

of the Auger yield for Ag and Br atoms and CNO atoms was made on this basis. (Hydrogen mesic atoms were not formed as the μ-meson would be transferred to one of the light element groups in the gelatine of the emulsion).

In more recent experiments, where Auger electrons have been observed associated with decaying μ-mesons, Pevsner et al.[82] and Vaisenberg et al.[83] have estimated that 60 per cent and 85-90 per cent respectively, of these Auger electrons must be attributed to heavy mesic atoms. Vaisenberg et al. estimated their figure for two reasons. 1) The energy distribution of the Auger electrons was similar to that expected for Ag and Br atoms from theoretical calculations. 2) Only two Auger electrons which satisfied their selection criterion were observed to have originated from 500 μ-meson stars in the light element group.

The Auger yields per captured μ-meson using each particular experimenter's interpretation have been summarised (Table 4). In the last two rows the yields for Auger electrons with energies greater than 30 keV have again been estimated.

A considerable degree of diversity exists, both in the experimental results and interpretation, where Auger electrons were observed associated with decaying μ-mesons, as can be seen by comparing the different values of the yield for the same energy range ($>$ 30 keV) (see the last column of Table 3).

Where μ-mesons were absorbed by a nucleus, it would appear reasonable to assign the Auger electrons to silver and bromine mesic atoms, as few of the μ-mesons will be absorbed by the lighter elements. If the interpretation of Vaisenberg was

correct (i.e. that 90 per cent of all Auger electrons associated with μ - e decays originated from Ag and Br atoms), then reasonable agreement exists between these results and those of Fry[80] for the energy range greater than 30 keV (Table 4). However, the theoretical yields (Table 5) for Ag and Br atoms are significantly larger than those of Fry's experiment[80] and nearly one order of magnitude greater than the results of Pevsner et al.[82]. (The relatively lower yields of Vaisenberg[83] in the energy range > 5 keV might be expected, as a more strict criterion for the selection of an Auger electron was used, compared with the others.)

Note on the estimation of Auger yields.

1) In Vaisenberg et al.'s experiment one out of fifteen decays were attributed to a μ-meson originally bound to an Ag or Br atom. One in sixty decaying μ-mesons had an associated Auger electron. As they have demonstrated that at least 75 per cent of all their Auger electrons originated from heavy mesic atoms, an even greater percentage would be expected for those electrons with energies > 30 keV. If all the electrons in this energy range are associated with Ag and Br mesic atoms, then from Vaisenberg et al.'s results, 133 Auger electrons should be assigned to approximately 4 x 166 mesic atoms. (The yield obtained from these values represents an upper limit, as any electrons not associated with Ag and Br have been included).

2) The 17 Auger electrons associated with 358 μ - e decays in Fry's experiment[81] were all considered to originate from light mesic atoms. However, if one in fifteen decaying mesons occur from heavy mesic atoms, then some 24 of these events should have been associated with Ag or Br mesic atoms. As 0.57 Auger electrons per stopped meson were observed (i.e. the yield for Ag or Br atoms), then 14 of these electrons must be attributed to the heavy group. Only the remaining three electrons would have been associated with mesic atoms of the light element group. The correct yield for Auger electrons per stopped mesic atom in the C, N, O group would be of the order of 0.01, if this correction were to be applied.

Auger electrons from μ-mesic atoms have been observed in a hydrogen filled diffusion cloud chamber[84]. The small admixture of carbon and oxygen atoms (in the form of alcohol condensant) was large enough to capture some of the μ-mesons originally bound to protons.

When the chamber was filled with 5 atmospheres of hydrogen, 10 Auger electrons were observed associated with 40 decaying μ-mesons. Three or four of these electrons appeared to have energies greater than 10 keV. As not all the μ-mesons were expected to be captured by a carbon or oxygen atom, a 3 per cent contamination of carbon dioxide was added to the chamber when at a pressure of 22 atmospheres of hydrogen. In this experiment 90 per cent of the μ - e decays had an associated

Auger electron.

As 95 per cent of the μ-mesons in this latter experiment were expected to be transferred to a carbon or oxygen atom before decaying, a very tentative estimation of the yield can be made. At least 90 per cent of μ-mesic carbon or oxygen produced an Auger electron of energy greater than 5 keV (if they were to be observed at 22 atmospheres of hydrogen), whereas just less than 30 per cent have Auger electrons with energies $>$ 10 keV.

The theoretical Auger electron yields[70] per captured μ-meson in carbon and oxygen together with the energy of the appropriate transition are shown (Table 6). An energy greater than 10 keV would most likely correspond to the L transition in both carbon and oxygen, whereas those of approximately 5 keV to the M transition.

As the number of events is small, the statistics of the experiment are necessarily poor, but the experimental yields (Table 7) appear to be at least as large as those calculated on the basis of capture in $\ell = n - 1$ states only (i.e. the calculation which would give the highest value for the yield).

Perhaps of greater significance is the large yield of this experiment compared with that of Fry[81] for light mesic atoms. The quoted yield of Fry is about five times smaller, whereas the corrected yield is at least one order of magnitude less than that computed from the observations in a diffusion cloud chamber[84].

TABLE 6

Theoretical Auger Electron Yields for the K, L and M transitions in Carbon and Oxygen[70]

Element	K yield	Energy (keV)	L yield	Energy (keV)	M yield	Energy (keV)
C	0.0012	77	0.256	14	0.91	4.8
O	0.0004	136	0.110	25	0.79	8.5

TABLE 7

Approximate experimental yields[84] of Auger electrons in Carbon and Oxygen

L yield	M yield
0.27	0.90

Conclusions concerning the X-ray and Auger electron yields.

In experiments expressly conducted to determine the X-ray and Auger electron yields per captured μ-meson in light mesic atoms ($Z < 8$) disagreement with the theoretical predictions has been recorded. These predictions are based on well established quantum mechanics. However, although the X-ray yields have been determined with some precision and agree in some respects with theory, the unexplained low yields in the lighter atoms still exist. As far as the Auger electron experiments are concerned, their results are less accurate and even inconsistent with each other as has been suggested by Condo et al.[85] and demonstrated in some detail in the last section.

In nearly all the nuclear emulsion experiments, the Auger electron yields are significantly smaller than the predicted rates, the disagreement being worse for lighter mesic atoms. Only when Auger electrons were observed in a diffusion cloud chamber[84] is the yield near to the theoretical value. However, the formation of the μ-mesic atom in this experiment[84] differs from that of the nuclear emulsion variety. The μ-meson is first bound to a proton and then transferred to either carbon or oxygen at the much lower quantum level of $n = 4$ or 5. As the energy available from this transfer process is of the order of 2 keV, it might be argued that some of the apparent Auger electrons occur during transfer and are not true Auger electrons caused by the de-excitation of the μ-mesic atom.

If the above consideration can be disregarded, the de-excitation would follow in an exactly similar manner to that of the normal mesic atom formed in a high state of excitation, the

only possible differences being in the actual population distribution of the $n = 4$ or 5 levels.

CHAPTER 6

THE AUGER ELECTRON YIELDS FROM μ-MESIC ARGON

Introduction

In an experiment[2] performed at Liverpool Nuclear Physics Laboratory negative μ-mesons from the cyclotron were stopped in the high pressure cloud chamber with a filling of 58 atmospheres of argon. Some 66 stopped μ-mesons were observed with no decay electrons. These events were used to determine the Auger electron yield produced during the de-excitation of μ-mesic argon.

Approximately, in one in every ten μ captures, an Auger electron of 45 keV energy should have been produced, whereas about half the μ-mesic atoms should have yielded electrons of 19 keV. Auger electrons of greater energy ($>$ 45 keV) were not expected in this number of events. If the Auger yield was to be measured, a method of detecting electrons of some 20 keV at the ends of μ-meson tracks would have to be developed. Although the range of such an electron in 58 atmospheres of argon is too small to produce an obviously visible track, the ionisation caused by this electron should be sufficient to increase the thickness of the μ-meson track at the stopping point.

A measurement of the μ-meson track thickness very close to its end point, together with a measurement of the track thickness at the very end of the track, was performed on examples of stopping μ-mesons, using a Cambridge Universal

Measuring Microscope. When the end thickness was significantly greater than the track thickness close to the end, then it was assumed that an Auger electron had occurred.

The energy of these Auger electrons was estimated by measuring the magnitude and frequency of knock-on electrons which were produced by μ-mesons traversing the chamber gas. The extent of the ionization produced by such electrons should have been similar to that of Auger electrons of the same energy.

Although it was possible by this microscope method to record both the existence and approximate energy of Auger electrons from μ-mesic atoms, some doubt concerning the validity of these results was inferred by a second less subjective method which gave a negative result.

Microscope Measurements

Two photographs of each event were recorded on the same film by the stereoscopic camera, the optical arrangement of which is shown (Fig. 1). The film containing the two views of a stopped μ-meson track, was clamped between the glass plates of the travelling microscope and the end point of the track located on the eye-piece crosswires. The distance D between the end points of the track on each view was measured, thus determining the magnification at that position.

Measurements of the track thickness was made by successively placing one of the crosswires along both edges of the track as near to the end point as was possible. Any increase in ionization at the very end of the track fell outside the region defined by

FIG I

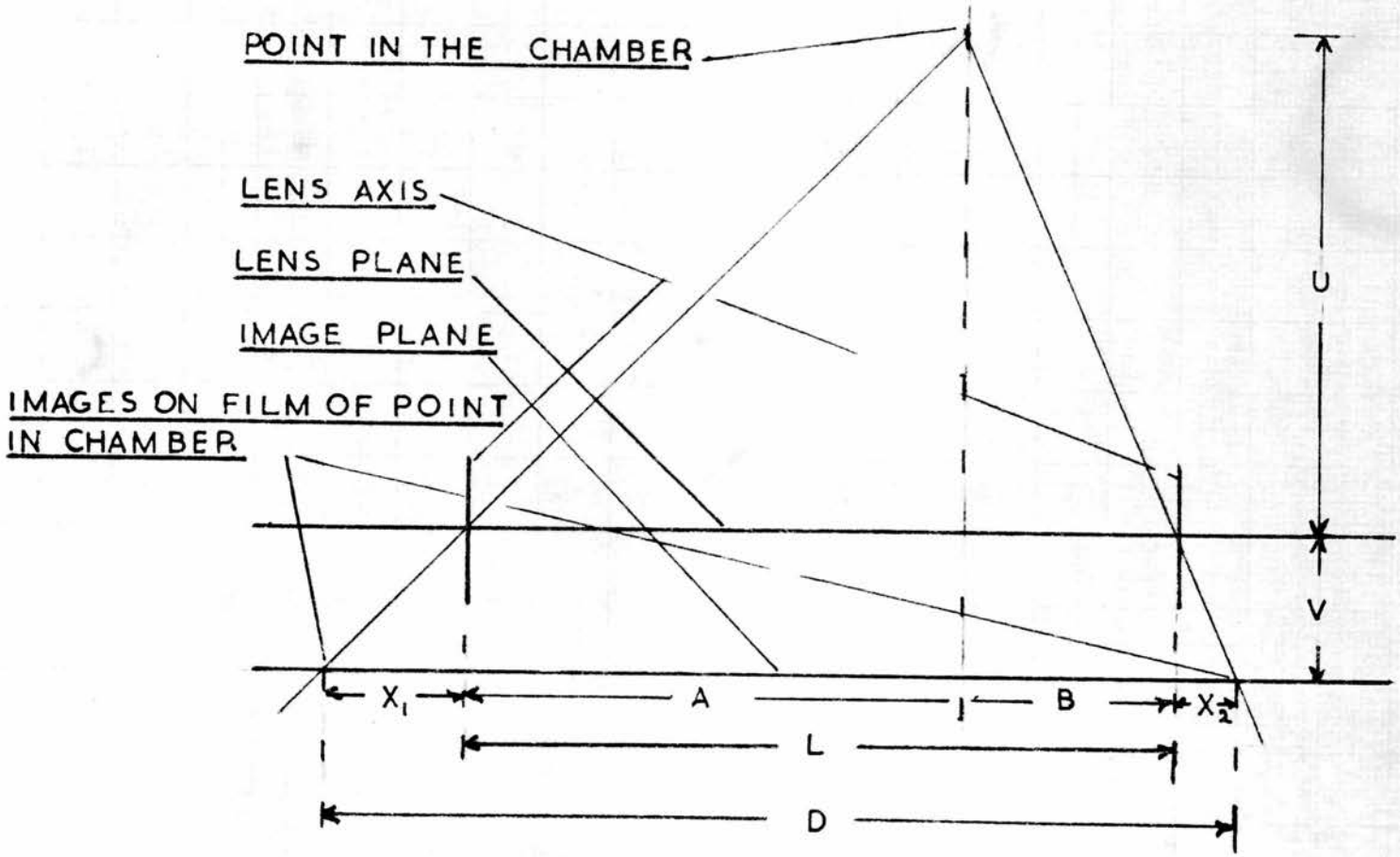

MAGNIFICATION $= V/U = X_1/A = X_2/B = M$

$(X_1 + X_2) = M(A+B)$ $\qquad M = (X_1+X_2)/(A+B) = (D-L)/L$

the two crosswire settings. This increase, where it occurred, appeared in the form of a roughly spherical blob of ions superimposed on the end of the μ-meson track. The diameter of this blob, measured at right angles to the μ-meson direction, was used to determine its magnitude.

Before an event was selected for analysis, measurements were made on both views. (In some cases, one view was obscured by another track.) Further events were rejected, if either the presence of heavy background cloud or poor illumination were sufficient to impair satisfactory measurement.

Track thickness measurements

The measured track thicknesses, recorded from one camera view, are shown in a graphical form (Fig. 2) plotted against the coordinate (D - L) which is proportional to the magnification. The errors shown on the graph were the resetting errors recorded on the travelling microscope ($\pm$ 0.0005 cm). A number of proton tracks, distinguished from μ-meson tracks by their range-track thickness properties, are also shown on the same diagram (Fig. 2). The measurements from this camera view and the (D - L) values are recorded in Table 1.

The track thickness measurements which did not lie on the curve were most probably caused by one of three effects. 1) A different intensity of background cloud. 2) Differing illumination from one position to another. 3) Differing times between the entrance of the particle into the chamber and photography. If measurements had been performed on tracks subjected

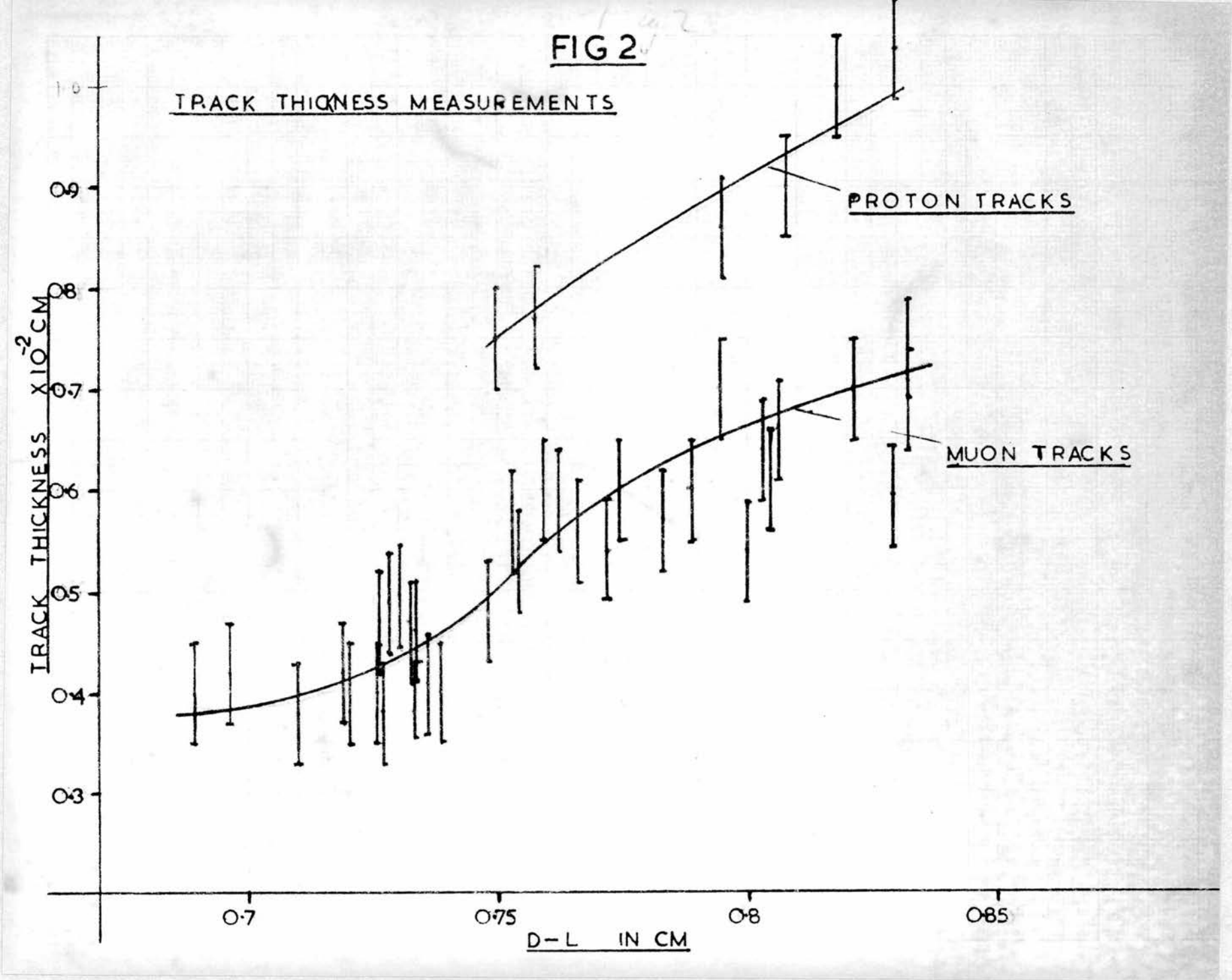
FIG 2
TRACK THICKNESS MEASUREMENTS
PROTON TRACKS
MUON TRACKS
TRACK THICKNESS X10^{-2} CM
0·9
0·8
0·7
0·6
0·5
0·4
0·3
0·7
0·75
0·8
0·85
D-L IN CM

TABLE 1

Event No.	Track thickness x 10^{-2}cm.	End thickness x 10^{-2}cm.	D - L x 10^{-1}cm.	Standardized end thickness x 10^{-2}cm.
1	0.38	0.53	7.098	0.67
2	0.60	0.76	7.892	0.60
3	0.38	0.38	7.268	
4	0.59	0.84	7.624	0.75
5	0.60	0.95	7.587	0.86
6	0.47	0.47	7.318	
7	0.46	0.46	7.338	
8	0.48	0.79	7.480	0.79
9	0.40	0.60	7.235	0.72
10	0.47	0.47	7.232	
11	0.53	0.60	7.543	
12	0.59	1.09	8.296	0.85
13	0.41	0.63	7.359	0.71
14	0.40	0.60	6.889	0.77
15	0.74	1.26	8.318	0.87
16	0.57	0.69	7.836	
17	0.64	0.64	8.029	
18	0.60	0.60	7.884	
19	0.49	0.49	7.284	
20	0.66	0.66	8.069	
21	0.69	0.91	8.327	0.63
22	0.70	0.94	8.206	0.67
23	0.46	0.94	7.333	1.03
24	0.40	0.58	7.200	0.71
25	0.38	0.55	7.333	0.63
26	0.54	0.74	7.988	0.61
27	0.57	0.79	7.527	0.76
28	0.42	0.42	7.188	
29	0.42	0.70	6.959	0.90
30	0.54	0.54	7.721	
31	0.56	0.98	7.661	0.86
32	0.50	0.67	7.300	0.78
33	0.70	1.15	7.942	0.88
34	0.40	0.40	7.385	
35	0.60	0.60	7.744	
36	0.61	0.79	8.041	0.60

to identical conditions, all the points would be expected to lie on the curve.

Increases in ionization at the ends of the tracks

If, in both views, an increase in ionization at the end of the track was measured which was 0.0015 cm greater than the track thickness on the film, then this was considered significant, as it represented three times the resetting error. However, it was accepted that the adoption of this criterion might produce a bias against detection of ionization increases at the ends of those tracks in positions of low magnification. In the 36 events analysed an increase in ionization was recorded in 22 cases.

In order to compare these blob sizes (increases in ionization) a two stage procedure was used. As it was assumed that all tracks at the same $D - L$ value should have the same thickness, those blob sizes which were associated with track thicknesses whose error did not include the curve (Fig. 2), were multiplied by a scaling factor sufficient to bring the track onto this curve. These corrected measurements were then multiplied again by the ratio y_1/y_2 to standardize the sizes to their expected value corresponding to a position of $D - L = 0.75$ cm.

y_1 = track thickness at $D - L = 0.75$ cm.

y_2 = track thickness at the $D - L$ value for the relevant blob.

Both the ordinates y_1 and y_2 were measured from the curve (Fig. 2).

These standardized blob sizes are shown in a histogram form

(Fig. 3) where the number of blobs, in groups of 0.0010 cm are plotted.

Reprojection Machine measurements

The events which had previously been measured on the microscope were reprojected using the same apparatus as had been used for multiple scattering measurements[51]. In each event, the track thickness was measured at the stopping point, together with measurements of thickness at each 0.25 cm along the last 1 cm of the particle range. The measurements were obtained by placing the point of the pin of the reprojection machine successively at each edge of the track, the displacement being recorded by a micrometer screw gauge.

Using this technique, track thickness of the order of 0.030 cm to 0.060 cm were obtained to an accuracy of $\pm$ 0.005 cm, where the error was again a resetting error. The average thickness of twenty tracks at the four points in the last 1 cm of range showed that no significant increase in thickness occurred in this distance (Table 2).

If the thickness recorded at the end of the track was greater than 0.01 cm of the average track thickness obtained from the four points in the last 1 cm, then it was assumed that a significant thickening had occurred.

When a blob of ionization had been recorded from the microscope set of measurements, then a corresponding increase was found when using the reprojection machine. Complete consistency between the two sets of results was obtained after

FIG 3

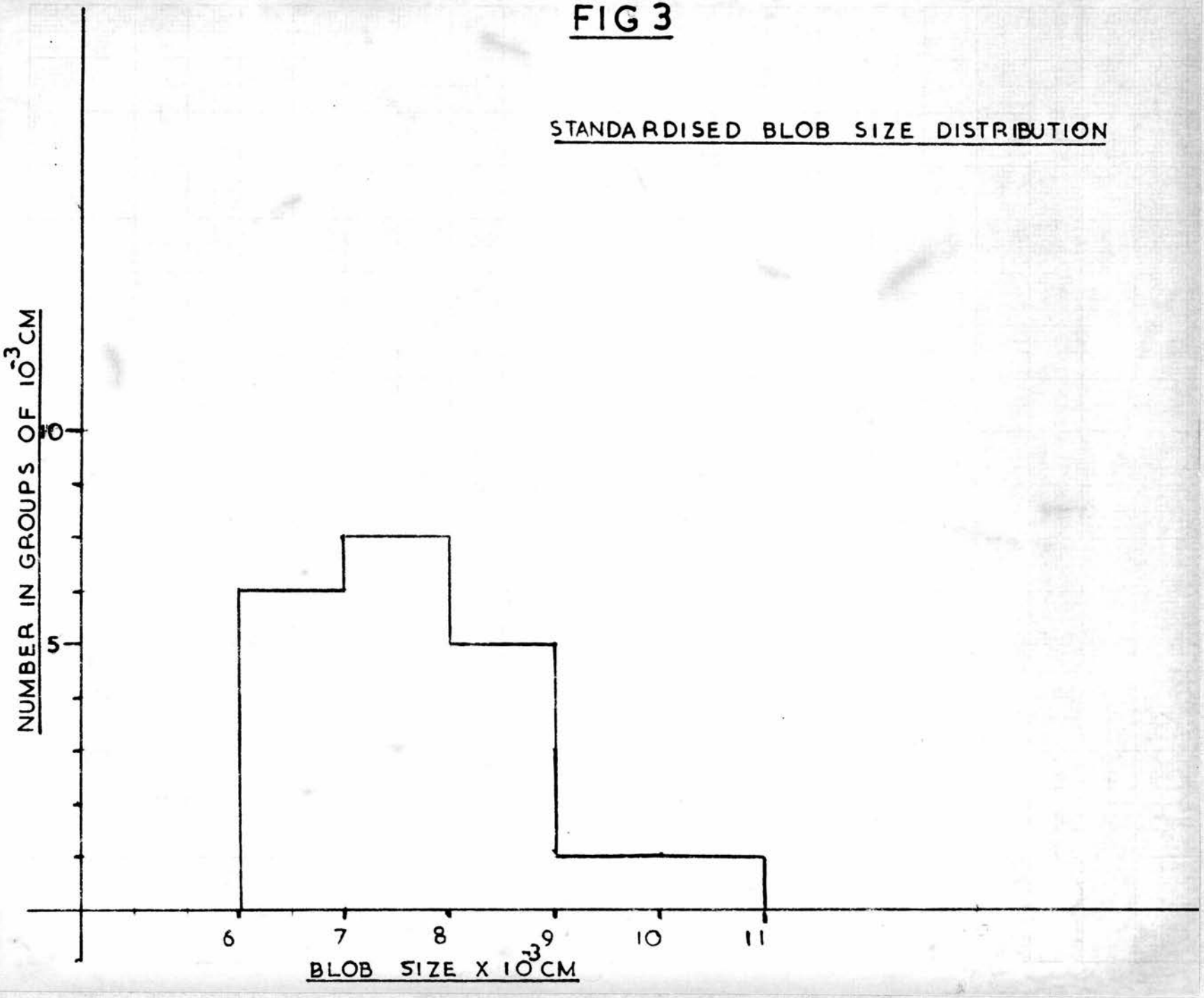
STANDARDISED BLOB SIZE DISTRIBUTION
NUMBER IN GROUPS OF 10^{-3}CM
10
5
6
7
8
9
10
11
BLOB SIZE X 10^{-3}CM

TABLE 2

Distance from the end of the track in cm.	0.25	0.5	0.75	1.0
Average track thickness ($\times 10^{-1}$ cm.)	0.452 ± 0.029	0.445 ± 0.026	0.444 ± 0.033	0.445 ± 0.028

remeasurement of two events which came close to the limit of the criteria.

However these results were only used to check the microscope measurements, as more consistent results were expected from that technique. The image obtained using the microscope was generally sharper, and the crosswire settings, rather than the point of a pin settings, were expected to yield better track thickness measurements.

Energy corresponding to the increases in ionization measured

An energy relationship for the blob sizes (Fig. 3) was obtained in the following manner. When a charged particle of energy E passes through a given thickness of matter, the probability, $\theta(E, E')dE'$, that an energy between E' and $E' + dE'$ is transferred to an atomic electron can be expressed as[87]

$$\theta(EE')dE' = K \frac{m_e c^2}{\beta^2} \frac{dE'}{E'^2} \qquad (1)$$

provided E' is small compared with E. $K = 0.0142$ in argon at 58 atmospheres, where $\theta(E, E')dE'$ is then the probability per centimetre of track.

Thus the number N of knock-on electrons per centimetre of path between energies E_1 and E_2 may be obtained by integrating equation (1)

$$N = K. \frac{m_e c^2}{\beta^2} \left(\frac{1}{E_1} - \frac{1}{E_2}\right) \qquad (2)$$

For the energies considered in this experiment, the μ-meson had $\beta < 0.7$. The maximum transferrable energy E_M is given by

$$E_M = 2m_e c^2 \frac{\beta^2}{1 - \beta^2} \qquad (3)$$

If μ-meson tracks of known β-value were inspected for knock-on electrons, which produced blobs of ionization of equivalent size to those previously measured, then a determination of their energy could be made from the above equations.

The maximum energy of μ-mesons entering the chamber was 40 Mev, corresponding to $\beta = 0.7$. If a μ-meson, having entered the chamber, produced a knock-on electron of some considerable range, then the minimum β-value for that track could be estimated from equation (3).

Three μ-mesons, which exhibited relatively long δ-rays were found, for which equation (3) set the lower velocity limit for the particles of $\beta = 0.5$ for two and $\beta = 0.65$ for the third. An average value of $\beta = 0.60$ for the three tracks was assumed to be reasonable. An attempt to measure their velocities by multiple scattering measurements gave results which were inconsistent with the above argument for two out of the three tracks. The poor results of the multiple scattering measurements were expected to be caused by track distortion which was sufficient to impair momentum measurements greater than $p\beta = 20$ Mev/c[2]. Thus no better estimation than the assumed average value of $\beta = 0.60$ could be achieved.

The numbers and sizes of knock-on electrons along these tracks were recorded using the measuring microscope, together

with the corresponding value of D (Fig. 1). The smallest size of δ-ray measured was that which produced a blob of ionization just greater than 0.0015 cm of the local track thickness.

The sizes of these knock-on electrons were standardized in a similar manner to the blobs observed at the ends of the stopped μ-meson tracks to a value of $D - L = 0.75$ cm. (It was not possible to use the first stage of the procedure as the tracks of particles with $\beta = 0.6$ would not be expected to have the same track thickness as those with nearly zero velocity.) This set of measurements and calculations are listed (Table 3).

Thus 41 knock-on electrons, which produced ionization in the form of short tracks or blobs of diameter greater than 0.0060 cm, were observed in 48 cm. of track.

Hence, using equation (2) and a velocity of $\beta = 0.60$, blobs having diameters $\geq$ 0.0060 cm. have energies $\geq 23 \pm 4$ keV or blob diameters $\geq$ 0.0080 cm. energies $\geq 41 \pm 6$ keV.

Thus an approximate relationship concerning the blob size produced at the ends of μ-meson tracks in terms of energy was established.

Origin of the blobs of ionization produced at the ends of μ-meson tracks.

It has been established that in more than 50 per cent of the cases of negative μ-mesons which stopped in argon, an increase in ionization at the end point was observed, which corresponded

TABLE 3

Knock on Electrons

Event	(10^{-2} cm) 40		(10^{-2}cm) 41		(10^{-2}cm) 42	
	(1)	(2)	(1)	(2)	(1)	(2)
	0.70	0.70	0.65	0.69	1.29	>1.00
	0.65	0.65	0.50	0.53	>1.00	>1.00
	0.92	0.92	0.90	0.96	>1.00	>1.00
	0.75	0.75	0.66	0.70	>1.00	>1.00
	>1.00	>1.00	0.80	0.85	0.82	0.70
	0.75	0.75	0.55	0.59	0.96	0.81
	>1.00	>1.00	0.81	0.86	1.34	>1.00
	0.80	0.80	0.98	>1.00	0.82	0.70
	0.76	0.76	0.96	>1.00	>1.00	>1.00
	0.63	0.63	>1.00	>1.00	0.98	0.83
	>1.00	>1.00	0.70	0.74	0.81	0.69
	1.05	L.05	0.65	0.69	0.99	0.84
	0.65	0.65	0.75	0.80	0.76	0.64
	0.76	0.76			0.89	0.75
					0.97	0.82
					1.08	0.91

(1) - Measured size of knock-on electrons.

(2) - Standardized size of knock-on electrons at D - L = 0.75 cm.

to an electron of energy greater than $\sim$ 20 keV.

The possibility that these observed electrons were knock-on electrons can be eliminated. The velocity of the μ-meson 0.1 cm. from the end of its range in these experimental conditions, was of the order of $\beta = 0.1$. The maximum energy of a knock-on electron would only be 10 keV. As the measurements of the blob diameters were made nearer to the end of the track than 0.1 cm., only a small contribution to the increase in ionization was expected from this source.

The thickening at the end of a track could have been caused by a μ-meson undergoing a large angle scatter close to the end point. However, the probability of a μ-meson, $\beta = 0.1$, being scattered through an angle of greater than 30° in a distance of 0.1 cm. is $\sim 1.5 \times 10^{-4}$ when calculated from the appropriate scattering formula[87]. Thus this effect was too small to be significant.

No effect, other than the existence of Auger electrons, could be established to explain the increase in ionization produced at the end points of μ-meson tracks. In 22 events out of the 36 analysed, Auger electrons having energy approximately $>$ 20 keV were observed. Thus the yield of Auger electrons per stopped μ-mesic atom was 0.61 ± 0.13 for energies $>$ 20 keV.

Discussion of the results

Some of the properties of μ-mesic argon are listed (Table 4) where the transition rates quoted are those between states n, n-1, $\rightarrow$ n-1, n-2 . The resulting yield of Auger electrons/

TABLE 4

Properties of μ-mesic Argon

Transitions of the form (n, n-1) → (n-1, n-2).

n	3	4	5	6
Energy of Transition (keV)	130	45	19	8.5
Radiative Rate (per sec)	1.5×10^{15}	3.7×10^{14}	1.2×10^{14}	4.0×10^{13}
Auger Rate (per sec)•	7.8×10^{12}	4.8×10^{13}	1.6×10^{14}	3.8×10^{14}
Auger Yield per stopped μ-meson	0.005	0.11	0.57	0.91

Yield of Auger electrons of energy > 19 keV = 0.68.

stopped μ-mesons, with energies $\geq$ 19 keV is 0.68 for μ-mesic argon. (The more realistic initial distribution of the initial n = 14 state computed by de Borde[64] and Eisenberg & Kessler[69] produced a yield of 0.61 for Auger electrons of energy $>$ 20 keV for μ-mesic bromine and silver, compared with 0.68 when calculated by the simpler theory[70].) As the difference between the yield predicted by the two theories became less with decreasing atomic number, a crude estimation of 0.62 Auger electrons/stopped μ-mesons for energies $\geq$ 19 keV was made for μ-mesic argon, if it were to be calculated using the more realistic initial distribution of the initial state n = 14. This experimental yield was in significantly better agreement with the theoretical prediction, than any of the nuclear emulsion experiments for the same electron energy range.

Comments on the method:

1) The adoption of the criterion - namely that the blob size had to be greater than the track thickness by 0.0015 cm., might have produced a bias in favour of selection of blobs on tracks where the magnification was large, (i.e. D - L = 0.8 cm). However, increasing this lower limit to 0.0020 cm. for tracks where D - L $>$ 0.75 cm. eliminated only two events, reducing the total number of observed Auger electrons to twenty.

2) The standardized blob sizes were dependent on the shape of the curve (Fig. 2). However an inspection of those blobs whose magnitude is $>$ 0.0080 cm. showed them to be equally distributed

throughout the chamber, with no preference for one region of D - L, indicating no obvious distortion produced by this process.

3) The histogram (Fig. 3) shows no peaks at the two transition energies 19 keV and 45 keV). In view of the variety of conditions under which the measurements were conducted, together with the relatively small effect detected, resolution of the two peaks could hardly be expected.

4) Due to the presence of track distortion, the velocities of the monitoring particles were not determined with any great precision. However, using a maximum value of $\beta = 0.7$ and minimum $\beta = 0.55$, then the blob sizes $\geq$ 0.0060 cm. correspond to energies $\geq$ 17 and 27 keV respectively. Both these values are reasonably consistent with the assumption that the observed Auger electrons originated from the 19 and 45 keV transitions.

5) The energies of the Auger electrons, when deduced from the magnitudes of knock-on electrons, appeared to be slightly greater than expected. However, the blob size of the lowest energy electrons (20 keV) might not be independent of the local track width, as measurements inevitably involved the combined effect of track width and blob size. Thus for a thicker track, the blob would appear larger for a given energy. The estimated blob size of 0.0060 cm. for electrons having energies $\geq$ 20 keV, when measured on the track of a particle with $\beta = 0.6$, might be too small when used to compute the energies of electrons occurring at the end points of stopped particles, where the measured track thickness was $\sim$ 20 per cent larger.

6) The existence of 20 keV Auger electrons at the end point of μ-meson tracks has been inferred from thesemicroscope measurements. If an increase in ionization was actually present, it should be possible to detect it by a less subjective method than that of measurements performed directly by the human eye.

Examples of tracks with which 20 keV electrons were apparently associated were analysed on a microdensitometer. No increase in track thickness at the end points could be detected from the densitometer traces obtained from appropriate regions of the track. Further, when a contour map of the structure of the ionization of one of these tracks was obtained from an isodensitometer trace, again no indication of a low energy electron was apparent. Local increases in thickness along the μ-meson track (Fig. 4) are visible and must correspond to knock-on electrons. However, no such increase at the end-point is visible.

Thus either it must be assumed that the microscope method was considerably more sensitive than the densitometer readings, or the validity of the former method was suspect. As the quoted sensitivity of the isodensitometer was not much less than that of the microscope, then some doubt must exist concerning the interpretation of the microscope measurements.

Suggested experiments to determine the μ-mesic Auger electron yields in gaseous elements.

The magnitude of the ionization produced by the Auger electrons (< 50 keV energy) was the most serious limitation of the technique previously described.

FIG 4

ISODENSITOMETER TRACE OF MUON TRACK

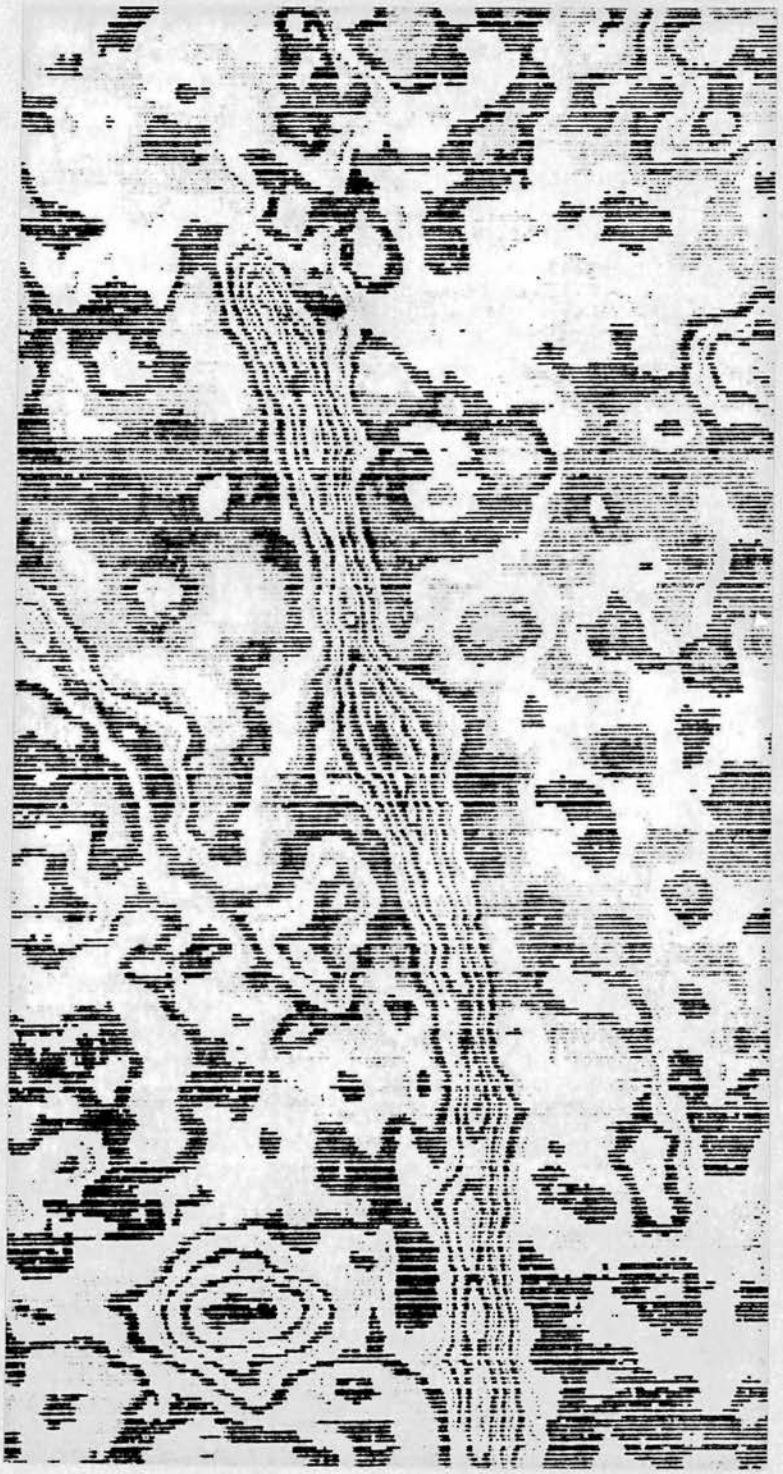

MUON TRACK

MAGNIFICATION X100

FIG 5

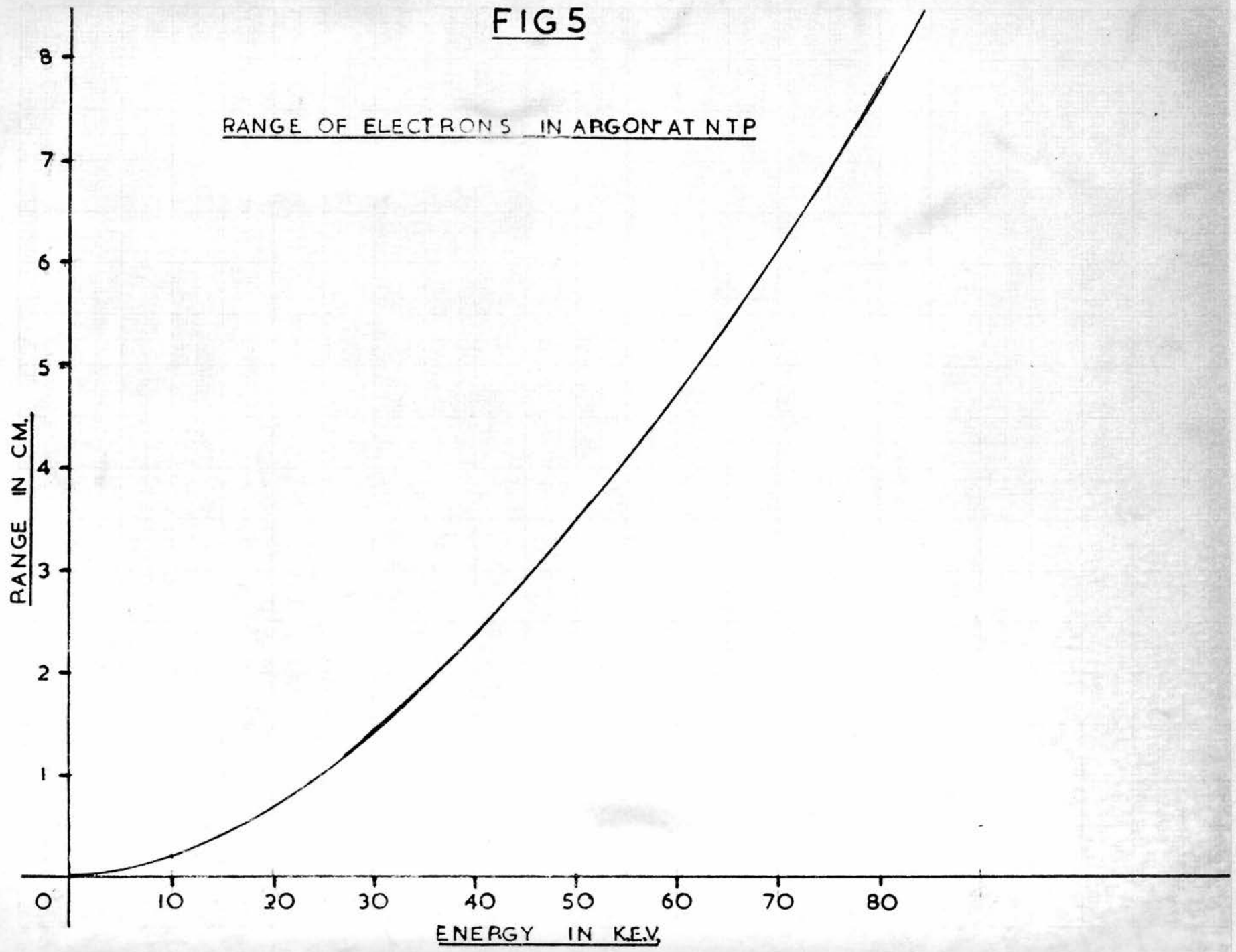
RANGE OF ELECTRONS IN ARGON AT NTP
RANGE IN CM.
0
1
2
3
4
5
6
7
8
10
20
30
40
50
60
70
80
ENERGY IN K.E.V.

It would be desirable to reduce the stopping power of the chamber gas to such an extent that the Auger electrons had a readily observable range. The range-energy curve (Fig. 5) for electrons in one atmosphere of argon indicated that energies, of the order of 5 keV, could be measured, if a minimum range of 0.1 cm. was considered as a lower limit. By increasing the pressure to 4 atmospheres, only electrons having energies > 15 keV would have this range or greater. Any lower energies could only be estimated by track thickness method.

Although a considerable increase in the energy resolution of electrons would be expected at this pressure (4 atmospheres), only 4 μ-mesons would stop in an equivalent run with a cyclotron, to that conducted in the high pressure cloud chamber. (In this experiment[2] 66 μ-mesons were stopped at a pressure of 58 atmospheres). Assuming a recycling time of one minute for a chamber at 4 atmospheres pressure, then a 50 hour run with a cyclotron would be required to obtain an Auger electron yield of the same statistical accuracy.

Only a small gain would be expected in the rate with which information could be gathered by increasing the volume of the chamber. Not only would it be difficult to operate a large expansion cloud chamber, but also the recycling time would be increased in proportion to its dimensions. The possibilities of using a counter control technique have been discussed, and if such a method could be rendered sufficiently efficient, then a considerable gain might be achieved.

The limitation of small dimensions and slow recycling time

do not however apply to diffusion cloud chambers. Although limited with a filling or argon, to a pressure of 2-3 atmospheres, a one metre long diffusion chamber operated at a cycling speed of 10 photographs/minute, would record approximately 5 times as many stopped μ-mesons as the 60 atmosphere expansion chamber in an equivalent time. Not only could the Auger yields be measured in argon, but also in the more interesting cases of oxygen and nitrogen, where most of the experimental values for both μ-mesic X-rays and Auger electron yields are in poor agreement with theory.

It has been demonstrated experimentally that when μ-mesons were stopped in a target of hydrogen with a small contamination of a heavier element, then the μ-meson has a very large probability of being transferred to the atom of the heavy element. Auger electron yields could be measured for elements which can be produced in a gaseous form, by adding a small percentage of the gas to a hydrogen filled chamber, provided the chemical properties of the gas do not impair the operation of the chamber. However, as the capture of the μ-meson by the heavier atom would be from a proton - μ-meson atom, rather than the simple capture of an unbound μ-meson, difficulties of interpretation might arise, if the exact nature of the transfer process were not understood.

Finally, the variable stopping of a cloud chamber, together with the simplicity of studying one type of mesic atom at a time, are distinct advantages over the nuclear emulsion technique.

CHAPTER 7

DIRECT PAIR PRODUCTION BY μ-MESONS

Introduction

Theoretical cross-sections for direct pair production by charged particles of spin ½ have been calculated by several authors[88-90] using classical quantum electrodynamics. Although initially the cross-sections obtained from alternative calculations differed, improved approximations made by Bloch et al.[91] indicated agreement between the theories. More recently, the differential and total cross-sections for direct pair production have been calculated by Murota et al.[92] using the Feynman formalism. Further calculations of the cross-sections from this theory for μ-meson have been made by Stoker and Haarhoff[93] and Roe and Ozaki[94].

An indefinite parameter α, which resulted from the cut-off factor in the momentum transfer from the primary particle , was introduced into the theory by Murota et al. The value of the cross-section could be altered by as much as 30 per cent by making reasonable changes in the magnitude of this parameter.

Several experiments[94-97] have been performed to investigate direct pair production by incident μ-mesons, in which multiplate cloud chambers were used. In these experiments incident μ-mesons, which caused electron showers by the processes of 1) knock-on electrons, 2) Bremsstrahlung, and 3) direct pair production, were observed in the cloud chamber. As the two

former processes were well understood, the events due to pair production could be separated from the total number, the energy transfer being calculated by shower production theory. However only the more recent experiments[96, 97] were in agreement with the predictions of Murota et al.'s theory, the two earlier experiments showing significantly different cross-sections for certain regions of energy transfer. Chaudhuri and Sinha[97] have suggested that these discrepancies were caused by fixing the low energy limit for momentum transfer at too small a value. The cross-section varies very rapidly in the region of energy transfer $\sim$ 30 Mev and any small uncertainties in energy assignment of the pairs could have produced a large error in the estimated cross-section. In one of these experiments[96] the most likely value for α was shown to be two, although the value was derived from evidence of only 24 events.

In a preliminary experiment conducted in the high pressure cloud chamber using cosmic ray μ-mesons at sea level, three examples of direct pair production were observed. An approximate experimental cross-section was obtained and shown to be in agreement with the accepted theory[92] evaluated by Stoker et al.[93]. Alternative processes, where events give the appearance of pair production were examined, together with the possibility that electrons rather than μ-mesons were the incident particles in the observed events.

Further experiments using a high pressure cloud chamber to observe this phenomena are discussed at the end of the Chapter.

Direct Pair Production in Argon

In the 5,000 photographs obtained in the argon-filled high pressure cloud chamber (Chapter 4) approximately 2 μ-meson per photograph were recorded with energies greater than 300 Mev. The quality of the tracks photographed was good enough to estimate whether they were caused by energetic incident particles by examining their straightness. It was assumed that practically all the energetic particles in the chamber were μ-mesons, provided they were not associated with cosmic ray showers. By counting the number of straight tracks (excluding those which were field separated) occurring in a randomly selected 20 photographs in each 400, a total number of 8,000 μ-mesons traversals of the 20 cm. cloud chamber were estimated to have occurred, giving a total path length of 1.6×10^5 cm.

On these 8,000 μ-meson tracks, 11 trident events were observed, in which two relatively low energy particles were produced, the incident particle continuing undeflected in its original direction. Both views of each of the 5,000 events were scanned twice for these trident events. Thus each event was effectively scanned four times, as the efficiency for observing events at this low frequency was expected to be rather poor. However on the second scan, only very low energy events were found to have been missed originally. No new events in which the energy transfer was larger than 1 Mev were found on the second scanning. It was assumed that the efficiency of scanning for trident events was thus relatively

good for energy transfers greater than 1 Mev.

All the photographs in which trident events occurred were reprojected, using the apparatus[51] previously mentioned. Where any of the secondary particles stopped in the chamber, range measurements were obtained. Multiple scattering measurements were conducted on those particles which did not stop in the chamber, their momenta in this case, being determined.

The range measurement of stopping particles was achieved by simulating the reprojected track image by a piece of wire. When a satisfactory copy of the track path had been made by manipulating the wire, it was straightened out, and its length measured. By repeated measurements of the range of one particle track, which suffered considerable multiple scattering, an estimated accuracy of $\pm$ 10 per cent was obtained for this technique of range determination.

The considerable multiple scattering of these particles, together with their low increase in ionization with residual range, indicated that they were electrons. However in one case (event 2) it was assumed that the more energetic particle was an electron, although it showed very little multiple scattering.

Thus the energies of these electrons were obtained, either from range-energy values or from the momentum determination. The energy values obtained are shown (Table 1) together with a photograph of one event (Fig. 1).

It was necessary to estimate the number of events giving the appearance of a trident which were not electron-positron

TABLE 1

Event Number	E_1	E_2	E
1	2.0	0.2	2.2
2	1.2	$40\ ^{+26}_{-12}$	42
3	2.5	1.3	3.8
4	0.29	0.18	0.47
5	0.29	0.38	0.67
6	0.20	0.18	0.38
7	$7\ ^{+4}_{-2}$	$8\ ^{+7}_{-2}$	15
8	0.26	0.18	0.44
9	0.70	1.2	1.9
10	0.22	0.25	0.47
11	0.29	$3\ ^{+4}_{-1}$	3.29

E_1 and E_2 are the energies of the two electrons resulting from the interaction (in units of Mev). $E = E_1 + E_2$ is the total energy transferred.

All the measurements quoted with no errors are accurate to approximately 10 per cent and were determined by range measurements.

FIG 1

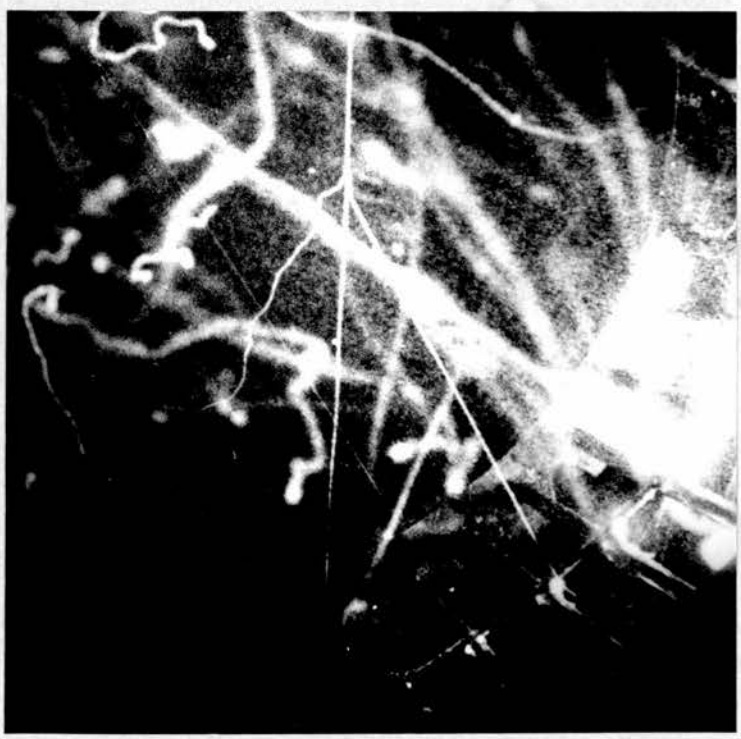

pairs produced by energetic charged particles.

1) Double knock-on electrons

Energetic charged particles produce knock-on electrons when passing through matter. In argon at 47 atmospheres the number N of knock-on electrons, per centimetre of track, which are produced with energies between E_1 and E_2 is:-

$$N = \frac{K}{\beta^2} \left(\frac{1}{E_1} - \frac{1}{E_2}\right)$$

where $\beta = \frac{v}{c}$, v = velocity of the incident particle.

K = 0.0132 for argon at this pressure.

The energies E_1 and E_2 are measured in units of $m_e c^2$. The maximum allowed energy for knock-on electrons for μ-meson (with energies = 300 Mev, $\beta^2 = 0.88$) is ∧ 7.5 Mev, hence the term $1/E_2 \rightarrow 0$ even at this low energy.

As practically all the cosmic ray μ-mesons will have energies > 300 Mev, $\beta^2 \simeq 1$ then the formula

$$N_1 = \frac{0.132}{E_1} \qquad (1)$$

will yield the number of knock-on electrons per centimetre, of energy greater than E_1, to a good approximation.

Thus the number of knock-on electrons (energy > E_1) expected in a track length of L cm was $N_1 \times L$.

A second knock-on electron could be observed in a distance ℓ cm from the first knock-on electron. If this distance was too small to be resolved on the photograph of the event, then it would have appeared as a trident process.

The total path length in which a second knock-on electron could be observed was thus, $N_1 \times L \times \ell$. Hence the number of events P' in which two knock-on electrons should have been observed with energies greater than E_1 and E_2 in the total path length of L cm was

$$P' = N_1 \times L \times \ell \times N_2$$

$$\text{where } N_2 = \frac{0.0132}{E_2} \quad .$$

However, as not only the primary particle but also the first knock-on electron could have given rise to a further knock-on electron, then the path length available for this second knock-on electron would be 2ℓ.

Thus

$$P = 2N_1N_2\ell L \quad .$$

The total track length = 1.6×10^5 cm.

The resolution length = 0.05 cm (of the order of a track width)

Thus $P \simeq \frac{3}{E_1E_2}$ where E_1 and E_2 are measured in units of m_ec^2 .

In order to compare the observed trident processes with this estimated number of double knock-on events, it was convenient to find the number of events Q in which a double knock-on process occurred, where the total energy $E = E_1 + E_2$ was greater than a certain value.

Thus $P = \frac{3}{x(E-x)}$ where $x = E_1$.

Hence the number of events Q in which the total energy $\gg$ E was obtained by averaging the value of P over all values of x between certain limits. The limit chosen for x was the lowest energy electron which was readily observable $x_o = 0.1\ m_e c^2$.

Thus $$Q = \frac{6}{(E - 2x_o)E} \ln\left(\frac{E - x_o}{x_o}\right) .$$

Table 2 gives the values of Q for certain values of E again in units of $m_e c^2$.

Table 2

E	Q
1	15
2	4
4	1.4
6	0.75

Thus 4 double knock-on events were expected with a total energy greater than $\gg$ 1 Mev or 0.75 events with a total energy greater than $\gg$ 3 Mev.

Hence by comparing the experimental values of E (Table 1), only events 2,3,7 could be caused by processes other than double knock-on electrons. Event 11 might just have been included in this category, but as the cross-section for direct pair production is very small for the energy sharing exhibited by this event, in this total energy range, E, and 0.75 events of the double knock-on

process were expected above 3 Mev, then this case was eliminated.

2) Trident events caused by coincidences between two tracks

It was possible that a random track could pass through the same point in space as a μ-meson track, thus giving the appearance of a trident process.

The smallest volume ∂v which could be resolved in the chamber was of the same order of magnitude as the length ℓ used in the previous section. Thus the probability of any track passing through any one volume ∂v was

$$n_1 \frac{\partial v}{V} \quad \text{where} \quad n_1 = \frac{\text{volume of this track}}{\partial v}$$

and

V = total volume of the chamber.

Thus the probability of a second track passing through this same volume was:-

$$n_2 \frac{\partial v}{V} \qquad n_1 \frac{\partial v}{V} \qquad \text{where} \quad n_2 = \frac{\text{volume of the second track}}{\partial v}$$

Thus the probability of this coincidence occurring in any of the ∂v volumes which made up the chamber volume was

$$n_1 n_2 \left(\frac{\partial v}{V}\right)^2 \cdot \frac{V}{\partial v} = \frac{n_1 n_2 \partial v}{V} \quad .$$

Thus the total number of chance coincidences R in N photographs was:-

$$R = \frac{N n_1 n_2 \partial v}{V} \quad .$$

Using the appropriate values :- $R = \frac{n_2}{12}$.

, The number of electron tracks in the cloud chamber which had 1) no definite origin, (i.e. knock on electrons were excluded), and 2) the same age as the μ-meson tracks in the relevant photograph, were counted. The number of points n_2 along these electron tracks, where a scattering had taken place which, had it coincided with a μ-meson track, would have been interpreted as a trident, was estimated to be of the order of 2 points per photograph, from an inspection of 100 randomly chosen photographs.

Thus the number of chance coincidence R was of the order of 0.2 and the effect could be neglected for this experiment.

3) Electron-Positron pairs

Three of the observed events could not be accounted for by either the double knock-on process or the possibility of a coincidence. Thus they were assumed to have been produced by either direct pair production of a charged particle, or a photon which was converted into a pair, the point of conversion coinciding with a particle track. However as the radiative losses by μ-mesons are much less than those due to collision processes for energies < 100 Gev, the chance of a photon being produced by a μ-meson nuclear scatter which subsequently was converted into a pair would be very small. Further as only one pair was observed in the chamber (unassociated with a particle shower) in the 5,000 photographs, it appeared most unlikely that the three events 2, 3, 7, could be accounted for by the conversion of photons into pairs. Thus if it is assumed that these events were caused by μ-meson, (the possibility of direct pair production

by electrons is discussed later), then the experimental cross-section σ for μ-meson direct pair production was:-

$\sigma \simeq 10^{-26}$ cm^{-2} for $E > 10$ Mev,

$\sigma \simeq 1.5 \times 10^{-26}$ cm^{-2} for $E > 3$ Mev,

where E is the total energy transferred to the pair.

Theoretical cross-section for direct pair production

The cross-section for direct pair production by μ-mesons in lead has been represented in a graphical form for μ-meson energies between 0.5 → 6.0 Gev. by Stoker and Haarhoff[93]. The second order differential cross-section derived by Murota et al.[92] was used as the basis of their calculations. By two integrations the cross-section was calculated for total pair energy > 10 Mev. However the limits of one of the integrations were such as to exclude all electrons which had energies < 5 Mev. This would tend to produce an underestimation of the total cross-section for low energy pairs ($E \sim 10$ Mev.). The indefinite parameter a which occurs in the theory due to a cut-off value of the momentum transfer was equal to unity in this calculation. The cross-section for direct pair production in argon was obtained simply, as for different elements it is proportional to Z^2.

As a significant number of μ-mesons would have energies greater than 6 Gev. the value of the cross-section at 25 Gev. was evaluated approximately for $E > 10$ Mev. from the partial cross-section section derived by Roe[94].

The approximate relationship obtained between the energy of the incident particle and the cross-section, in this way, was

expected to be an underestimation for the experimental condition considered:-

1) The indefinite constant was equal to unity for that part of the cross-section obtained from the calculation of Stoker and Haarhoff

2) The cut-off, imposed by the limits of the integration, on the low energy electrons, would also reduce the true value of the cross-section.

The energy distribution of cosmic ray μ-mesons at sea level was obtained from the results of the experiments performed by Gardner et al. and Hayman & Wolfendale[98]. As the value of the cross-section σ changes rapidly with incident μ-meson energy, it was necessary to calculate an average cross-section $\bar{\sigma}$ for the whole of the μ-meson spectrum. By selecting an energy interval E_L to $E_L + \partial E_L$ with a corresponding μ-meson intensity $I_L(E_L)$ and cross-section $\sigma_L(E_L)$, the contribution to the average cross-section from this interval was:-

$$\frac{I_L \partial E_L \sigma_L}{\sum_L I_L \partial E_L}$$

where the intensity I_L was in units of number of particle per unit energy interval.

Thus the total average cross section $\bar{\sigma} = \dfrac{\sum_L I_L \partial E_L \sigma_L}{\sum_L I_L \partial E_L}$.

The value of $\bar{\sigma} = 0.25 \times 10^{-26}$ cm^{-2} was thus obtained for direct pair production by cosmic ray μ-mesons with $E > 10$ Mev.

Although this value was a factor of four lower than the experimental value obtained, the statistical error involved in

this value from only two events together with the expected underestimation of $\bar{\sigma}$, suggested reasonable agreement between the two values.

A calculation of $\bar{\sigma}$ with $E > 3$ Mev was not performed. However qualitative agreement can be inferred as the experimental cross section σ ($E > 3$ Mev) was of the same order of magnitude as that for $E > 10$ Mev. An inspection of the differential cross-section[94] indicated that only a 25 % increase in σ would be expected between the values of σ for $E > 10$ Mev and $E > 3$ Mev, at incident μ-meson energies of 25 Gev.

The cross-section for direct pair production by cosmic ray electrons

It has been assumed that all the straight tracks, which were not associated with cosmic ray showers, were caused by μ-mesons. However, as the cross-section for direct pair production by incident electrons is much larger than μ-mesons of the same energy, it was necessary to calculate the number of pairs produced from this phenomena.

The intensity of cosmic ray electrons is of the order of 1% of the total cosmic ray intensity at energies of > 300 Mev[99] and is approximately proportional to $E^{-1.5}$ at high energies[100].

All particles which arrived in the chamber passed through at least 7 centimetres of steel. Energetic electrons passing through this thickness lose energy by 1) inelastic collisions, 2) radiation, the later process dominating at high energies.

The rate of energy loss/unit length for inelastic collisions is:-

$-\frac{dE_1}{dx}$ = 15 Mev/cm. for steel at minimum ionisation when calculated from the appropriate formula[101].

For radiation processes the energy loss per centimetre $-\frac{dE_2}{dx} = 0.53\,E$ again calculated from the relevant formula (Heitler[101]).

This calculation yields the maximum value of energy loss/cm. by radiation. As at an energy of ~ 25 Mev the energy loss per centimetre has reached ~ 80% of its maximum value, little approximation will be incurred by using the maximum value, for the electron energies considered.

Thus the total energy loss/cm (Mev/cm)

$$-\frac{dE}{dx} = 0.53E + 15 .$$

Hence for an electron of initial energy E_1 and final energy E_2 travelled through x cm. of steel

$$x = \int_0^x dx = \int_{E_1}^{E_2} \frac{-dE}{0.53E+15}$$

if x = 7 cm

$$\text{then} \quad \log\left(\frac{0.53E_1+15}{0.53E_2+15}\right) = 3.6 .$$

Thus knowing the approximate intensity distribution of electrons outside the chamber, the average intensity of electrons inside the chamber was calculated.

The cross-section for direct pair production by electrons derived by Murota et al.[92] was used to determine the number of trident events due to electrons, in conjunction with the electron energy spectrum inside the chamber, in a similar

manner to the μ-meson case. From this calculation only 0.1 events of pair production were expected to have occurred by incident electrons.

However, in many cases the incident electron would have produced observable secondary particles in the form of a cascade shower in the wall of the chamber. If all the secondaries were not absorbed in the walls of the chamber, then the event would have been eliminated by the selection criterion. It would be possible to calculate the number of single incident electrons which passed through the chamber wall without producing observable secondaries by using the method developed by R.R. Wilson[102].

The calculated 0.1 events would be an upper limit to the number observed, as practically all the electrons would be expected to produce some observable secondaries which entered the chamber. Thus the chance that any of the three genuine directly produced pairs were caused by incident electrons, appeared small.

Possible further experiments to determine the cross-section for direct pair production by μ-mesons.

The small number of events obtained in the previously described experiment were hardly sufficient to confirm the correctness of the theoretical prediction about direct pair production. In other experiments[94-97] conducted to investigate this phenomena, multiplate cloud chambers, operated at near atmosphere pressure, have been used. As the event took

place in one of the plates of the cloud chamber, energy transfers of lower than 50 Mev could only be determined with relatively poor accuracy, a feature which rendered theoretical comparison difficult, for this low energy range.

However, where a high pressure cloud chamber is used, the event occurs in the gas of the chamber. Accurate determination of the electron energies between 1 and $\sim$ 50 Mev could be made, by either range or multiple scattering measurements, provided distortion in the cloud chamber was small. As approximately 60% of the events occur with energy transfers less than 100 Mev, the increased accuracy in the determination of the low energy events would in some way compensate the poorer resolution at higher energies.

Watson[6] has suggested another method of utilizing a cloud chamber to determine the experimental cross-section for direct pair production. A simple counter arrangement could be used to select μ-meson of energy $>$ 1.5 Gev by placing the cloud chamber and a suitable thickness of lead absorber between them. In this method the quality of the tracks of the event would be superior to the random photography method, and a higher limit could be set on the momentum transfer. However, to achieve a similar rate with which information could be collected one coincidence about every three minutes would be required, necessitating the use of relatively large counters. (As the μ-meson selected by the counter system would have energies greater than 1.5 Gev, the average cross-section for the μ-meson spectrum would be greater, and proportionally less tracks would be required to produce an equivalent number of events.).

In both methods, the equivalent of some 100,000 photographs would be required, to obtain significant results, the expected number of events being in the region of 50-100 for energy transfers greater than 10 Mev. If such a number of events were achieved, a determination of the indefinite parameter could be expected. With the present high pressure cloud chamber such a large number of photographs is not out of the question, although a complete year of 24 hour operation would be necessary.

APPENDIX I

Introduction

The majority of μ-mesons present in cosmic radiation have energies > 300 Mev and corresponding velocities > 0.94 c. However those μ-mesons which would stop in the high pressure cloud chamber, equivalent to approximately 2 gm/cm^2 of absorber would require a velocity of less than 0.4c on entering the chamber gas. Thus provided two scintillation counters could be arranged so that relatively little absorber was present, both between scintillator phosphors and the chamber gas, slow μ-meson which could stop in the chamber could be detected by a time of flight technique.

As the degree of ionization produced by a charged particle is approximately proportional to $1/\beta^2$ (where $\beta = \frac{v}{c}$), the larger energy loss of slow particles whilst passing through the scintillator phosphors might further be used to detect stopping particles. However the advantages of using this property of increased ionization of slow particles might be offset by several factors, when cosmic ray μ-mesons were anticipated as the particle source. Two coincident particles, which would produce twice the ionisation of a single particle, would give the appearance of a slow particle. Particles which passed diagonally through the counters or near the edge of the phosphor would give light outputs which were functions of the geometry of the system rather than the velocity of the particle.

The counter system was designed which used predominantly a time of flight technique, with the possibility of monitoring

the detectors by a control which depended on the ionization of the particle.

The number of μ-mesons in cosmic radiation which were liable to stop in the chamber was estimated from the experiments conducted using the random photography method. In 5,000 photographs, equivalent to a total of 15,000 μ-meson tracks (if field separated tracks are included) approximately 30 μ-meson either decayed or stopped in the cloud chamber. Thus, of the order of 1 in 500 μ-meson could be expected to stop in the chamber.

If an equivalent number of events were expected from this counter technique (i.e. stopped μ-mesons) as compared with the method of random photography, then the counter system would be required to encompass a solid angle through which about one fast μ-meson passed each minute, yielding about three stopped μ-mesons per day.

The incident μ-meson would pass through the phosphors of both counters and then some window which allowed it to enter the chamber. An inspection of range energy curves for μ-mesons[103] indicated that if the μ-meson passed through the total thickness of the steel chamber wall (7 cm. or 50 gm./cm^2 of absorber), then its velocity prior to reaching the chamber wall would have to be > 0.95 c. Some difficulty would be experienced in selecting these mesons by a time of flight technique.

One of the chamber illumination windows (Fig. 1) was first envisaged as a suitable entry point. The 2.5 cm thick

armour plate glass presented an absorber of some 8 gm/cm^2. A useful reduction in this quantity was obtained by replacing the glass window with a duralumin one of effective thickness of 1 cm. (Fig. 2) (A stress calculation had indicated that this new window could withstand pressures up to 500 atmospheres before fracture was likely). Although the loss of one illumination window was not desirable, it appeared to be the best compromise.

The phosphors of the two counters were 2 cm thick. An incident μ-meson would require to pass through a total of some 5 gm/cm^2 of absorber after leaving the top counter (Fig. 3). The velocity of a μ-meson between the two counters which would just stop at the bottom of the chamber would be 0.67c, whereas one just reaching the chamber gas would have a correspondingly smaller velocity of 0.63c. The average angle through which these slow μ-mesons would be scattered when passing through the lower counter and duralumin window was calculated from the appropriate scattering formula(52) and found to be less than 10° in each case. Thus the increase in range through scattering and the loss of slow μ-mesons caused by deflections into the steel wall, were small effects and not expected to alter these tentative calculations severely.

The current state of fast coincidence circuitry and scintillation counter techniques (1963) suggested that resolving times of the order of 1 nsec were practicable possibilities. Thus if resolution by a time of flight method between particles of 0.65c and c was to be achieved, a path length of the order of 1 metre should be sufficient.

This separation of 1 metre would govern the sizes of the

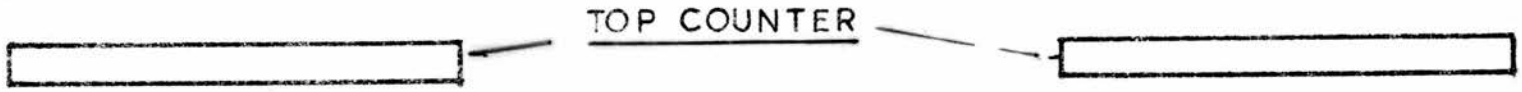

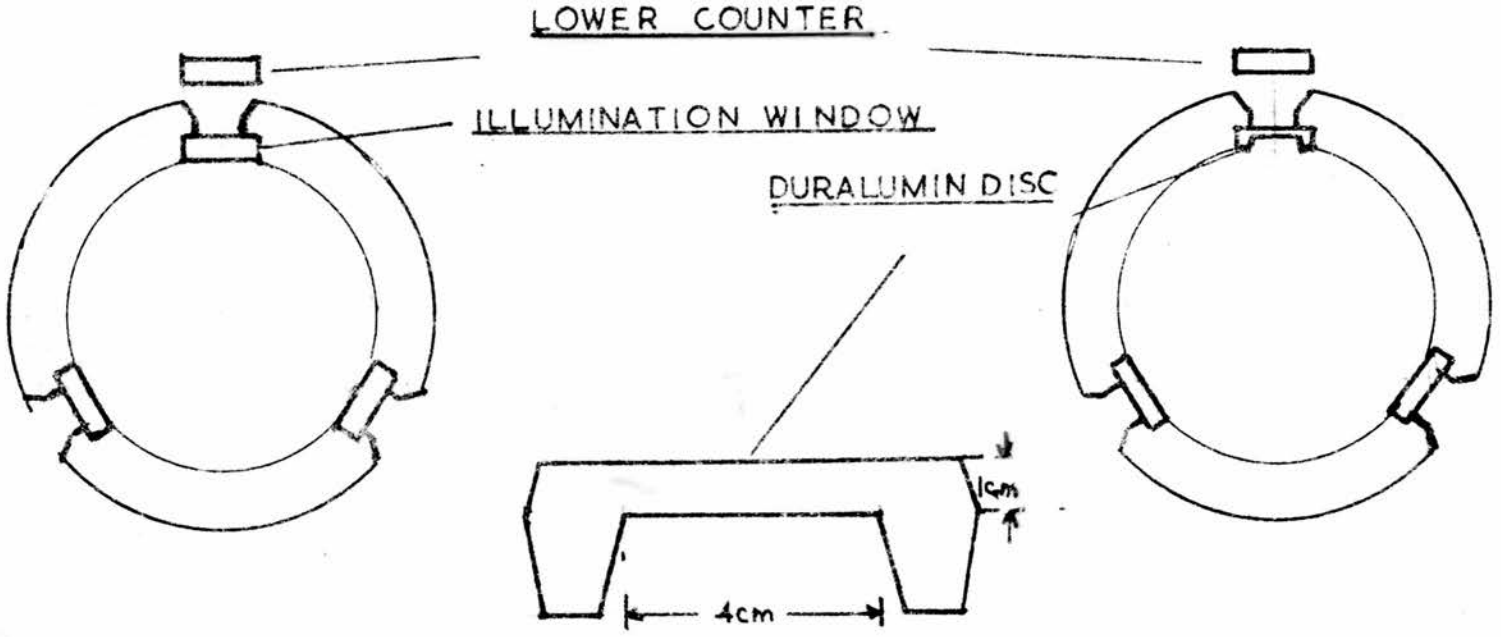

FIG1

FIG 2

FIG 3

two counters, as the total counting rate of 1 μ-meson per minute was required. Thus as the lower counter had to be held to approximately the same dimensions as the duralumin window, the diameter of the phosphor of the top counter, when computed from the cosmic ray μ-meson intensities[98], was of the order of 30 cm.

The Details of the Counters

The top counter (C1)

The design of the top counter (C1) is shown in Fig. 4. A 2 x 30 x 30 cm slab of Nuclear Enterprise NE102 phosphor was connected optically to the photomultiplier (Mullard 56AVP) by means of a perspex light pipe. Optical contact between the scintillator, sections of the light pipe (fabricated from three conical sections) and the photomultiplier was obtained with a thin film of glycerine. (The use of glycerine rather than the recommended contact grease was adopted, as a uniform contact over such large areas was found difficult to achieve with silicone grease).

The outside of the light pipe was coated with reflecting paint to facilitate diffuse reflection at its surface. The optics of this pipe were such that, without reflecting paint, most of the light would escape after the first reflection.

A clamping arrangement of wooden discs was used to hold the phosphor, light pipe and scintillator together, the whole assembly being enclosed in a light tight box. The top and bottom of the box were detachable to allow assembly.

FIG 4

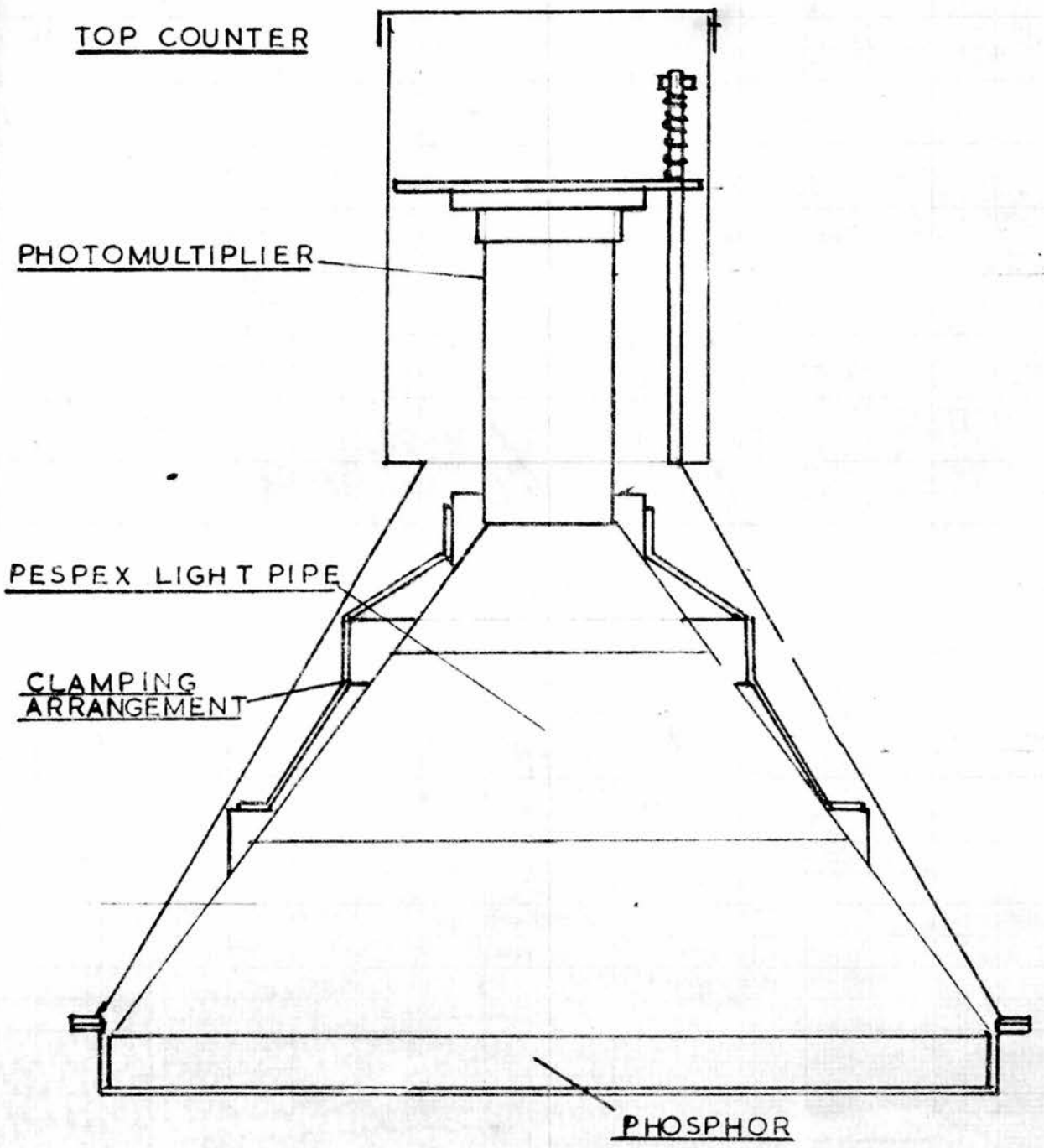
TOP COUNTER
PHOTOMULTIPLIER
PESPEX LIGHT PIPE
CLAMPING ARRANGEMENT
PHOSPHOR

FIG 5

LOWER COUNTER

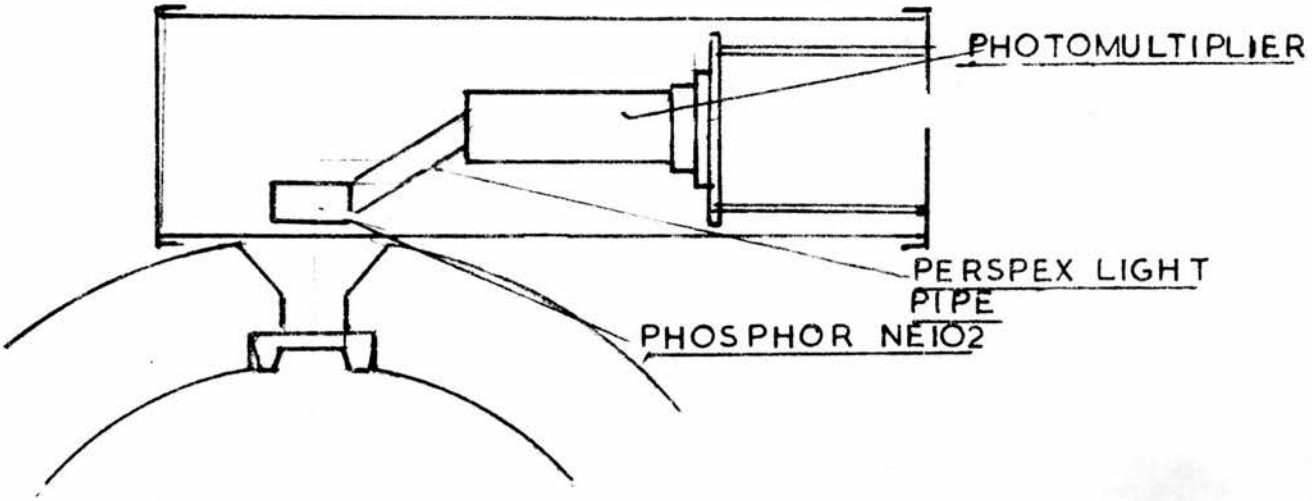

FIG 6

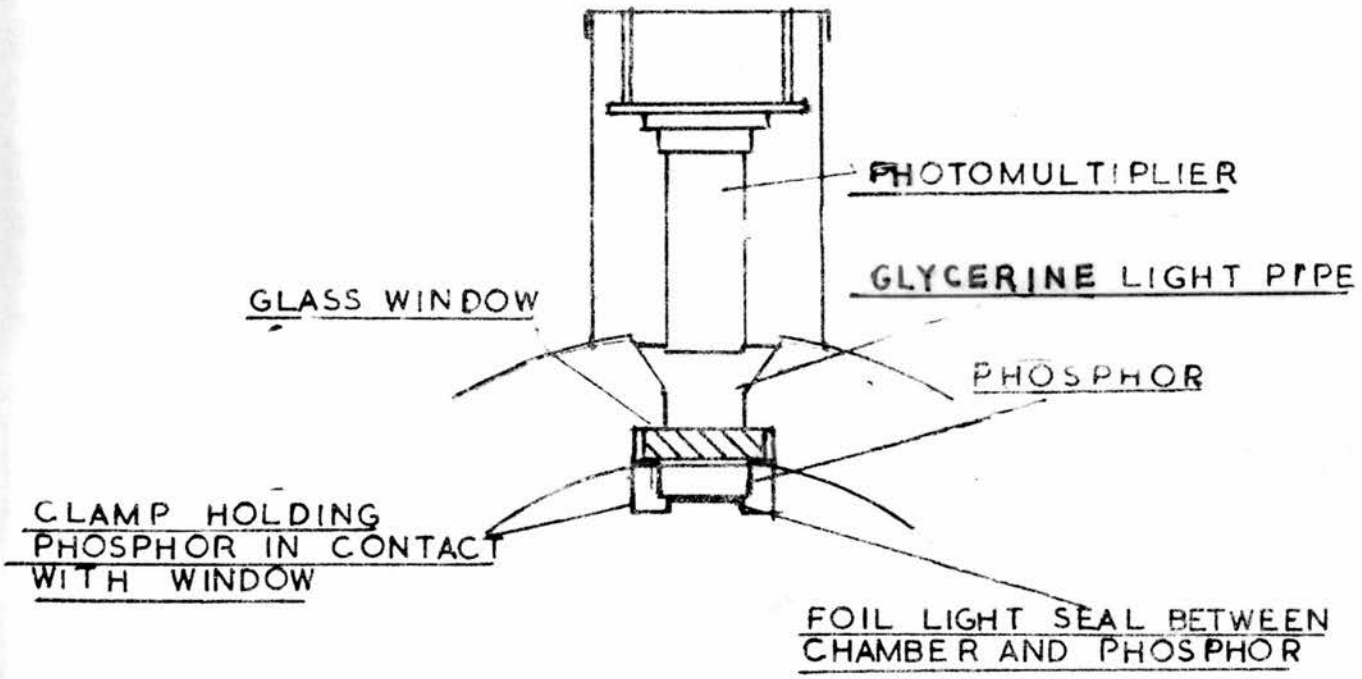

The lower counter C2

The lower counter (Fig. 5) shown in position on top of the chamber consisted of a 5 x 5 x 2 cm block of NE102 phosphor connected to its photomultiplier by a perspex light pipe. This arrangement allowed the scintillator to be as close to the duralumin window as possible, without producing any absorber between the two counters.

The original design of this lower counter (Fig. 6) had been discarded. In this arrangement, the phosphor was actually inside the chamber, the light from it being collected through the plate glass window and then a glycerine light pipe to the photomultiplier. However the total amount of absorber between the two phosphors of C1 and C2 was considerable, the photomultiplier representing some 12 gm/cm^2. The calculation of the previous section would not have been valid, the minimum velocity between the counters for a μ-meson which would now enter the chamber being 0.82 c. Although this system contained the desirable features of better light collection and geometry, the large amount of absorber placed between the counters made it impracticable.

The geometry of the system

Only slow particles which passed through the dural window could be expected to be detected and then seen to stop in the chamber. Those slow particles, which "missed" the window, would stop in the chamber wall before reaching the gas.

As the solid angle enclosed by the two counters, when projected, included a greater area than the dural window (Fig. 7),

FIG 7

GEOMETRY OF COUNTER SYSTEM

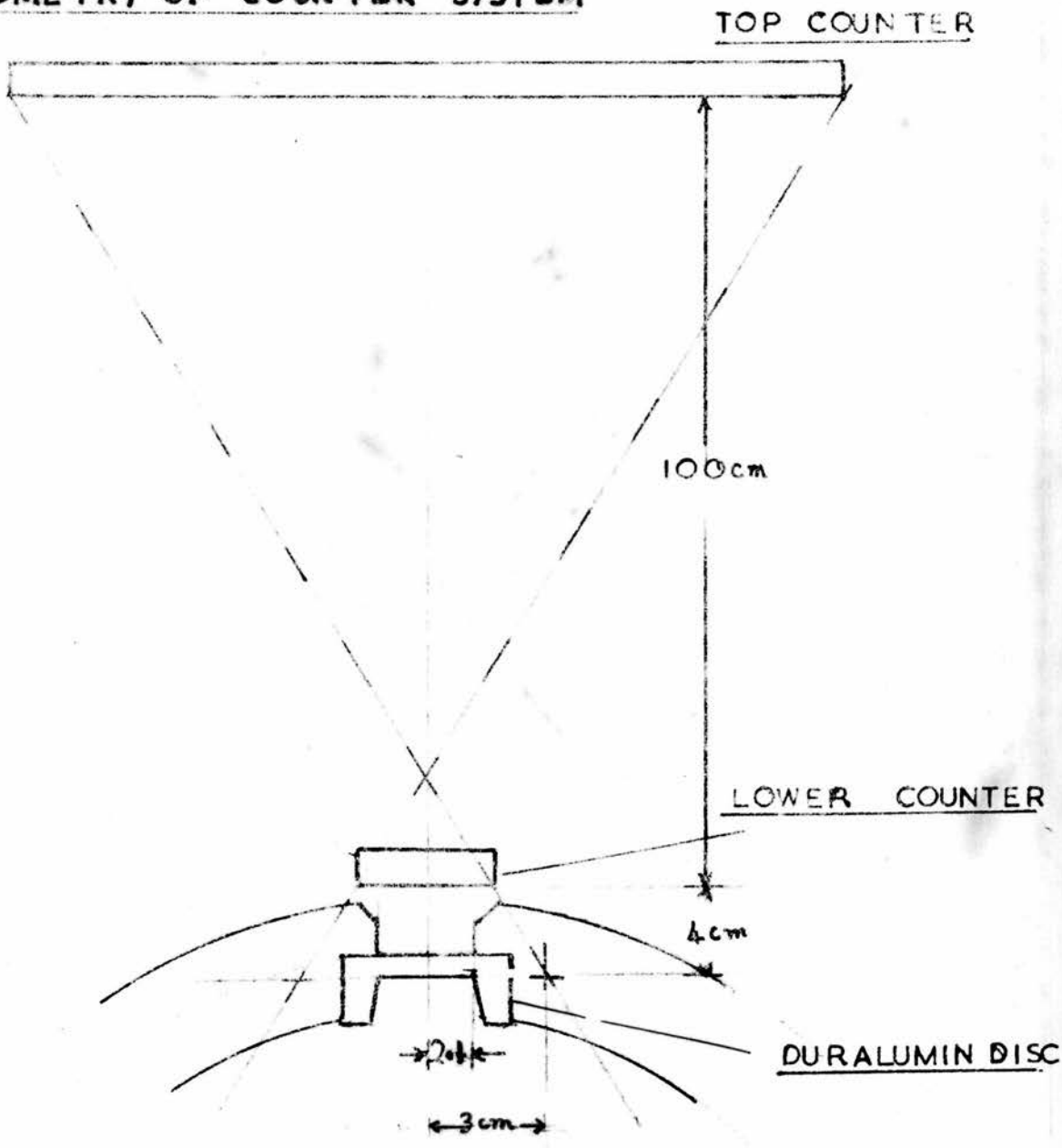

$$\frac{\text{EFFECTIVE AREA OF DURALUMIN DISC}}{\text{PROJECTED AREA OF COUNTER SYSTEM}} = \left(\frac{2.1}{30}\right)^2 = 0.49$$

the apparatus would have an inherent inefficiency where slow particle detection was concerned. The ratio of the projected area of the counter telescope to that of the acceptance area of the dural window was approximately 2.1, yielding an efficiency of some 49%.

Although a smaller counter (C2) would have been sufficient to yield the same overall result, the size of this counter was not changed. Positioning of this counter would not be critical and any effects of scattering in the phosphor might be expected to be minimized, by using a larger size than the minimum necessary.

The electronics of the counter system

For a photomultiplier operated with a scintillation crystal it has been shown that the time variance[104] of the R-th photoelectron from the cathode of the tube is $\sim \frac{\tau}{Q}\sqrt{R}$, where τ is the decay time of the scintillator and Q the total number of photoelectrons given off. Thus from this consideration alone, the minimum time variance of the system would be achieved, by triggering the electronics after the counter, with the pulse from the first photoelectron.

However, where real photomultiplier tubes are concerned, a further time variance exists for the tube itself due to the finite time between the initiation of the photoelectrons and the arrivel of the amplified pulse at the anode. The theory of time resolution in scintillation counters has been evaluated in some detail by Gatti and Svelto[105]. They have demonstrated that the above assumption about the minimum time variance for

real tubes is not true and have shown that the best results, concerning time resolution, should be obtained when the triggering level of the electronics was a fixed ratio of the total pulse height. This ratio would depend on the parameters of the actual tube, the decay time of the phosphor and the manner in which the associated electronics was operated. For certain conditions, the results of this theory have been tested experimentally[106] and good agreement shown.

From these considerations, where scintillation counters which used NE102 phosphor (decay time - 3 nsec) and 56AVP photomultiplier tubes, the minimum time variance of the counters would be achieved by operating at a triggering level which was between 0.2 and 0.3 of the total anode pulse height, and by using the maximum light collection efficiency.

Both the counters mentioned in the previous section were expected to have fairly large variation in light input to the cathode of the photomultiplier tube for a fixed loss of energy in the phosphor, because of the optical arrangements. It would therefore appear advisable to eliminate small pulses at the anode which could be caused by poor light collection, because of their relatively larger time variance.

Thus a conventional fast-slow coincidence system was envisaged as the necessary arrangement for optimum time resolution, where the timing was achieved by the fast side, the slow part being used to discriminate against small pulse. A block diagram to the complete system in shown in Fig. 9A.

The electronics of the counters

The circuit of both counters was the same and a diagram is shown (Fig. 8). Negative pulses from the anode were fed into 100 Ω AS50 transmission line cable, and similarly positive pulses from the 15th dynode. The two pulses were mixed together, in network A, the negative one delayed 2n secs with respect to the positive one. As the rise time of the pulses from these photomultipliers was of the order of 2n secs, the positive pulse had reached 90% of its maximum value before the arrival of the start of the negative pulse. The mixing network effectively quartered the height of the positive pulse, the resulting compound pulse swinging across the zero line at a point corresponding to 25% of the total pulse height from the anode. The shorted delay line clipped the pulse to 6n secs producing a positive overswing at the tail end of the output pulse.

The pulse for the slow coincidence unit was taken from the 10K Ω load resistance attached to the 12th dynode. It was then fed into an emitter follower which operated also as a discriminator, inverted in the next stage to produce a negative pulse and then passed through a further emitter follower of low enough output impedance to feed a 100 Ω line.

The Coincidence Unit

Several varieties of fast coincidence units were built initially, similar to those designed by Franzini[107], Gygi and Scheinder[108] and Larsen and Shera[109], all of which used

FIG8

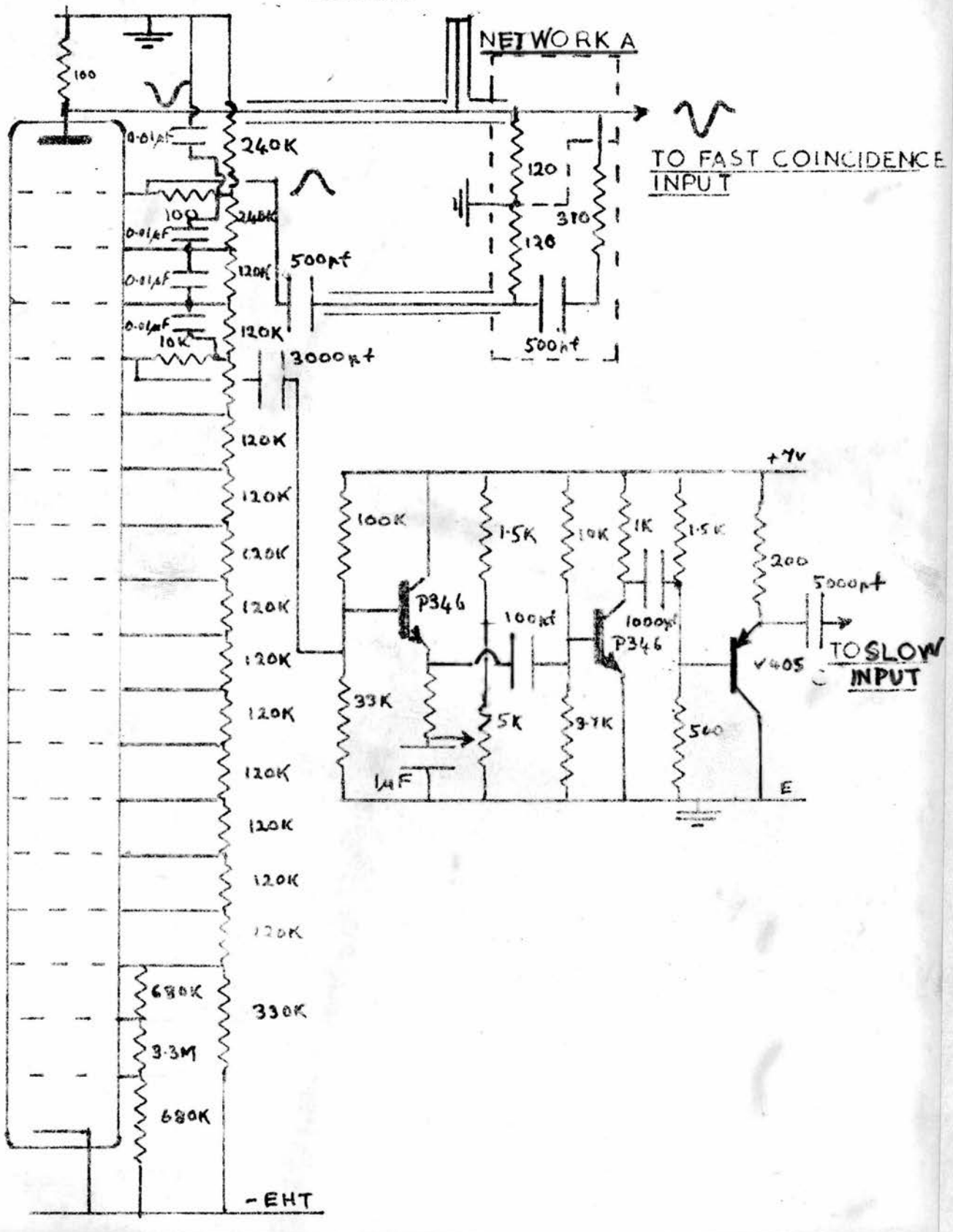
NETWORK A
TO FAST COINCIDENCE INPUT
100
0·01μF
240K
100
240K
0·01μF
0·01μF
120K
0·01μF
10K
120K
500μf
3000μf
120
310
120
500μf
120K
120K
120K
120K
120K
120K
120K
120K
120K
680K
3·3M
680K
330K
-EHT
+7v
100K
1·5K
10K
1K
1·5K
200
5000μf
P346
100μf
1000μf
P346
TO SLOW INPUT
33K
5K
3·7K
540
1μF
E

solid state elements. However, only the type similar to that of Larsen and Shera was found to be completely satisfactory.

The output pulse from the mixing network of the counters, which, for a typical cosmic ray particle passing through one of the counters, would be at least 50 ma in a 100 Ω load, was fed into the input tunnel diode of the fast coincidence unit (Fig. 9B). The tunnel diodes, normally held in the high resistance state, required only 1 ma to switch over to the low resistance part of their characteristics, this being achieved by a very small fraction of the input pulse. The condition that the trigger level of the coincidence unit should be 20%-30% of the total pulse height was thus satisfied for all large pulses. The positive overswing at the tail end of the input pulse switched the tunnel diode back to its normal state.

Thus, a standard pulse of 0.45 volts and 6sec length was achieved and used as a time marker for the next stage of the circuit. (Very large pulses tended to produce slightly larger than standard pulse from the tunnel diode due to feed through, the increase being of the order of 0.1 volts.).

This standard pulse from the tunnel diode was sufficient to trigger the transistor of the next stage operated in the avalanche mode. The differentiated output pulse from this section (4.8 volts) was then fed into one side of a simple diode adding gate. When a similar pulse was received in the other side of the diode gate, which was coincident in time with the first, an output pulse from the adding gate was

FIG 9A

BLOCK DIAGRAM OF COMPLETE SYSTEM

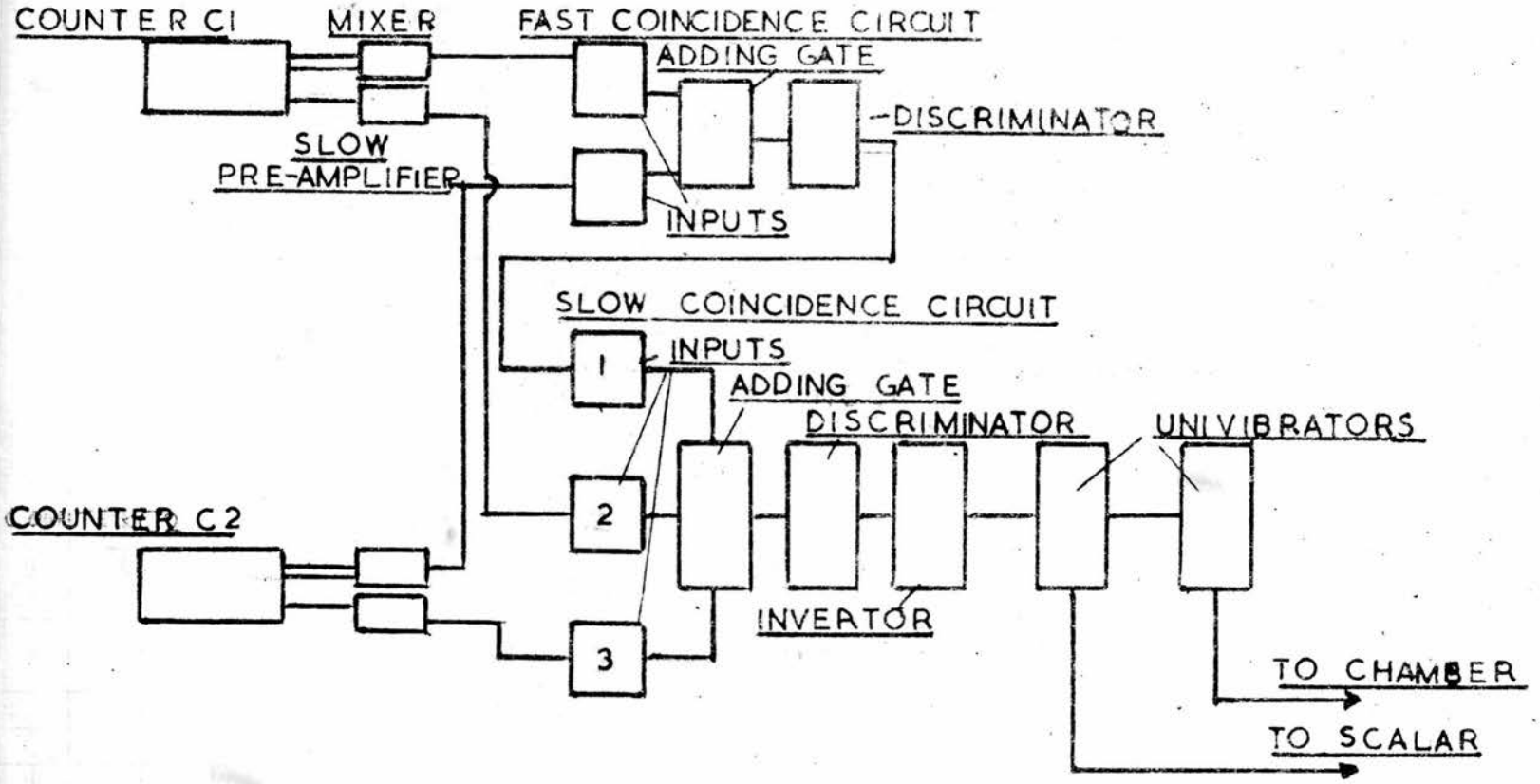

FIG9B

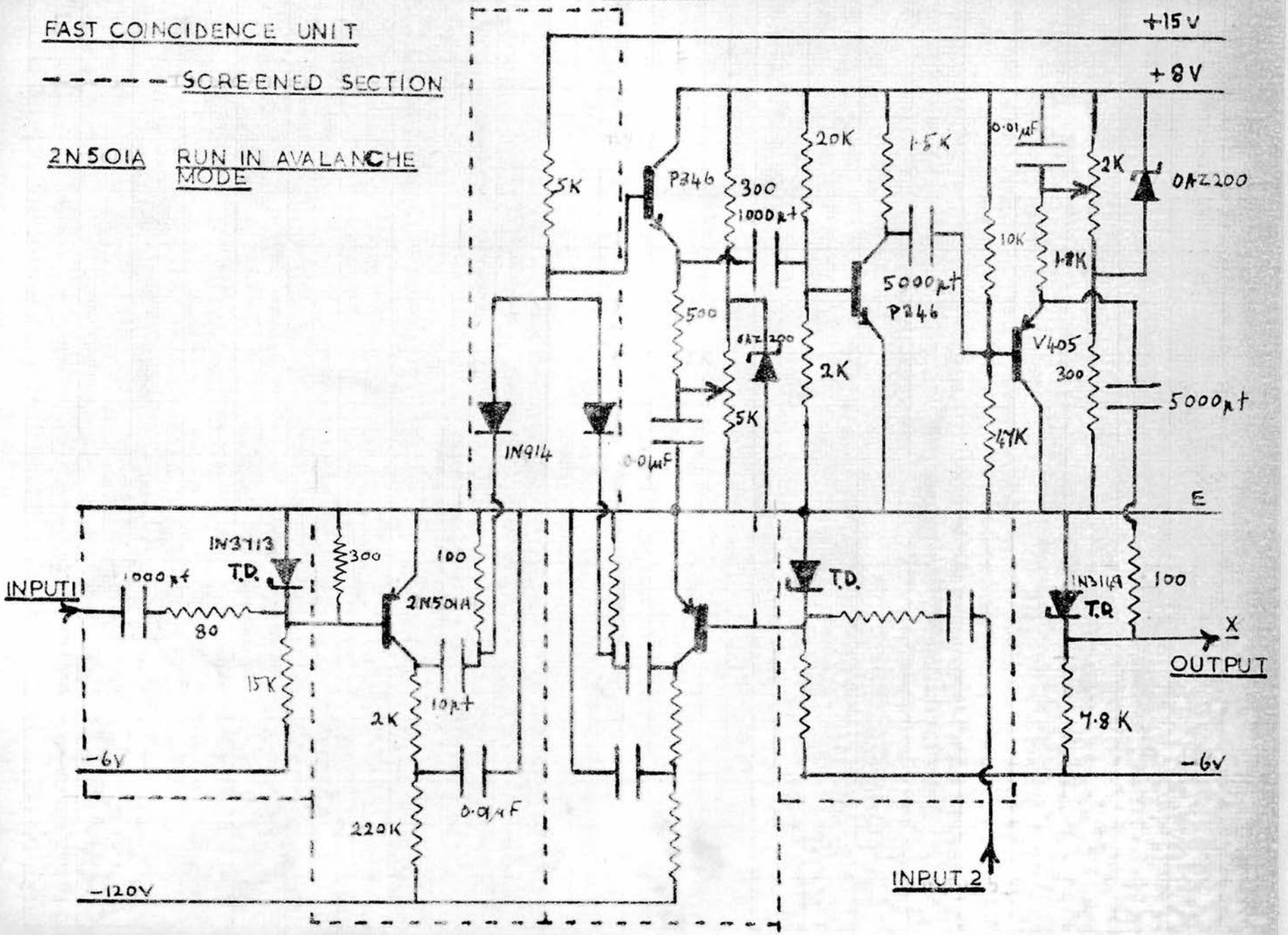
FAST COINCIDENCE UNIT
SCREENED SECTION
2N501A RUN IN AVALANCHE MODE
+15 V
+8V
5K
P346
300
1000μf
20K
1·5K
0·01μF
2K
OAZ200
10K
1·8K
5000μf
P346
500
OAZ200
V405
300
2K
5K
5000μf
IN914
0·01μF
47K
E
IN3113
T.D.
300
100
INPUT1
1000μf
2N501A
80
15K
2K
10μf
0·01μF
220K
-6V
-120V
T.D.
IN3149
T.D.
100
X
OUTPUT
7·8 K
-6V
INPUT 2

FIG9C

SLOW COINCIDENCE UNIT

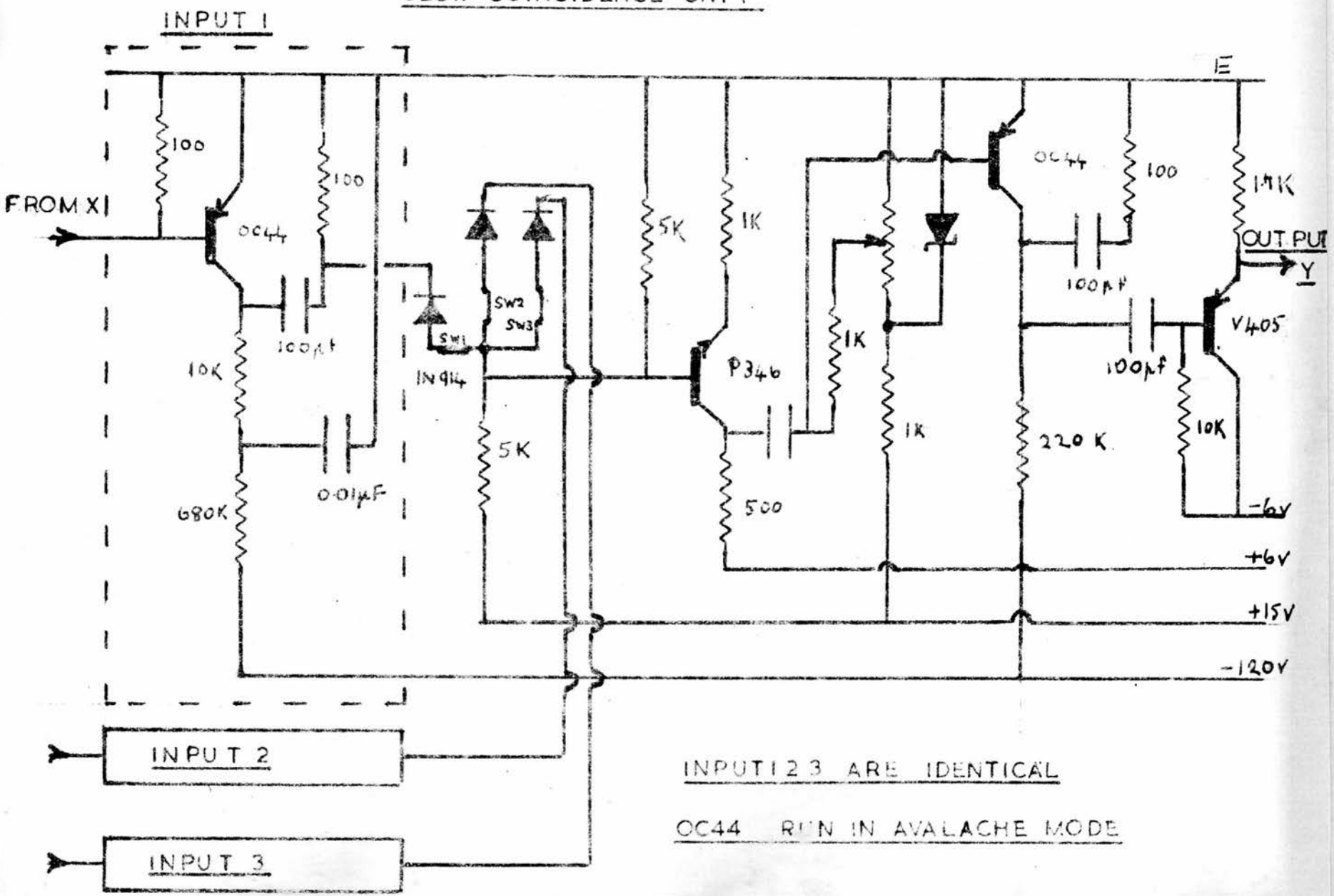

INPUT 1 2 3 ARE IDENTICAL

OC44 RUN IN AVALACHE MODE

FIG 9D

UNIVIBRATOR CIRCUITS

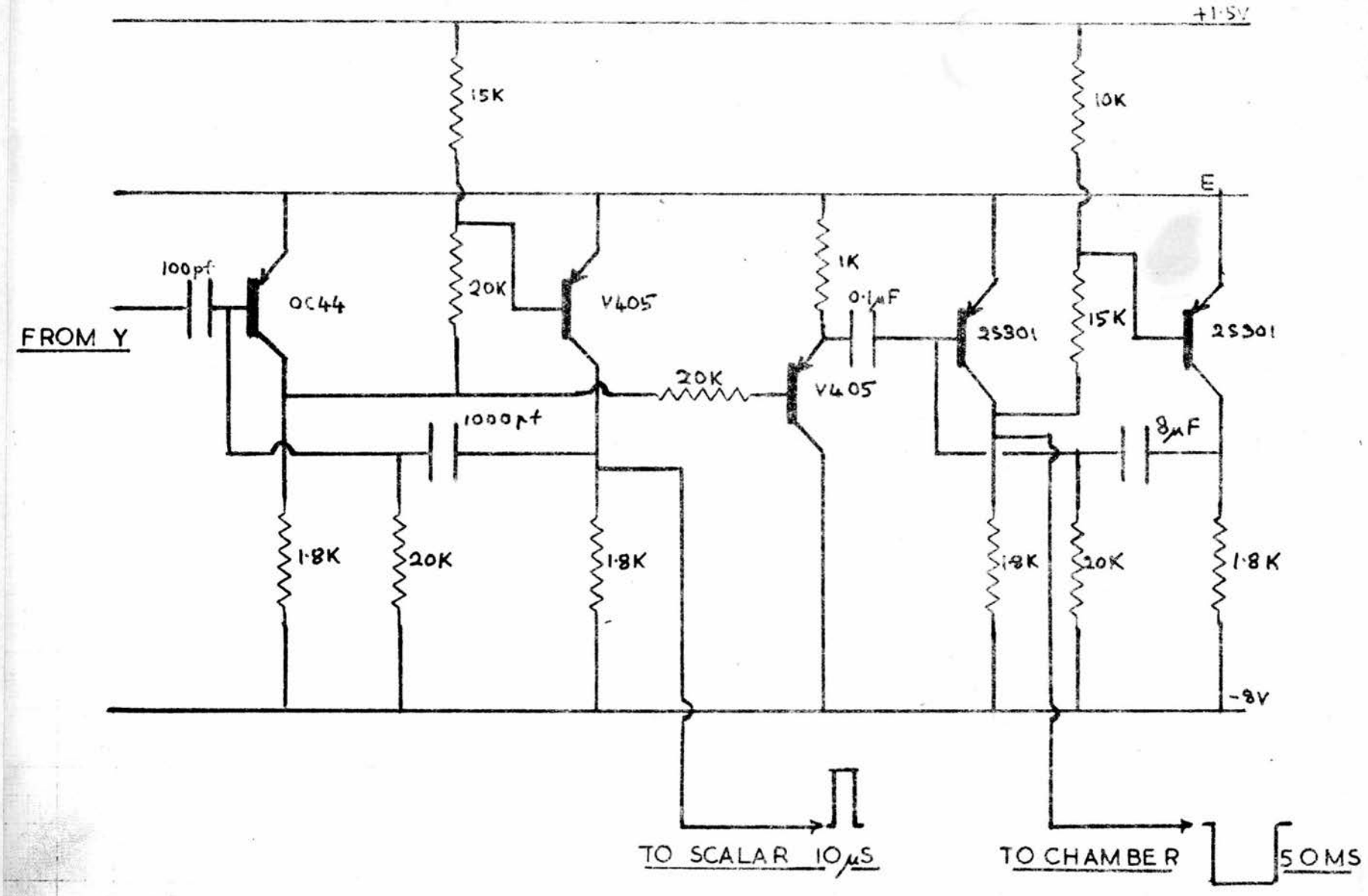

detected.* This pulse was further discriminated and amplified by the transistors of the next section and finally fed into a tunnel diode which produced a yes-no pulse of 0.45 volts. The accepted overlap in time of the two input pulses could be varied by altering the bias settings of the discriminator amplifier section.

The amplified pulses from the 12th dynode of the counters were also fed into avalanche transistor input circuits (Fig. 9C). The differentiated output pulses from these three avalanche circuits (two for the slow coincidence circuit and one for the output pulse from the fast coincidence circuit) were added in a triple diode adding gate and after inversion, further discriminated by an avalanche transistor circuit. The bias of this discriminator was set to give an output pulse if the three pulses arrived within a time interval of 20 n secs.

The switches SW1, 2, 3 were provided for test purposes, so that the slow coincidence unit could be used as a single, double or treble coincidence unit if desired.

Further pulse shaping and lengthening was achieved by two univibrator circuits (Fig. 9D), one output being suitable for a scalar, the other being used to trigger the control circuit of the cloud chamber.

---

* The idea of adding the differentiated pulses without any further shaping was suggested by R.D.L. Mackie.

Note on the use of avalanche transistors

It has been of practical knowledge for some time[110] that certain types of transistor are suitable for operation in the avalanche mode, although not specifically designed for this purpose. The two transistors used in the fast coincidence circuit were selected from batches of the same type of transistor, so that the differentiated pulse in the same circuit gave similar pulse heights. (This pulse height was both a function of the break down voltage and the rise time of the avalanche pulse.). It was established that a variety of types were suitable for this circuit (2N501, 2N501A, 2N617, 2N1500) provided a matched pair could be found.

The tunnel diode standard trigger pulse was used, because the time of the initiation of the avalanche pulse is known to be a function of both the size and length of the input pulse. Thus feeding the input pulses from the counters straight into the avalanche circuits would produce an undesirable time jitter into the fast coincidence circuit.

The OC44 transistors, used in the avalanche mode elsewhere in the circuit, were selected for nearly equal break down voltages. Any time jitter introduced by triggering the avalanche transistors of the slow side directly, was considered unimportant, as this section was in effect used for discrimination rather than time resolution.

Performance of the system

In order to test the ultimate resolution of the coincidence unit alone, pulse from a test counter, similar in electronic

circuit to those previously described, was used in conjunction with a C^{60} source. This counter (C3) consisted of a 10 cm diameter disc of phosphor of depth 2.5 cm. connected directly to the photocathode of a 56AVP tube.

The output pulses from this counter were split by a PET T connector, the two resulting leads being fed into each side of the fast unit. The lengths of cable in one of these leads was varied, resulting in the delay curve (Fig. 10).

The stability of the circuit, with respect to time variation over long periods was less than 0.1 nsecs. The points at either end of the steep sides of the curve were found to be consistently reproducible.

The resolving time of 1.8 n secs, shown, was that maintained for the rest of the experiment, although smaller resolving times could be achieved (by increasing the appropriate biases). However, for reasons of reliability, these biases were maintained at levels well below the maximum working values of the transistors.

Although (Fig. 10) represents the time resolution of the coincidence unit, no information concerning the time resolution of two counters when triggered by coincident particles can be inferred. In order to calibrate the overall performance of the two counters and unit, coincident pulses obtained from counters C2 and C3, when placed near to a Co^{60} source, were used.

The curve (Fig. 11) was obtained when the length of cable between one of the counters and the coincidence unit was varied. The slow coincidence unit was switched out whilst this set of

FIG 10

SPLIT PULSES FROM ONE COUNTER

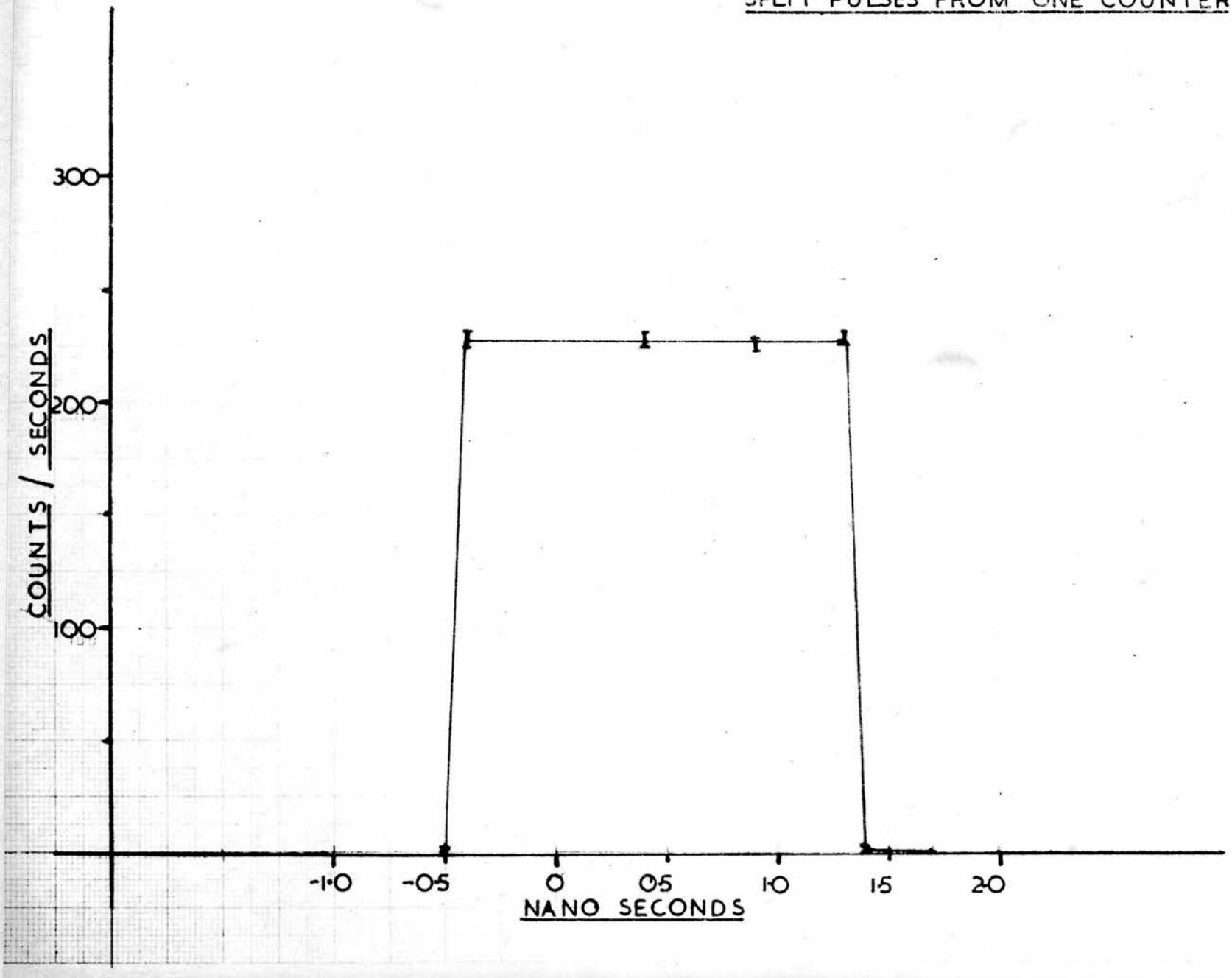

FIG 11

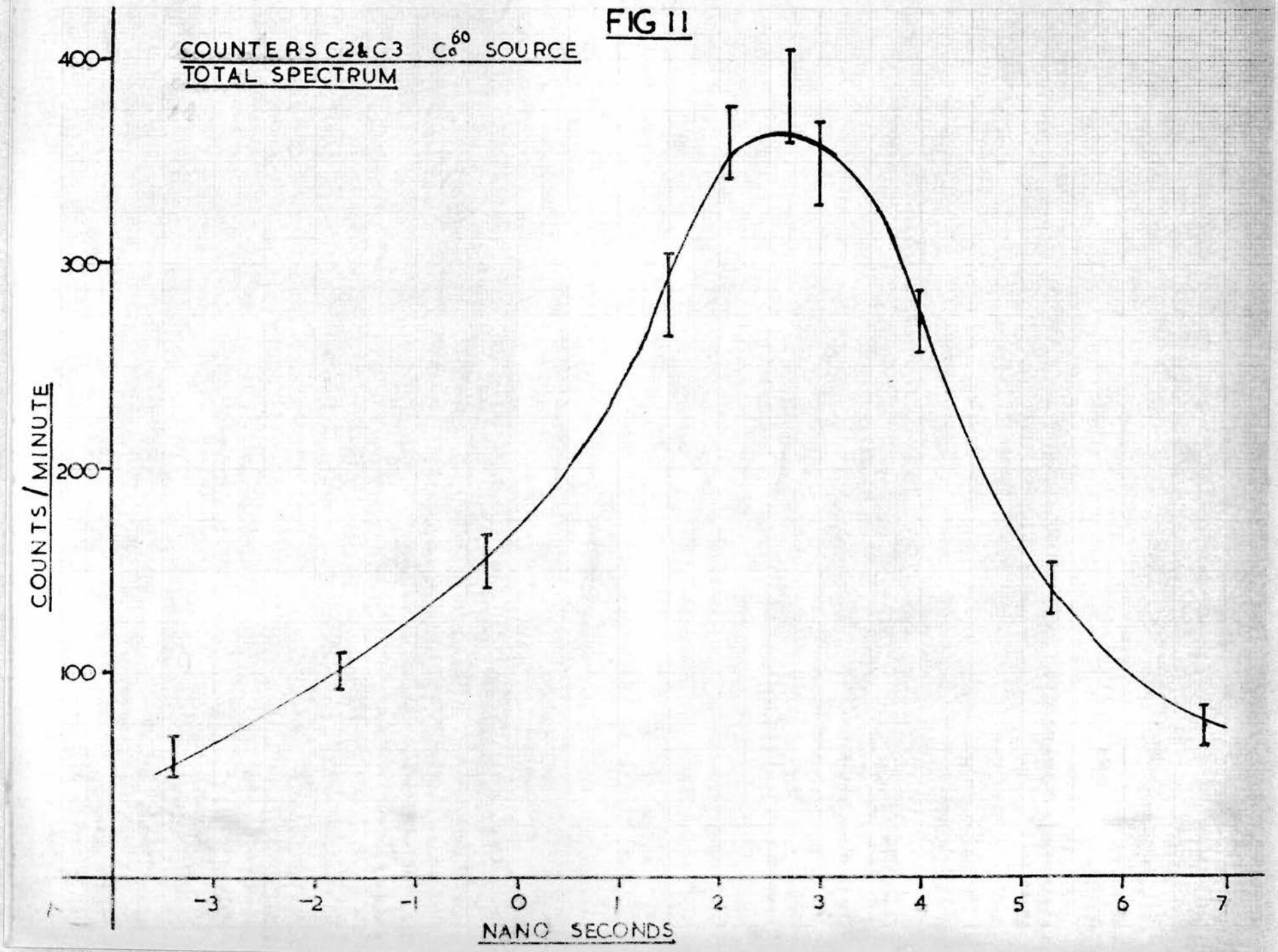
COUNTERS C2&C3 Co^{60} SOURCE
TOTAL SPECTRUM
400
300
200
100
COUNTS / MINUTE
-3
-2
-1
0
1
2
3
4
5
6
7
NANO SECONDS

FIG 12

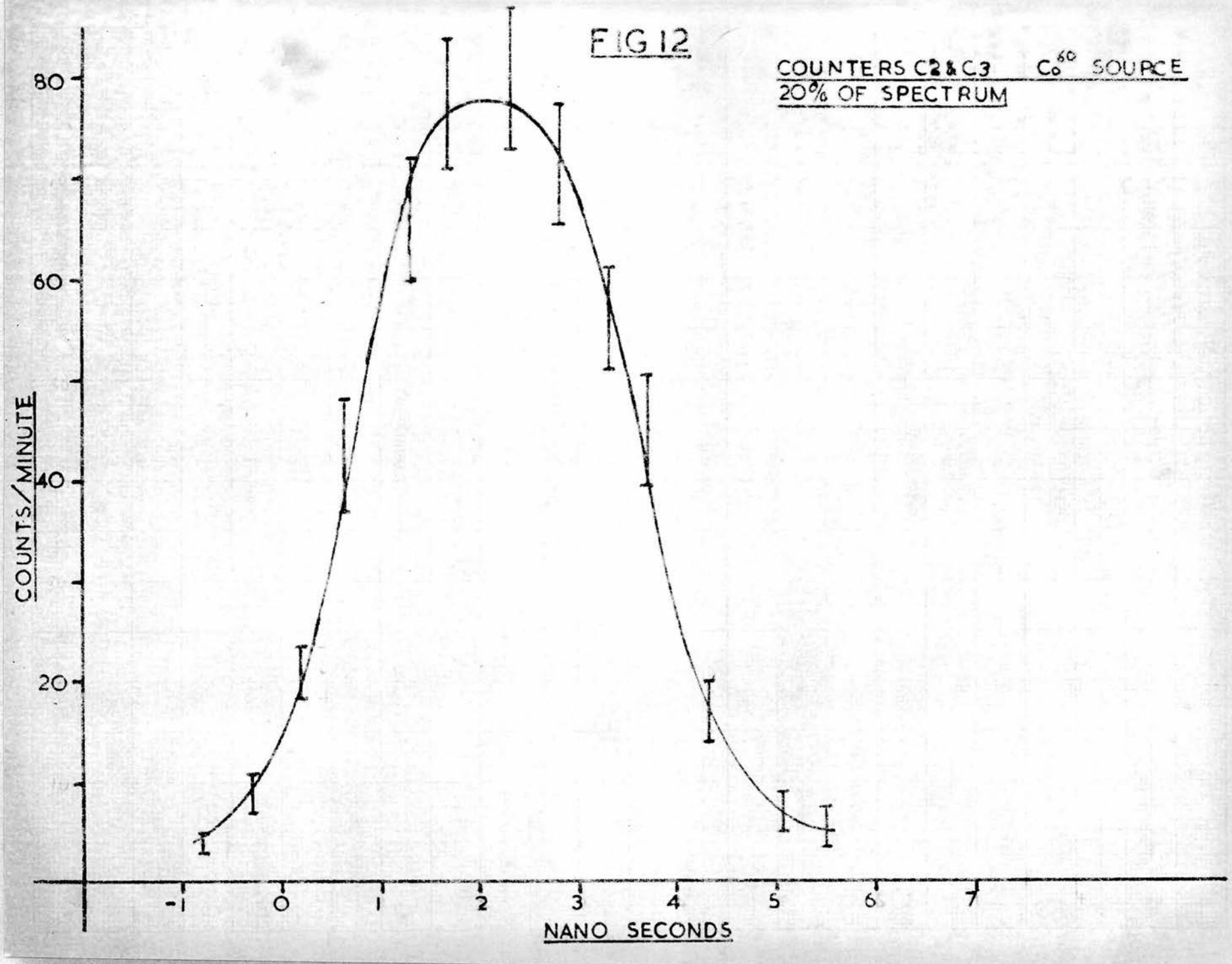
COUNTERS C2 & C3 Co^{60} SOURCE
20% OF SPECTRUM
COUNTS/MINUTE
80
60
40
20
-1
0
1
2
3
4
5
6
7
NANO SECONDS

FIG 13

COUNTERS C2 & C3 Co^{60} SOURCE
3% OF SPECTRUM

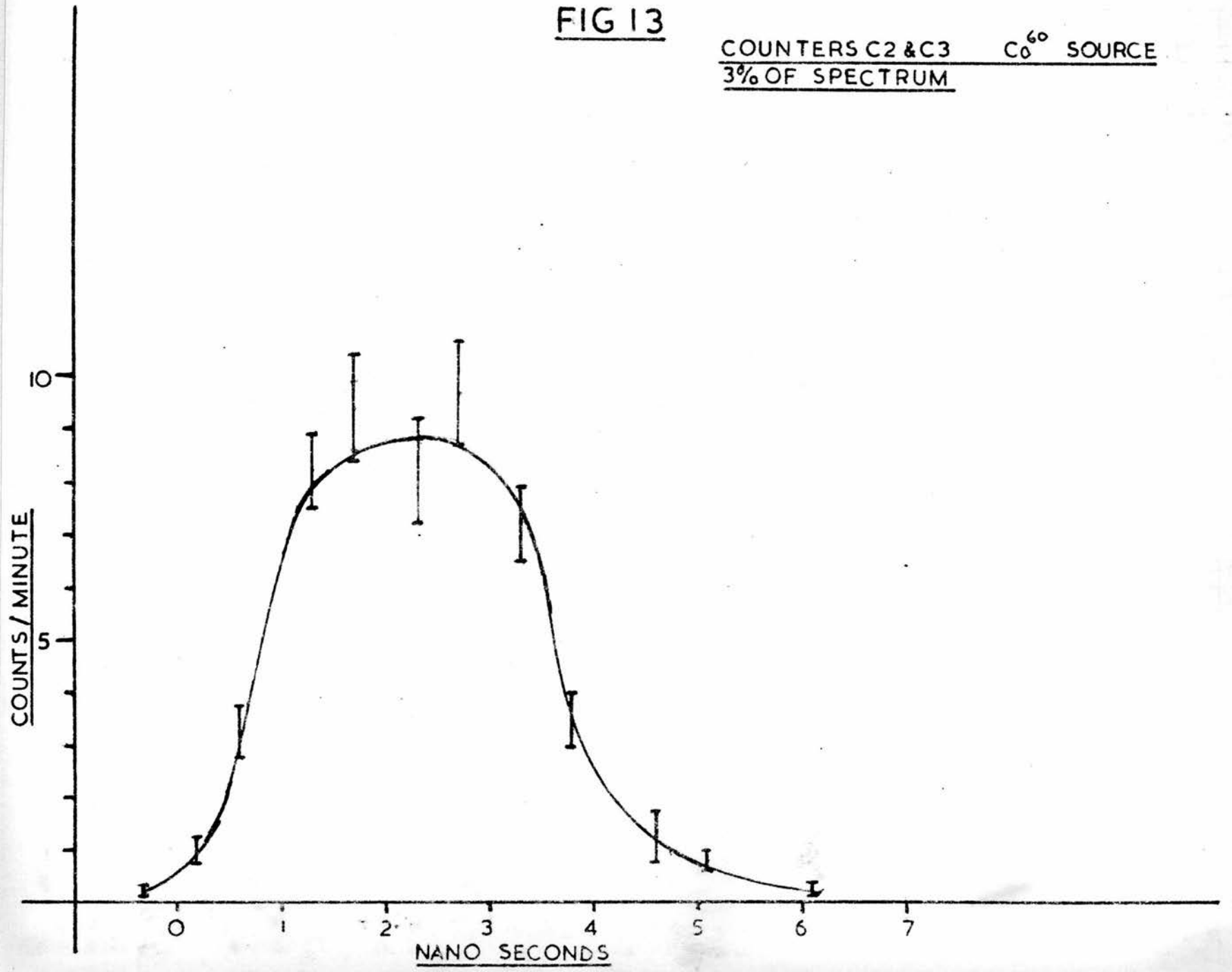

FIG 14

COUNTER C2 & C3 COSMIC RAY MUONS

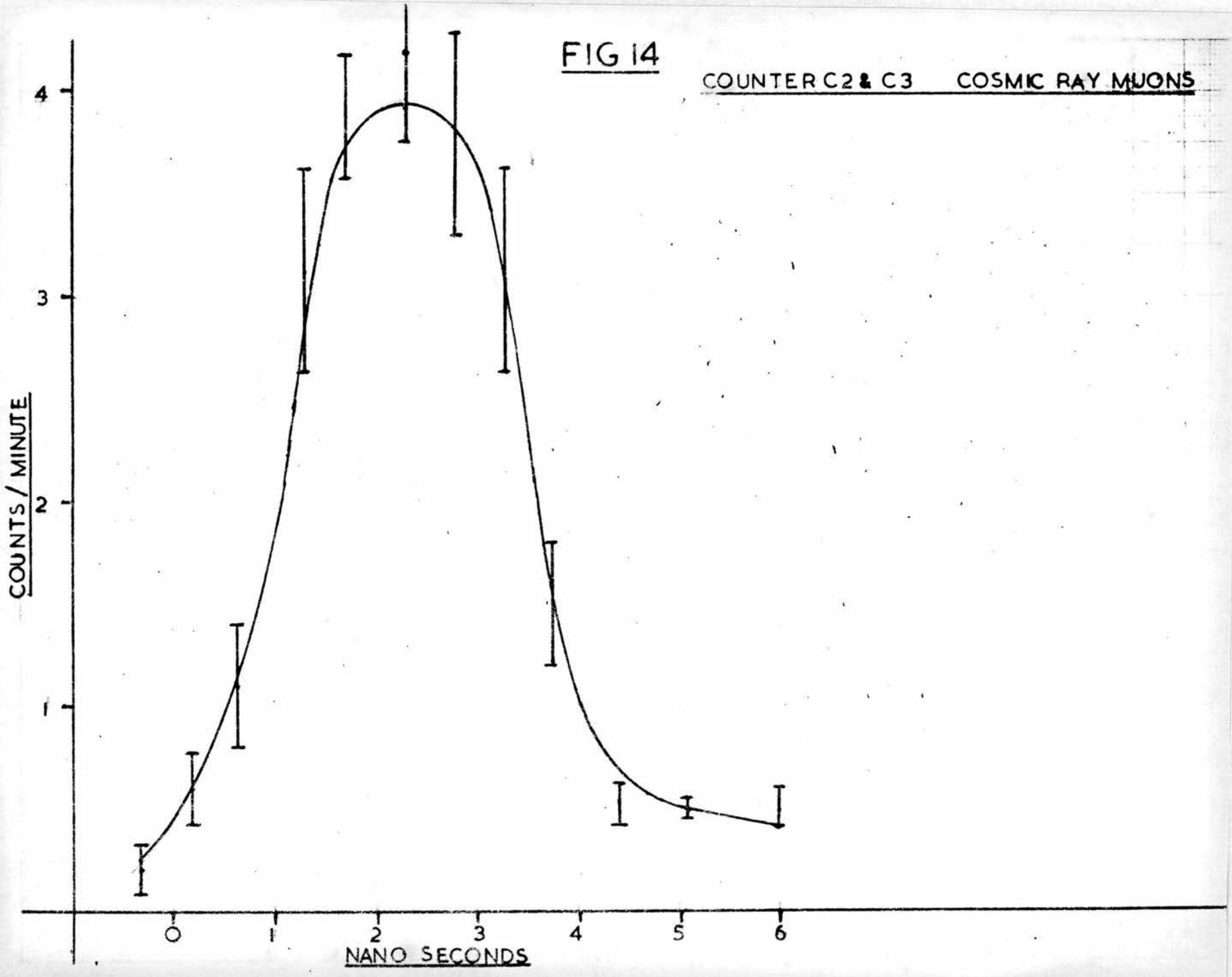

FIG 15

COUNTERS C1 & C2 COSMIC RAY MUONS
5 CM APART

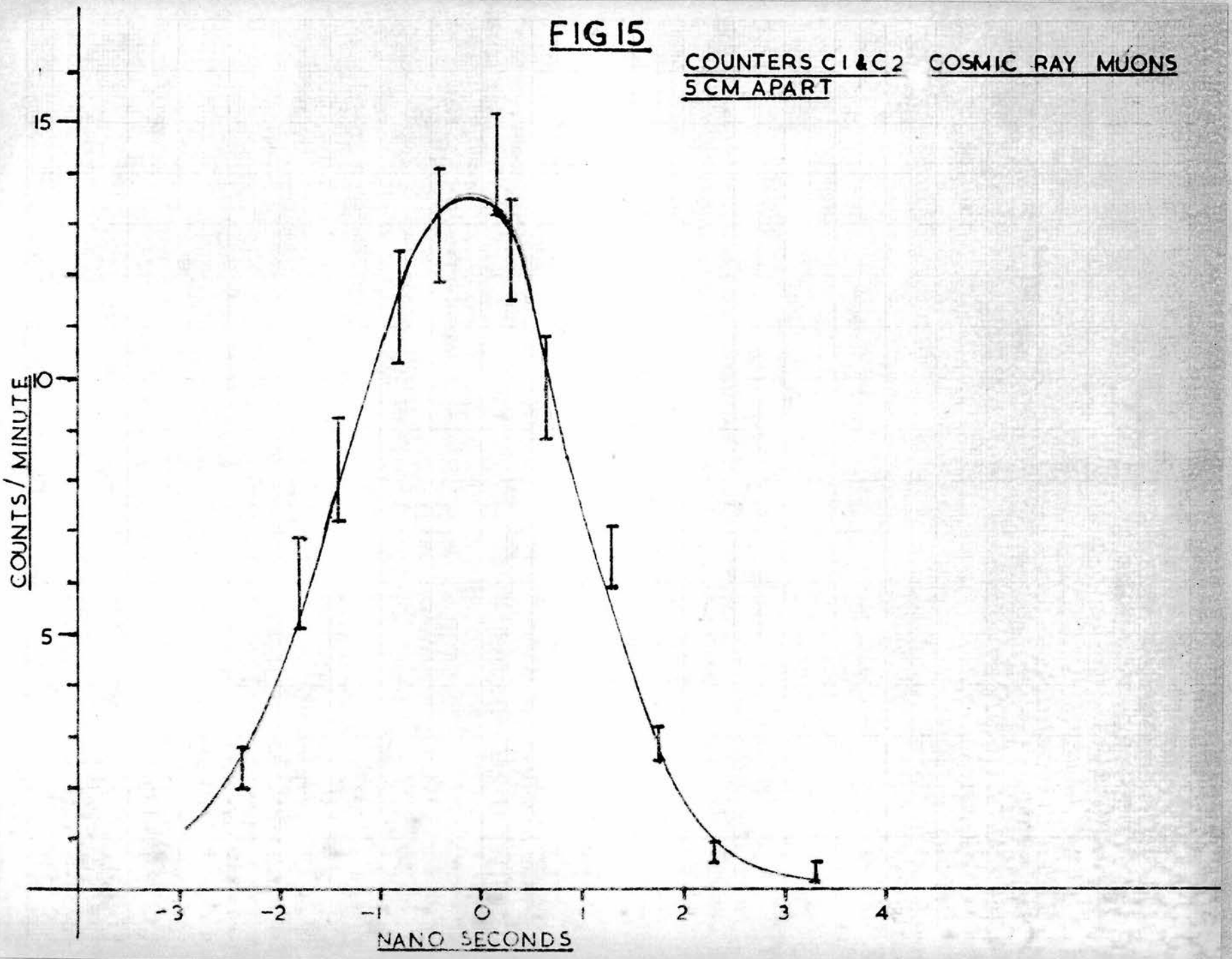

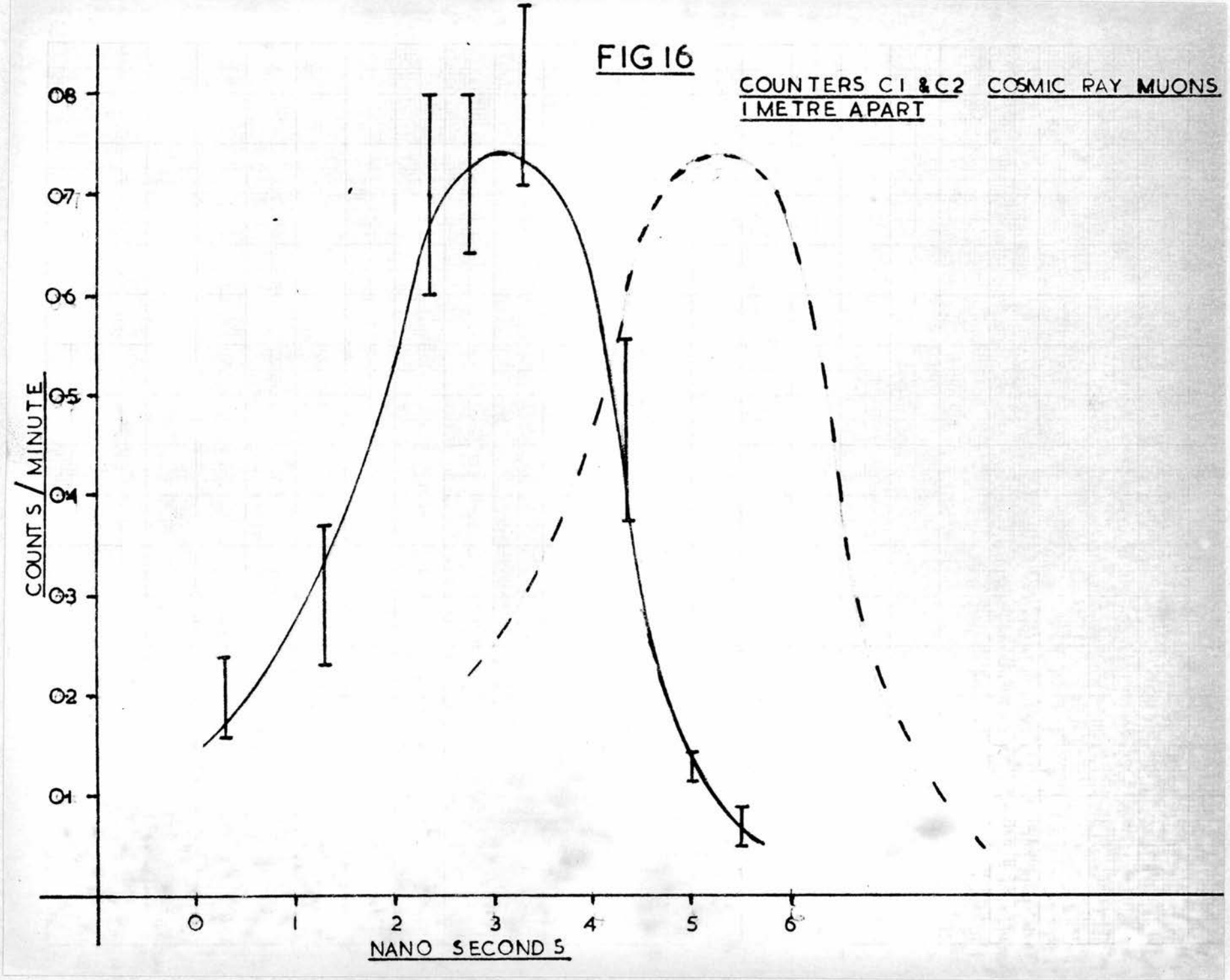
FIG 16
COUNTERS C1 & C2 COSMIC RAY MUONS
1 METRE APART
COUNTS / MINUTE
0·8
0·7
0·6
0·5
0·4
0·3
0·2
0·1
0
1
2
3
4
5
6
NANO SECONDS

results was taken, thus allowing all pulses which could trigger the tunnel diodes of the fast side to be counted. When the slow coincidence unit was switched in, and the appropriate bias levels set to accept only the top 20% of the total spectrum of pulses from the counters, considerable improvement in time resolution can be seen from Fig. 12. A further slight increase in resolution was possible if only the top 3% of the pulses was accepted (Fig. 13).

The γ-rays of the Co^{60} source produced a continuous spectrum of Compton electrons in the scintillator phosphors. Thus the height of the anode pulse would be expected to be roughly proportional to the energy of these electrons. As indicated by the theoretical considerations, the time variances of pulses produced by different energies of electrons (i.e. different numbers of photoelectrons given off the photo-cathode) would decrease with increasing energies. Thus, if almost all the Compton electrons were accepted, the time resolution would be poor as in Fig. 11. By increasing the biases on the slow side, only higher energy electrons could be selected, resulting in an improvement in the shape of the coincidence curves.

The coincidence curves (Fig. 14, 15 and 16) were obtained when coincident pulses from cosmic ray μ-mesons were used with the system. The bias levels of each counter were set to accept pulses where the apparent energy dissipation was greater than approximately 600 keV.

Curve Fig. 14 was obtained by placing counter C3 directly above counter C2 in such a manner as to accept the maximum cosmic ray flux. The other curves (Fig. 15, 16) were achieved

by placing the large counter C1 immediately above and one metre above counter C2, respectively.

The vast majority of counts fell in a region $\pm$ 2n secs on each side of the peak of the curves. The slightly poorer time resolution of Fig. 15 and 16 were expected, as the light collection efficiency of counter C2 would not be as high as that of the test counter C3.

The coincidence curve (Fig. 16) obtained when the two counters were separated by one metre indicated that particles of velocity ~ 0.6 c could clearly be separated from those of the velocity c. The dotted curve (Fig. 16) would be the curve expected if a beam of particles having velocities 0.6 c had been available, the two peaks being separated by 2.2 n secs. Thus the system would have a 100% efficiency for the selection of particles with velocity 0.6 c but only a 9% efficiency for those of velocity c, when a delay of 5.5 n secs was used.

The relatively broad coincidence curve (2.8 n secs at half height) would suggest, that for the selection of particles in the region of velocity 0.6 c, the actual value of the delay would not be critical. A region of velocities 0.5c to 0.7c would be selected with relatively high efficiency rather than just a narrow band about the velocity 0.6c.

When the delay setting of 5.5 n secs was used, a counting rate of one in fourteen minutes was recorded. Thus, provided the recycling time of the cloud chamber was small (of the order of 4 minutes) less than one quarter of the total available time would be lost on this account. Although it would be desirable

to reduce the efficiency for counting fast particles at this delay (5.5 n secs delay) even further, the total time which the experiment would take could not be reduced appreciably. By increasing the biases on the slow side of the system, the counting rate could no doubt have been reduced. In case this might have been at the expense of losing some of the slow particles this was not attempted.

The trigger circuit for the cloud chamber control system

The cycle of the cloud chamber had been started by the closure of a switch, which then operated relay Q of the control circuit. In order to trigger the start of the chamber with the 50 m secs output pulse of the coincidence unit an additional circuit was designed. (Fig. 17). The 50 m secs pulse, after feeding an emitter follow, was used to operate a second transistor which closed relay Q, thus starting the cycle. The time taken for this relay to swing into its energised position was of the order of 50 m secs, and thus gave rise to the slight field separation of counter controlled tracks mentioned in Chapter 4.

As the input line was fed via the normally open contacts of relay RL1, no pulse could be received unless the chamber cycle was completed.

In order to increase the contrast of counter controlled tracks, a slight delay was introduced between the switching off the clearing field and opening of the expansion valve. A 120 μF condenser (shown dotted on the control circuit Fig. 4, Chapter 2)

FIG 17

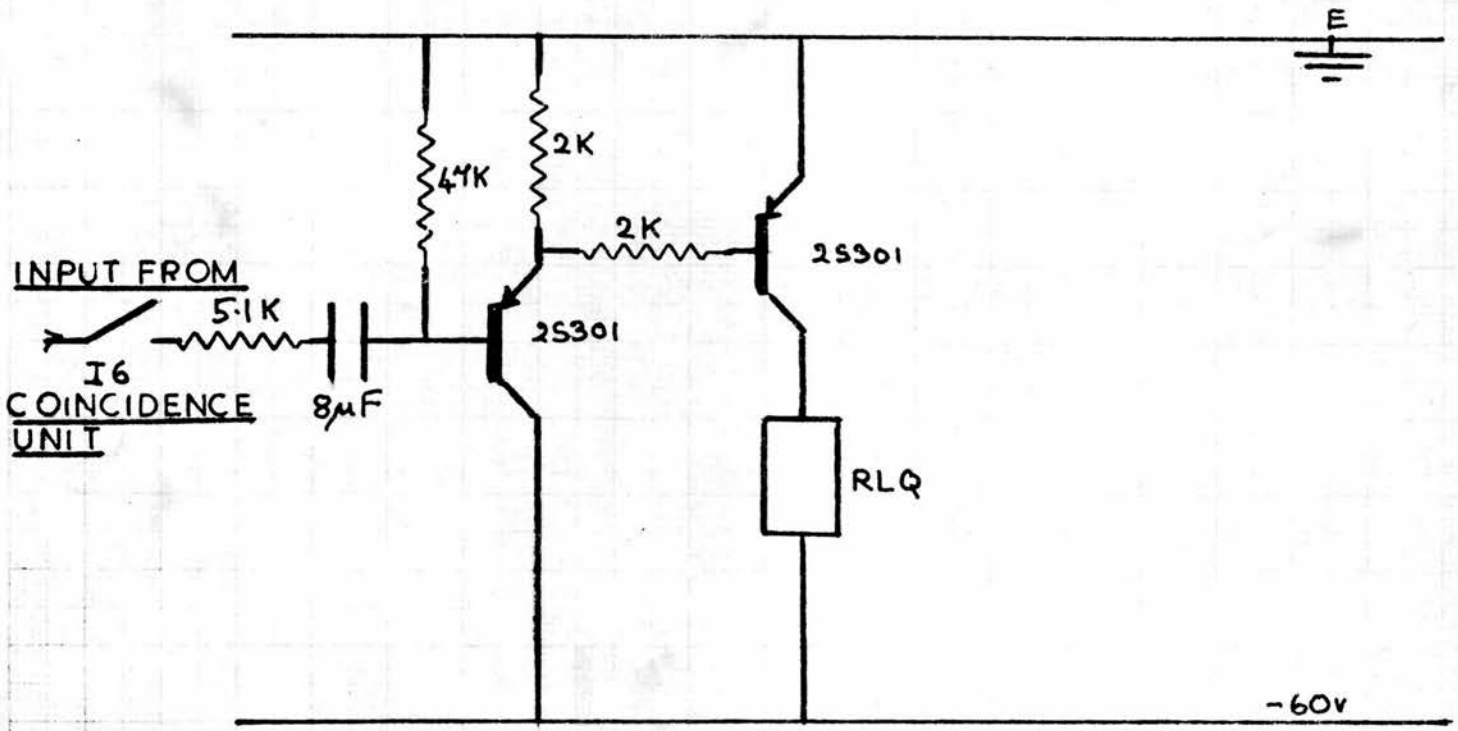
E
4·7K
2K
2K
2S301
INPUT FROM
5·1K
2S301
I6
COINCIDENCE
UNIT
8μF
RLQ
-60v

FIG 18

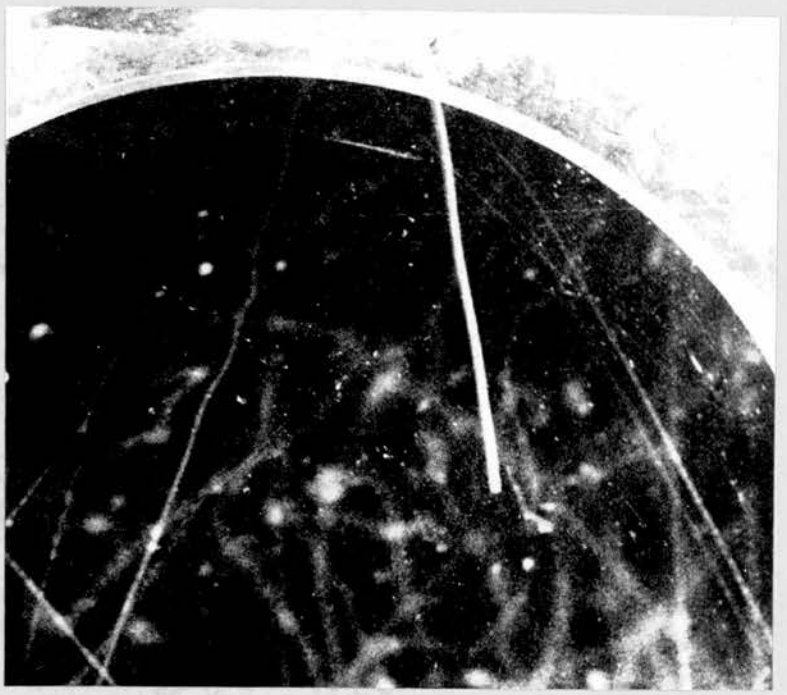

STOPPED PROTON

facilitated this function by delaying the switching on of relay RLA.

The efficiency of the system for the selection of stopping μ-mesons

Among the 3,800 cloud chamber photographs obtained with this system, 21 events of either μ - e decays or capture μ-mesons were obtained. As the efficiency for the selection of fast particles when set at a delay of 2.2 n secs off the coincidence peak was of the order of 10%, this number of photographs represented the passage of some 38,000 fast μ-mesons through the counter system. As the ratio of stopping μ-mesons to the total number was about 1 to 500 from the random photography run, then about 76 events should have been detected by the counter system. However, as the geometry of the counters produced an efficiency of only 49%, the number of events actually seen in the chamber should have been 37.

If the statistical significance between the estimated and observed number could be granted, then scattering of slow μ-mesons by both the scintillator phosphor of the lower counter and the duralumin window could account for the lower counted number of events.

As a further test that the system actually selected slow particles, the delay was increased to 4.5 n secs from the peak, given the flight time of 7.8 n secs between the two counters. For this delay, slow protons present in cosmic radiation should be selected. An example of a stopping proton obtained in this manner is shown in Fig. 18.

APPENDIX 2

Multiple Scattering Measurements

When a charged particle passes through a finite thickness of matter, it is subjected to a large number of collisions which produce, in general, very small angular deflections.

A formula for the projected average scattered angle $\bar{\theta}$ has been established by Goldschmidt-Clermont[52] which incorporated the probability function for this multiple scattering process derived by Moliere[53]. The formula is valid for all values of $\Upsilon = \frac{zZ}{137\beta}$.

$$\bar{\theta} = \frac{2ze^2\sqrt{t}\sqrt{NZ^2}}{pBc}\,\phi \qquad (1)$$

$$\phi = 1.45 + 0.8\left[\ell n\left\{0.2\pi t\, Z^{-\frac{2}{3}} N\left(\frac{\hbar^2}{m_e e^2}\right)^2 \left(\frac{1}{\frac{0.3}{\Upsilon^2}+1}\right)\right\}\right]^{1/2}$$

$$\beta = \frac{v}{c}$$

z = ratio of the charge of the incident particle to that of the electron.

t = the thickness of the matter over which the average deflection $\bar{\theta}$ occurs.

In all the previous measurements, $z = 1$ and for electrons it can be assumed that $\beta = 1$ if the energy of the electron is large compared with mc^2.

The formula (1) reduces to the following imperial formula

for charged particles (z = 1) in a gas at a pressure of P atmospheres:-

1) In argon

$$\bar{\theta} = \frac{\sqrt{tP}}{p\beta} 0.0268 \quad 1.45 + 0.8 \quad \ell n \frac{3.83\ Pt}{\beta^2 + 0.058}^{\frac{1}{2}} .$$

2) In nitrogen

$$\bar{\theta} = \frac{\sqrt{tP}}{p\beta} 0.0147 \quad 1.45 + o.8 \quad \ell n \frac{2.20\ Pt}{\beta^2 + 0.0087}^{\frac{1}{2}}$$

where the momentum p is in units of Mev/c.

The measurements of multiple scattering were performed using the reprojection apparatus[51] and in a manner similar to that by Tait[2]. A cell length t = 1 cm was used where the particle track was sufficiently long, this length being about that required to reduce the signal to noise ratio to the optimum value. (The signal was the actual measurement performed on the reprojection machine, the noise arose from the setting error due to the track having a finite width.).

REFERENCES

(1) Donald, R.A., Ph.D. Thesis (1957).

(2) Tait, R.S., Ph.D. Thesis, (1960).

(3) Duff, M.J.B. and Morris, N. Conference on the recent developments in Cloud Chamber and Associated Techniques, p. 78 (1955).

(4) Hazen, W.E., Rev. Sci. Instrum. 13, 247, (1942).

(5) Emigh, C.R. & Fisher, P.C. Conf. on recent developments in Cloud Chamber and Associated Techniques, p. 155 (1955).

(6) Watson, A.A., Ph.D. Thesis (1964).

(7) Wheeler, J.A., Rev. Mod. Phys. 21, 133 (1949).

(8) Tiomno, J. and Wheeler, J.A. Rev. Mod. Phys. 21, 153 (1949).

(9) Keufell, J.W. et al. Phys. Rev. 87, 942 (1952).

(10) No reference.

(11) Kennedy, J.M. Phys. Rev. 87, 953 (1952).

(12) Tolhoek, H.A. and Luyten, J.R. Nuclear Physics 3, 679 (1957).

(13) Primakoff, H. Proc. 5th Rochester Conference, p. 174 (1955).

(14) Primakoff, H. Rev. Mod. Phys. 31, 802 (1959).

(15) Sens, J. Phys. Rev. 113, 679 (1959).

(16) Fujii, A. and Primakoff, H. Nuovo Cimento 12, 327 (1959).

(17) Goldberger, M.L. and Treiman, S.B. Phys. Rev. 111, p. 335 (1958)

(18) Feynman, R.P. and Gell-Mann, M. Phys. Rev. 109, 193 (1958).

(19) Filippias, T.A. et. al. Phys. Letters 6, 118 (1963).

(20) Klein, R. and Wolfenstein, L. Phys. Rev. Letters 9, 408 (1962).

(21) Luyten, J.R. et al. Nuclear Physics 41, 236 (1963).

(22) Telegdi, V. Phys. Rev. Letters 8, 327 (1962).

(23) Zaimidoroga et al. Phys. Letters 6, 100 (1963).

(24) Rothberg, J.E. et al. Phys. Rev. 132, 2664 (1963).

(25) Blesser, E. et al. Phys. Rev. Letters 8, 288 (1962).

REFERENCES (Contd.)

(26) No reference.

(27) Godfrey, T.N.K. Phys. Rev. 92, 512 (1953).

(28) Wolfenstein, L. Nuovo Cimento 13, 319 (1959).

(29) Flamand, G. and Ford, K.W. Phys. Rev. 116, 1591 (1959).

(30) Morita, M. and Fujii, A. Phys. Rev. 118, 606 (1961).

(31) Burgman, J.O. et al. Phys. Rev. Letters 1, p. 469 (1958).

(32) Argo, H.V. et al. Phys. Rev. 114, 626 (1959).

(33) Fetkovich, J.G. et al. Phys. Rev. 118, 319 (1960).

(34) Maier, E.J. Phys. Rev. Letters 6, 417 (1961).

(35) Cohen, R.C. et al. Phys. Rev. Letters 11, 134 (1963).

(36) Duck, I. Nuclear Physics 35, 27 (1962).

(37) No reference.

(38) Conversi, M. et al. Phys. Rev. 136, B1077 (1964).

(39) Rood, H.P.C.) Phys. Letters 6, p. 121 (1963).
Tolhoek, H.A.)

(40) Yovnovich, M.L. and Evseer, V.S. Phys. Letters 6, 333 (1963).

(41) Donald, R.A. and Evans, G.R. Nuovo Cimento 9 (Supp.) 385 (1958).

(42) Rossi, B. High Energy Particles, p. 190 (1952).

(43) Morinaga, H. Phys. Rev. 103, 504 (1956).

(44) Burhop, E.J.S. Conf. on Recent Development in Cloud Chambers and Associated Techniques, p. 86 (1955).

(45) No reference.

(46) Endt, P.M. and Van Der Leun, C. Nuclear Physics 34, 1 (1962).

(47) Siegbahn, K. Beta- and Gamma-Ray Spectroscopy, p. 286 (1955).

(48) Fermi, E. Nuclear Physics, p. 82 (1950).

(49) Talmi, I. Phys. Rev. 107, 1601 (1957).

REFERENCES (Contd.)

(50) Beltrametti, E.G. and Radicati, L.A. Nuovo Cimento 11, 793 (1959)

(51) Williams, E.J. Conference on Recent Development in Cloud Chambers and Associated Techniques, p. 95 (1955).

(52) Goldschmidt-Clermont, Y. Nuovo Cimento 7, 331 (1950).

(53) Moliere, Zeits. Naturforschung 3a, 78 (1948).

(54) No reference

(55) No reference

(56) No reference

(57) Wheeler, J.A. Phys. Rev. 71, 320 (1947).

(58) Fermi, E. and Teller, E. Phys. Rev. 72, 399 (1947).

(59) Conversi, M. et al. Phys. Rev. 71, 209 (1947).

(69) West, D. Reports on Progress in Physics, p. 271 (V. 21) (1958).

(61) Fitch, V.L. & Rainwater, J. Phys. Rev. 92, 789 (1953).

(62) Ford, K.W. and Wills, J.G. Nuclear Physics 35, 295 (1962).

(63) Krall, N.A. and Gerjuoy, E. Phys. Rev. Lett. 3, 142 (1959).

(64) De Borde, A.H. Proc. Phys. Soc. A67, 57 (1954).

(65) Mann, R.A. and Rose, M.E. Phys. Rev. 121, 293 (1961).

(66) Day, T.B. et al. Phys. Rev. 123, 1051 (1961).

(67) Baker, G.A. Phys. Rev. 117, 1130 (1960).

(68) Martin, A.D. Nuovo Cimento 27, 1359 (1963).

(69) Eisenberg, Y. and Kessler, D. Nuovo Cimento 19, 1195 (1961).

(70) Burbridge, G.R. and De BBorde, A.H. Phys. Rev. 89, 189 (1953).

(71) Ruderman, M.A. Phys. Rev. 118, 1632 (1960).

(72) Stearns, M.B. and Stearns, M. Phys. Rev. 105, 1573 (1956).

(73) No reference.

(74) No reference.

(75) No reference.

REFERENCES (Contd.)

(76) Lanthrop, J.L. et al. Phys. Rev. Lett. 7, 147 (1961).

(77) Scott Johnson, C. et al. Phys. Rev. 125 (2), 2102 (1963).

(78) Eisenberg, Y. & Kessler, D. Phys. Rev. 130 (2), 2349 (1963).

(79) Cosyns, M.G.E. et al. Proc. Roy. Soc. A62, 801 (1949).

(80) Fry, W.F. Phys. Rev. 83, 594 (1951).

(81) Fry, W.F. Nuovo Cimento 10, 490 (1953).

(82) Pevsner, A. et al. Nuovo Cimento 19, 409 (1961).

(83) Vaisenberg et al. Soviet Physics J.E.T.P. 14, 734 (1962).

(84) Dzhelepov, V.P. et al. Nuclear Physics 34, 424 (1963).

(85) Condo, G.T. et al. Phys. Rev. 133, A1280 (1964).

(86) No reference.

(87) Rossi, B. High Energy Particles, p. 137 (1952).

(88) Bhabha, H.J. Proc. Camb. Phil. Soc. 31, 394 (1935).

Quoted by (93) (89) Racah, G. Nuovo Cimento 14, 93 (1937).

(90) Nishima et al. Sci. Paper Inst. Phys. Chem. Research (Tokyo) No. 27, 137 (1935).

(91) Block, M.M. et al. Phys. Rev. 96, 1627 (1954).

(92) Murota, T. et al. Prog. Theoretical Physics, p. 482 (1956).

(93) Stoker, P.H. and Haarhoff, P.C. Nuclear Physics 14, 512 (1960).

(94) Roe, B.P. and Ozaki, S. Phys. Rev. 116, Lo22 (1959).

(95) Gaebler, J.F. et al. Nuovo Cimento 19, 265 (1961).

(96) Stoker, P.H. et al. Nuclear Physics 45, 505 (1963).

(97) Chaudhuri, N. and Sinha, M.S. Nuovo Cimento 32, 853 (1964).

(98) Gardner, M. et al. Proc. Phys. Soc. 80, 697 (1962).
Hayman, P.J. and Wolfendale, A.W. Proc. Phys. Soc. 80, 710 (1962).

(99) Williams, E.J. Proc. Roy. Soc. 172A, 202 (1939).

(100) Barker, P.R. Phys. Rev. 100, 860 (1955).

REFERENCES (Contd.)

(101) Heitler, W. Quantum Theory of Radiation, (1954).

(102) Wilson, R.R. Phys. Rev. 86, 261 (1952).

(103) Rossi, B, High Energy Particles, p. 42 (1952).

(104) Neiler, J.H. and Good, W.M. Fast Neutron Physics (Part 1), p. 552 (1960).

(105) Gatti, E. and Svelto, V. Nucl. Inst. & Method 4, 189 (1959).

(106) Bartl, W. and Weinzierl, P. Rev. Sci. Inst. 34, 252 (1963).

(107) Franzini, P. Rev. Sci. Inst. 32, 1222 (1961).

(108) Gygi, E. and Schneider, F. Nucl. Inst. & Method 20, 352 (1963).

(109) Larsen, R.N. and Shera, E.B. Nucl. Inst. & Method 32, 168 (1963).

(110) Hendry, W.M. Rev. Sci. Instr. 32, 168 (1965).

ACKNOWLEDGEMENTS

I wish to thank Professor N. Feather, F.R.S., for the use of his laboratory facilities in the Department of Natural Philosophy.

I am indebted to Dr. G.R. Evans for suggesting the subject of this thesis and for his advice and encouragement during the project.

I should like to extend my thanks to Mr. Headridge and his staff for their valuable help in the design and construction of apparatus.

I am indebted to D.S.I.R. for the provision of a post-graduate grant.